Microfluidics: Functionality Integration for Proteomic Applications

Petersen, Daria

Publication date:
2006

Document Version
Early version, also known as pre-print

MICROFLUIDICS: FUNCTIONALITY INTEGRATION FOR PROTEOMIC APPLICATIONS

Daria Petersen

Ph.D. Thesis

May 2006, Department of Micro and Nanotechnology (MIC)
Technical University of Denmark (DTU)

Microfluidics: Functionality Integration for Proteomic Applications

Daria Petersen

Ph.D. Thesis

May 2006

Supervisor:

Oliver Geschke, Assoc. Professor, POEM group leader (Polymeric Environmental Microsystems)

Co-supervisors:

Jörg P. Kutter, Professor in μ-TAS (micro- Total Analysis Systems)
Pieter Telleman, Professor in Bio/Chemical Microsystems, Director of MIC

Department of Micro and Nanotechnology (MIC), Technical University of Denmark (DTU), Building 345 East, DK-2800, Kongens Lyngby, Denmark

Preface

My work was coordinated by associate professor Oliver Geschke, Group Leader, POEM (Polymeric Environmental Microsystems). My co-supervisors have been, Professor Jörg P. Kutter, Group Leader, μTAS (Micro-Total Analysis Systems), and Professor Pieter Telleman, Director. All supervisors are from Department of Micro and Nanotechnology (MIC), Technical University of Denmark (DTU). This thesis represents a part of the requirements for obtaining the Ph.D. degree at the Technical University of Denmark.

The experimental work was carried out at MIC and in collaboration with other institutes. Some of the microsystems with integrated electrospray needles which were fabricated during this study were tested at the Analytical Chemistry Department of Helsinki University, Finland under the supervision of professor Marja-Liisa Riekkola. One year of this study was carried out at Oak Ridge National Laboratory (ORNL), where I worked on a Micro Chem Lab / Bio Detection project, with Sandia National Laboratory as the lead partner. This project involved on-chip integration of several functional elements for protein analysis. The research was carried out under the supervision of Dr. Robert S. Foote in the Laser Spectroscopy and Microtechnology Group at ORNL, and J. Michael Ramsey, Minnie N. Goldby Distinguished Professor of Chemistry at University of North Carolina at Chapel Hill (UNC), USA.

Acknowledgments

I would like to thank my supervisors at MIC for their support and patience during my study. I would especially like to thank associate professor Oliver Geschke and professor Jörg P. Kutter for their supervision and scientific input regarding the microfabrication techniques and the ideas for designing electrospray interfaces. I am very grateful to my supervisor Oliver Geschke for his input into the thesis correction process, which became a very valuable part of my education. I am grateful to all members of μ-TAS and POEM groups for helpful discussions and making my study at MIC a pleasant experience. I would especially like to thank Ph. D. Ramona Matieu for her input to the structure and style of this thesis.

I sincerely thank J. Michael Ramsey and Robert S. Foote for their supervision and financial support during my external research at Oak Ridge National Laboratory. All the group members should be credited for fruitful scientific discussions and sharing their knowledge with me. I thank Christopher D. Thomas and Leslie Wilson for their help with fabrication of integrated microchips for protein analysis. I would also like to thank Jean Pierre Alarie for correcting the English language in this document.

I would like to thank Marja-Liisa Riekkola for giving me the opportunity to visit her group at Helsinki University. I would also like to acknowledge Professor Jörg P. Kutter for organizing this visit.

I would like to sincerely thank my husband and our daughters for their understanding and support and apologies to them for all they suffered from me being stressed and busy during my study. I would also acknowledge my husband for giving the valuable advises within the course of my study. Everything I learned of practical things whether useful for experiments in the lab, for literature search and management, data treatment and interpretation, or Danish language, I learned from him.

The Ph. D. project was sponsored in part from the Danish Research Council, on frame program "Micro Total Analysis Systems", case number 9901288, and in part by U. S. Department of Energy, National Nuclear Security Administration, under contract DE-AC05-00OR22725 with Oak Ridge National Laboratory, managed and operated by UT-Batelle, LLC. This research was also supported in part by an appointment to Oak Ridge National Laboratory Postmaster's Research Participation Program administrated jointly by Oak Ridge Institute for Science and Education and Oak Ridge National Laboratory.

Summary

Interest in miniaturization of chemical and biological analyses is growing. In this work, the design, fabrication and characterization of microfluidic analytical tools is studied. The focus is set on glass microchips for chemical analysis.

The work consists of three parts:

1) Design, fabrication and characterization of integrated microchips for protein processing with enhanced limit of detection (LOD);

2) A novel bonding process of glass devices for miniaturized total analysis systems (μ-TAS);

3) Design and fabrication of glass microchips with novel monolithically integrated electrospray ionization interface for capillary electrophoresis to mass spectrometry (CE-ESI-MS).

Sample preconcentration, injection, separation, fluorescence labeling, postcolumn dilution (destaining) for signal enhancement and detection of proteins are combined and optimized in a single glass microdevice. On-column as well as post-column non-covalent protein labeling strategies are demonstrated to be compatible with protein preconcentration using a sol-gel filter followed by capillary sieving electrophoresis (CSE) as a separation method. This is the first demonstration of on-chip protein preconcentration integrated with on-chip non-covalent labeling. It is demonstrated that post-column labeling and dilution (destaining) performed simultaneously in a single step result in better separation efficiency and limits of detection similar to these compared to on-column labeling combined with destaining.

The novel bonding process for glass chips involves a sputtered-on polysilicon layer which is employed both as an adhesion layer for the etch mask and as an intermediate layer for field-assisted bonding, thus reducing the number of microfabrication steps. A mechanism of field-assisted anodic bonding is discussed. This bonding scheme is found to be superior to direct bonding methods such as high temperature fusion bonding in terms of process yield, and the relatively low bonding temperature (~ 350 ºC) makes it suitable for packaging of microsystems having integrated layers with different thermal expansion coefficients or low melting points. This novel fabrication process is used to fabricate CE glass chips with an electrospray needle for capillary electrophoresis coupled by electrospray ionization to mass spectrometry (CE-ESI-MS).

The ESI interface is designed and fabricated in conjunction with a CE-separation channel. Microfabrication procedures are developed and optimized to create a zero dead volume monolithically integrated electrospray needle.

Resume (in Danish)

Interessen for miniaturiserede kemiske og biologiske analyser er voksende. I denne afhandling er der set på design, fabrikation, og karakterisering af miniaturiserede analytiske systemer. Fokus er lagt på mikrochips fabrikeret i glas til kemiske analyser. Rapporten består af tre dele:

1) Design, fabrikation og karakterisering af integrerede mikrochips til protein analyser med forøget detektionsgrænse;

2) En ny bindingsproces af glas-mikrosystemer til 'miniaturized total analysis systems' (μ-TAS);

3) Design samt fabrikation af glas mikrosystemer til kapillær elektroforese (CE) separering integreret med elektrospray ionisering til massespektrometer analyse (CE-ESI-MS).

Prøve koncentrering, injektion, separering, fluorescensmærkning, fortynding (affarvning) efter separation for signal forøgelse og detektion er blevet kombineret og optimiseret i et enkelt mikrochip-system. I-kolonne og efter-kolonne protein mærkningsstrategier påvises i rapporten at være forenelig med protein koncentrering, ved brug af et silika gel ('sol-gel') filter, efterfulgt af en kapillar 'sieving' elektroforese (CSE)-separation. Dette er den første demonstration af 'on-chip' protein koncentrering integreret med 'on-chip' ikke-kovalent mærkning. Det demonstreres ligeledes, at når efter-kolonne mærkning og fortynding (affarvning) udføres samtidigt i et enkelt procestrin, opnår man en bedre separationseffektivitet og detektionsgrænse som er på niveau med i-kolonne mærkning kombeneret med fortynding.

Den nye bindingsproces indbefatter et 'sputtered-on' polysiliciumlag, der både fungerer som et fæstelag for ætsemasken og som et mellemlag for elektrisk-ledsaget anodisk bonding. På denne måde forenkler den nye bindingsproces fabrikationen ved at reducere antalet af procestrin. En mekanisme for elektrisk-ledsaget anodisk binding diskuteres i rapporten. Proces-udbyttet for denne binding metode er bedre end direkte binding metoder, som f.eks. høj-temperatur fusions binding. Den relativt lave temperatur (ca. 350 °C) gør elektrisk-ledsaget anodisk binding særligt velegnet til samling af mikrosystemer bestående af integrerede lag med forskellige termiske udviddelseskoefficienter eller med lave smeltepunkter. Denne nye fabriaktionsproces er blevet anvendt til fabrikation af et glas microsystem med en integreret nål for elektrospray ionizering for CE-ESI-MS.

Et ESI interface er designet og fuldt integreret i en CE-mikrochip. Fabrikationsproceduren er udviklet og optimiseret for at lave en monolitisk integreret spray til uden dødvolumen.

Table of contents

Abbreviations

2DE – two-dimensional electrophoresis
BOE – buffered oxide etch
c – concentration (mol/L)
CE – capillary electrophoresis
cmc – critical micelle concentration
CSE – capillary sieving electrophoresis
Da – Dalton, atomic mass unit (g/mol)
DI – deionized water
DMSO - dimethyl sulfoxide
DNA – deoxyribonucleic acid
DR – dilution ratio
EDTA – ethylenediaminetetraacetic acid
EOF – electroosmotic flow
ESI – electrospray ionization
FASS - field amplified sample stacking
FITC – fluorescein isothiocyanate
GRAVY – average hydropathicity for all the amino acids in a protein calculated according to Kyle and Doolittle [1]
H –theoretical plate height
HF – hydrofluoric acid
HMDS – hexamethyldisilazane
HUPO – Human Proteome Organization
LIF – laser induced fluorescence
LOD – limit of detection
LPA – linear polyacrylamide
MALDI – matrix assisted laser desorption ionization
MAPTOS - 3-methacryloxypropyltrimethoxysilane
MS – mass spectrometry
M_r – relative molecular mass with a unit of 1 Da
mRNA – messenger RNA
MW – molecular weight (g/mol)
N_a – Avogadro's constant
N - separation efficiency
ODS - octadecylsilane
PAGE – polyacrylamide gel electrophoresis
PDMS - polydimethylsiloxane
pI – isoelectric point
PSI – protein standard initiative
PVC – polyvinyl chloride
R_s – resolution
RNA - ribonucleic acid
rpm – rounds per minute
rRNA – ribosomal RNA
SDS – sodium dodecyl sulfate
SPE – solid phase extraction
TBE – Tris-borate-EDTA
TEMED - tetramethylethylenediamine
TEOS - tetraethylorthosilane
TMOS - tetramethylorthosilane
t_R - migration time of an analyte peak
w_b – analyte peak width at the baseline
$w_{1/2}$ – analyte peak width at half peak height

1. Introduction

In this chapter, the motivation for protein analysis is described as well as the challenges in the field of proteomics. The argumentation for miniaturizing and integrating the steps for protein analysis is presented. The conventional methods for protein analysis are compared to the miniaturized systems.

1.1 What is "proteomics"?

The concept of "*proteome*," which is an acronym for PROTEin complement expressed by a genOME, has emerged as a complement to genomics in order to understand the biological functions of proteins. *Proteomics* deals with characterization of the entire protein complements within a cell, tissue or organism. A proteomic analysis of levels, activities, regulations and interactions of cellular proteins in response to unique stimuli has now become a frontier of cell biology, pharmacology, clinical diagnostics and analytical science, to name a few.

For a better understanding of biological systems, it is desirable to know which proteins a given cell is expressing at a particular point in time, and how the concentration of the expressed proteins changes in response to external stimuli. Furthermore, it is desirable to know location of the expressed proteins within a cell of interest and to be able to monitor any variations that occur as a function of time.

Proteomics is a more complex field than genomics because it is aimed at not only the structure and quantification of a protein but also at its function. Structural proteomics defines the primary, secondary and tertiary structure of proteins, whereas functional proteomics makes predictions of protein function based on genomic information. There are many possible interactions between proteins, and there are many more proteins than genes. The genome of an organism is static (humans have 30,000-50,000 genes), but its proteome varies depending on the particular cell type, and on dynamic alterations of its environment. Current estimates indicate that organisms express an order of magnitude more proteins than genes [2]. In addition, expressed proteins are typically modified in a variety of ways by post-translational modifications such as phosphorylation and glycosylation. The proteome is highly dynamic, responding to both the cellular microenvironments and the physiological states of the organism.

Proteins are required for the structure, function, and regulation of the body's cells, tissues, and organs. Each protein has unique functions, acting for examples as hormones, enzymes and antibodies.

Proteins can be divided into homoproteins consisting only of amino acids, and heteroproteins which also contain a non-protein part (the so-called prosthetic group). Depending on the type of prosthetic group, these proteins are further divided into nucleo-, lipo-, glyco-, phosphor-, hemo-, flavo-, and metalo- proteins. Proteins typically have molecular weights of approximately 5,000-100,000 Da for single chains to over 400,000 Da for oligomeric structures. The size of globular conformations for single chains is about 1-6 nm with oligomers and membrane proteins being much larger than that.

Environmental conditions can induce changes in the secondary, tertiary, or quaternary structure of the protein and thereby change its properties including solubility, enzymatic activity, and potentially chemical breakdown due to exposure of less stable bonds. Various physical processes such as heating, cooling, mechanical treatment (including ultrasound) and radiation can induce protein denaturing. Proteins can also be chemically denatured with acids, bases, metals, organic solvents or at high ionic strength. The result of protein denaturing can be reversible or irreversible. Protein denaturing produces conformers and different aggregation states.

Human serum contains approximately 300 proteins; mitochondria and organelles from blood cells contain about 5,000 different proteins each, all present at different abundance levels. Analyzing such a complex mixture of native proteins is a very difficult task due to the large variations in molecular weight, charge, solubility and concentration of the individual proteins. “Native” protein refers to the naturally occurring conformation of the protein molecule in which it possesses its biological activity. One approach to reduce sample diversity is to perform a digest of native proteins. An enzymatic digest of single human cell protein content (approximately 10,000-20,000 proteins) can produce up to 1,000,000 peptides. No single chromatographic or electrophoretic method is capable of separating such a complex mixture effectively enough to identify a reasonable percentage of peptides. Another disadvantage is that post translational modifications of proteins can not be monitored after a digest has been performed. Therefore, it is desirable to perform a separation of native proteins prior to digest in order to reduce the complexity of the sample.

1.2 Conventional protein analysis

For analyzing complex protein mixtures, several separation technologies are available as presented in Figure 1. Isotope-Coded Affinity Tags (ICAT) developed by Aebersold et al. in 1999 [3] is used for comparison of relative protein abundance between two samples. The two samples are

labeled with two different isotopes prior to being separated together on the 2D gel. The different isotopes as labels allow comparing the amount of a specific protein in either sample.

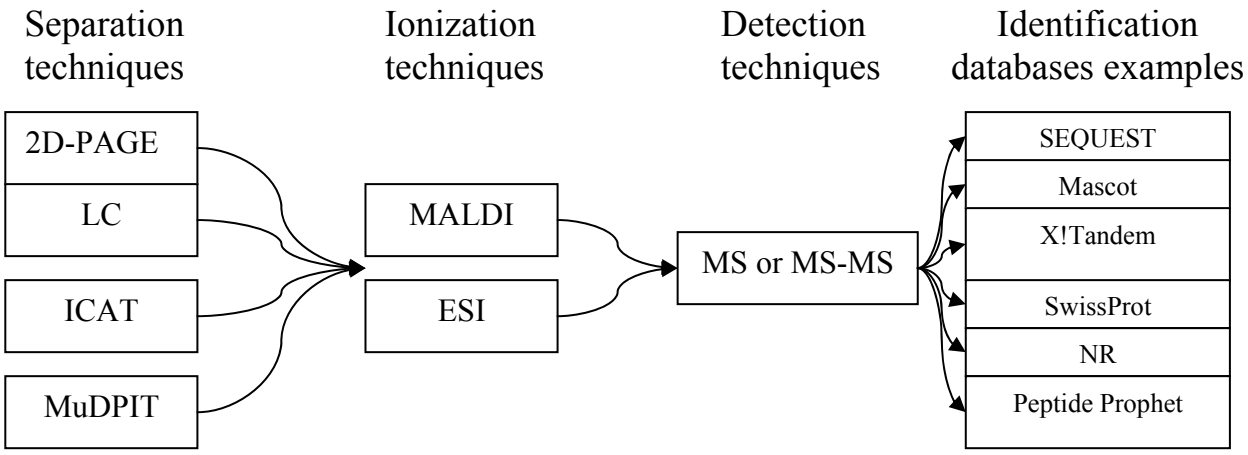

Figure 1. An overview of conventional schemes for analyzing complex protein mixtures. Separation techniques include two-dimensional Polyacrylamide Gel Electrophoresis (2D-PAGE), Liquid Chromatography (LC), Isotope-Coded Affinity Tags (ICAT) and Multidimensional Protein Identification Technology (MudPIT). Mass Spectrometry can be employed for the detection by all methods, after the sample has been ionized by either Matrix-Assisted Laser Desorption and Ionization (MALDI) or by Electro Spray Ionization (ESI). The resulting MS spectra can be searched in various databases in order to confirm the identities of biomolecules.

Two-dimensional polyacrylamide gel electrophoresis (2D-PAGE) has long been recognized as a powerful tool for the analysis of complex protein mixtures extracted from cells, tissues, or other biological samples. This technique separate proteins according to two independent properties: their isoelectric points (pI) and their molecular weights (MW). In the first dimension the proteins are separated by isoelectric focusing (IEF) and in the second-dimension SDS-polyacrylamide gel electrophoresis (SDS-PAGE) is performed. IEF is achieved by having a pH gradient in the SDS-PAGE gel in one dimension. When the electrical field is applied, proteins migrate along the pH gradient until they reach the pH value where they become neutral and therefore have no net mobility. This location of the proteins in the gel constitutes their apparent pI values. For the 2-D gels to be reproducible, careful attention should be paid to sample preparation, first- and second-gel dimension preparation and running, as well as reproducible protein detection. Once the protein spots of interest have been revealed from the quantitative analysis of the 2-D PAGE patterns, the problem of identification is encountered. In 1993, Biomedical Proteomics Research Group (BPRG) of the Geneva University Hospital and the Swiss Institute of Bioinformatics (SIB) established the Expert Protein Analysis System (ExPASy) world wide web server, www://expasy.org. It includes SWISS-2DPAGE, a database for (2-D PAGE) and SDS-PAGE. The SWISS-2DPAGE database assembles data on proteins identified on various 2-D PAGE and SDS-PAGE maps [4]. Each entry

in this database contains textual data on specific protein, including mapping procedures, physiological and pathological information, experimental data (isoelectric point, molecular weight, amino acid composition, and peptides masses), bibliographical references and images showing the experimentally determined locations of the individual proteins. It also suggests a theoretical region computed from the sequence of the protein, indicating where the protein might be found in the gel.

Two main approaches for the protein identification after most two-dimensional electrophoresis gels (2DE gels) are immunoblotting and peptide-mass fingerprinting. The 2DE database search give an opportunity to predict a probable identity of a particular protein spot from 2DE gel which then can be confirmed or denied the by immunoblotting. Western blotting (also referred to as protein blotting, or immunoblotting) has evolved for the detection of proteins post-electrophoresis since the protocol for protein transfer from an electrophoresed gel to a membrane was described in 1979 [5]. The various procedures that have been used to transfer proteins from a gel to a membrane based on the principles of diffusion, vacuum-assisted solvent flow and electrophoretic elution, as well as a brief description of methods generally used to detect antigens on blots, is described in review by Kurien et al. [5]. Immunoblotting is used where only small quantities of sample are available as it can detect as little as picogram amounts of protein, depending on the specificity of the antibodies. However, immunoblotting is a slow technique, as it is only possible to identify a few proteins per gel per day. Blotting techniques also require the prior existence of monoclonal or polyclonal antibodies, which may be expensive to make or obtain commercially. The other approach to identification of protein is peptide mass fingerprinting, performed by obtaining accurate peptide masses from specifically cleaved proteins band and then using these masses to search protein sequence databases to identify a previously sequenced protein or to confirm that it is novel.

2D-PAGE methods are not able to display the complete proteome present in a native biological sample like a body fluid and works better for the high abundant proteins. The dynamic range of most 2DE gels is from 10 to 200 kDa. Proteins with limited solubility and extremely acidic or alkaline isoelectric points ($pI < 4$ and $pI > 9$, [6]) are not observed on 2DE gels. Also the concentration range of proteins observed in body fluids (six- to nine-orders of magnitude) cannot be covered by 2DE gels. Three approaches to fluorescence labeling of proteins in two-dimensional gels are currently practiced: covalent derivatization of proteins with fluorophores, intercalation of fluorophores into the sodium dodecyl sulfate (SDS) coated protein, and direct electrostatic

interaction with proteins by a Coomassie Brilliant Blue-type mechanism, all methods reviewed in [7].

The reproducibility of 2DE gels is another challenge. For instance, differential imaging gel electrophoresis (2DE-DIGE) uses the possibility to analyze two samples in one gel by using different fluorescent tags to address the reproducibility. The limitations of conventional protein staining techniques are being gradually overcome as electrophoresis methods are interfaced with automated gel stainers and image analysis workstations, followed by robotic spot excision instruments, which transfer samples to protein digestion work stations, and finally the sample is introduced to mass spectrometers. However, two-dimensional electrophoresis remains a low throughput technique and full automation of it is still not commercially available. Another bottleneck challenge in using 2D-PAGE for protein identification is a necessity of the sample preparation for the isolated spots from gel protein before MS analysis, typically requiring various enzymatic digestions after the spot was excised.

Unique mass spectra of many proteins allow for high certainty identification by mass spectrometry, but it requires as pure separated proteins in the sample as possible for the successful identification. Chromatography can be used for the high efficiency separation of biomolecules in complex mixtures, but the identification of analytes based on the retention times alone is not possible. Thus the ability of chromatographic methods to provide relatively ‘pure’ analytes into the MS combined with possibility of differentiation between analytes with close retention time by their mass spectra provides for very powerful identification ability of chromatography-MS. Out of a big family of chromatographic methods including gas chromatography (GC), high performance liquid chromatography (HPLC), supercritical fluid chromatography (SFC), capillary electro chromatography (CEC), micellar electrokinetic chromatography (MEKC), it is mostly HPLC that is being widely employed for analysis of complex biological samples. The combination of GC with mass spectrometry originated in 1958 and was commercialized in 1967. The popularity of ‘tandem’ or ‘hyphenated’ GC-MS technique is easily explained by the similar requirements to the sample in both GC and MS. For GC, the sample has to be volatile at temperatures suitable for the separation, yet the sample has to be stable at these temperatures. MS analyses gas phase ions and thus the analytes eluting from GC can be ionized for MS and the interfacing of the two techniques is relatively straight forward. Such a compatibility and ease of interfacing is not the case for using MS as a detection method for HPLC. An interface to transfer the analytes to the gaseous phase and to

ionize them is needed. Unlike the case of GC-MS hyphenation, there is no single interface existing that would allow efficient transfer of all analytes for LC-MS.

The HPLC can easily separate proteins and peptides also in the low-molecular weight range, an area which is largely inaccessible to standard 2DE gels. Multidimensional chromatographic methods can have an enormous dynamic range of protein concentrations needed for proteomics (approximately nine-orders of magnitude). There is an abundance of retention mechanisms for normal-phase and reverse-phase HPLC, such as hydrophobic interaction chromatography, ion-pair chromatography, ion-exchange chromatography, size exclusion chromatography, etc.

Multi-Dimensional Protein Identification Technology (MudPIT) invented by Yates et al. [8] in 2002 requires a digest of protein sample with resulting peptides being analyzed by in-line two-dimensional chromatography (2D-LC). MudPIT technology employs the digestion of proteins into peptides in order to overcome the solubility, handling and ionization problems inherent to working with large proteins. MudPIT employs two dimensional chromatographic separations of the digested samples containing the complex peptide mixtures. An ion-exchange column with a high loading capacity is placed before a reversed phase chromatographic column, acting as a peptide reservoir. This separation allows gradually eluting and separating different fractions by controlling the gradient and thus can achieve a good signal even from the low abundance peptides. Thus, MudPIT demonstrates equal sensitivity for sample peptides, independent of their size, abundance and pI. The detection for MudPIT is performed by tandem MS-MS where peptide ions are first measured in intact form according to their m/z ratio, the individual ions are then subjected to a collisionally induced dissociation (CID) and analyzed in a subsequent MS. This process is often referred to as tandem mass spectrometry, or MS/MS. The CID patterns of peptide ion fragments are predictable, and thus a theoretical spectrum can be constructed for the protein sequence. Proteins are then identified by comparing the experimentally derived sequence information with databases.

MudPIT technology requires desalting of the peptide sample prior to loading it on the first column. With a well optimized separation, MudPIT allows routine analysis of 1500-2000 proteins in a sample derived from whole cell lysate [9], generating about 70,000 spectra. A single run typically takes 6 to 24 hours after 2 to 7 additional hours used for loading the sample. An advantage of MudPIT technology is that no pre- or post-column labeling of sample is needed. It could therefore be very attractive to miniaturize and integrate the sample preparation, digestion and multidimensional separation on a single microfluidic device together with an electrospray interface for MS/MS detection.

To transfer the separated biomolecules into gaseous phase for MS analysis, two different ionization techniques can be used. One ionization technique is matrix – assisted laser desorption and ionization (MALDI), developed by Koichi Tanaka in 1988 [10]. Another ionizations technique, electrospray ionization (ESI) first demonstrated by John B. Fenn et al. in 1989 [11, 12] is especially advantageous for proteins with high molecular weight. The inventors of both techniques shared a half of the Nobel prize in Chemistry in 2002 for the development of proteome research technology. More details on these ionization techniques are given in Chapter 4.1. Ion spectra obtained by an MS instrument are then correlated with databases to identify the protein.

There are numerous challenges in the rapidly developing field of proteome analysis, like the limitations of resolution of MS instrumentation required for interpretation of multiple charged biomolecules. Another serious issue is the facilitation of data comparison, exchange, and verification. To address this issue, the Proteomics Standards Initiative (PSI) was founded at the Human Proteome Organization (HUPO) in 2002 [13] in order to define community standards for data representation in proteomics: mass spectrometry and protein-protein interaction data, as well as a standardized general proteomics format.

In the human body, there are 1 to 100 million of different proteins at various abundance. The main requirements for the analytical tools are to be rapid and cheap. The techniques described above have a great potential for high-throughput proteome analyses. However, the automation and high throughput of the traditional techniques is unlikely to be the final solution. The main bottleneck of the field is completely left out of the scheme presented on Figure 1, being the sample preparation issue. This is one of the areas where miniaturized analytical tools for protein processing can be useful due to the low costs, possible integration of various sample preparation steps, short analysis times, and the potential for automation without the need of large quantities of samples.

An example of how microfluidics can reinforce sample pretreatment for MALDI-MS in proteomics is new automated technology introduced in 2004 by Gyros AB (Uppsala, Sweden) [14]. The microfluidic device from Gyros® is based on a compact disc (CD) layout with 96 individual microchannels having modified inner surfaces to ensure controlled sample loading by capillary action. The channel is designed with hydrophobic patches that assure that filling occurs only up to a predetermined point and no further, until the CD is rotated at a speed where enough force is generated to force solutions over hydrophobic regions. For desalting and preconcentration, the sample is first passed through a reversed-phase chromatographic phase. There the analytes are

washed to remove the unwanted components to a waste chamber and then an eluent containing MALDI matrix is used to elute the analytes to open MALDI target areas on the CD. Once the sample is loaded, liquid transport is controlled by varying the speed of the CD rotation. There is no risk of sample losses as the target plate is integrated on the same device. Concentrated crystallized samples are obtained when the analytes elute into the dedicated open areas on the CD.

1.3 Miniaturized systems for protein analysis

A comparison of conventional protein analysis methods from Figure 1 (2D-PAGE, HPLC, ICAT, MudPIT) with miniaturization technologies is given in Table 1. Parameters as peak capacity, typical required sample volume and concentration, analysis time, limit of detection (LOD), automation and integration possibility, are selected to highlight the advantages and disadvantages of miniaturized analytical systems compared to conventional methods.

Table 1. Comparison of conventional protein analysis methods with microfluidics. Limit of detection **(**LOD) refers to the limit of detection of the proteins prior to the identification by mass spectrometry.

	Peak capacity	**Typical sample ammounts**	**time**	**LOD**	**Possibility of full automation / integration**
2D-PAGE	3000-10000 [15]	20 µl with 20 µg/µl [16]	2 days [6]	silver stain : 1 ng [17], Coomassie blue : 8-10 ng [17] Sypro Red: 10^{-12} M [18]	no
LC-LC	2000-3000 [19]	100 µl with 50 µg/µl [16]	96 min [16]	0.35 µg [20]	no
MudPIT	3200 [21]	15 ml urine [22] 100 µg total protein [23]	7- 31 h [9]	only MS detection	no
Protein Microarrays	1340 sampels/cm^2 [24]	10 µl of 16.6 ng/µl protein content for PMA [25]	1.5 h [24]	63 amol/spot [26]	yes
2D Microfluidics	500-1000 [27] 4200 [28]	1 pl of 30-150 µg/µl [27] 5 pl of 1 µg/µl [28]	10 min [27] 15 min [28]	Sypro Orange 16 nM	yes

One of the directions of miniaturization of analytical tools, microarrays, has already revolutionized genomics [29, 30]. Microarray technology is a powerful tool of studying genes interactions and cell's regulatory network. It is a high-throughput automated technique for simultaneously analyzing thousands of different DNA sequences or proteins spotted by a high precision robot on a glass or silicon slide. DNA microarrays are used to monitor changes in the

expression levels of genes in response to changes in environmental conditions or during a disease, by studying the binding of fluorescently pre-labeled DNA from cells of interest to complementary DNA strands pre-immobilized on the slide; fluorescence occurs in the spots where gene activity is present. Protein microarrays are used to study protein expression, protein–protein interactions, and interactions between proteins and other molecules. Microarray technology employs advanced computers and software programs connected to a scanning microscope. Nearly comprehensive lists of literature reviews on microarrays and companies offering gene microarrays, chip-reading systems and related software can be found in [31]. Commercial microarrays have reported sensitivity in a range from 50 fM to 10 pM messenger RNA. Typically, between 20 to 40 million of identical individual molecules must be present in the sample for microarray detection without amplification. Since only RNA and DNA can be amplified, the protein analysis depends upon an assumed correlation between effective concentrations of given proteins and their corresponding mRNA.

Commercially available protein arrays are reviewed in [26]. Microarrays for protein analysis can be subdivided into the protein microarrays (PMA) consisting of the purified recombinant proteins, antibody microarrays (AMA), and the reverse protein microarrays (RPM) containing the whole cell lysate. In all schemes, the binding partners are incubated with the arrayed proteins and the binding is detected. A major advantage of RPMAs is the small sample volume needed (5000 cells/10 μl or 10 μl of sample with 16.6 ng/ μl of a model protein). The main challenge in the protein assay technology is that there are only relatively few specific antibodies available on the market, and they are very costly. The main application of array technology today is the identification of specific proteins and the investigation of enzymatic or binding activities of proteins.

Miniaturized devices for chemical analysis are often referred to as microchip**s.** In microarray technology, definition “microchips” refers not to analytical instrument itself but to the glass or silicon slide with the immobilized sample.

Another direction for miniaturization of analytical tools, which can be applied in fields of genomics and proteomics, is microfluidics. In such devices, all materials are transported in a microchannel network, where reactions, separations and detection can take place. The typical channel dimensions are 5 to 200 μm in width and 150 nm to 200 μm in depth. The analytes are typically moved around valve-less, by pressure or electrochemically (in electrophoretic manner or

by electroosmotic flow). Microfluidics is a technology developing towards the creation of Miniaturized Total Analysis Systems (μTAS), small devices that will perform the functions of large analytical instruments including all steps of sampe pretreatment, chemical reactions, separations and detection. Microfluidic devices are manufactured by techniques adapted from the microelectronic industry for fabrication of electronic integrated circutes (microchips). Microsystems on silicon or glass are typically formed by the exposure of photoresist deposited on respectively silicon or glass followed by chemical etching. For polymeric microsystems, hot embossing, molding and direct laser writing techniques are frequently employed.

A vision for a microfluidic proteomics-on-a-chip device is to sample, separate, detect, and identify the proteome close to the sampling point. The main advantage of miniaturized systems compared to conventional systems for proteomic research (see Table 1) is an opportunity for integration of all analysis steps such as cell sorting, cell lysis, chemical derivatization/digest, extraction/separation, concentration, labeling, and detection, on a single microdevice. This high integration potential is due to the possibility to realize 2-D and even 3-D channel networks on the same chip. Beside the possibility of integration, the size reduction leads to:

- Less reagent consumption and less waste generation results in cheaper cost of a single analysis
- The possibility of mass fabrication of microfluidic devices is economically advantageous compared to traditional analytical instruments
- Improved thermal diffusion, allowing fast heating and cooling of microfluidics. For electrophoretic separations, the fast energy dissipation allows the use of high electric field strengths without occurrence of Joule heating. In turn, this improves the speed and efficiency compared to conventional electrophoretic methods.
- Small dimensions lead to laminar flow profiles
- Faster separation speeds/shorter analysis times.
- Several analyses can be performed in parallel on the same device.

The small channel dimensions as well as lengths scale makes it possible to analyze minute sample volumes with short separation times. An example of the high separation efficiencies that can be obtained on microchips was demonstrated by Culbertson et al. in 2000 where a separation of 19 amino acids was achieved in 165 s with an average plate number of 280000 [32]. The high

separation efficiencies with the short separation lengths are possible mainly because of the narrow, well defined injection volumes with widths typically only 20 - 50 μm.

The first paper about proteomics-on-a-chip was published in 2001 by Figeys [33]. The recent developments in proteomic analysis; available technologies; opinions about elements required for an envisaged proteomics-on-a-chip device; required microfabrication processes, and the integration of the elements into one device are covered in review articles [34-38]. The relevant to this work advances in on-chip protein separations, labeling and preconcentration, as well as the state of the art in coupling microfluidic devices to mass spectrometry, will be given more attention in the introduction parts of the respective chapters below.

The challenge to gain all the benefit of the miniaturized devices is to combine the different steps to provide highly integrated devices. The devices not only have the opportunity to gain high throughput at low cost but may also allow ease of operation as well. The possibility of connecting functionalities together on the same device may allow obtaining real time information about signaling pathways. For example, cells can be brought into contact with a drug, lysed and analyzed all in a time scale of seconds on a miniaturized device.

Presented in this thesis projects (the highly integrated microfluidic system for protein preconcentration, labeling and sizing, the anodic bonding adapted for glass microsystems and the novel design of a monolithically integrated electrospray needle for interfacing microfluidics with the mass spectrometry detection) are all steps towards the ultimate goal of creating a Miniaturized Total Analysis System.

1.4 Outline of the thesis

Chapter two of this thesis is dedicated to the work on integrating microfluidic device for protein preconcentration, labeling and separation. The theory for the on-chip separation methods for proteins, the protein molecular weight determination background, on-chip labeling and preconcentration methods is described. The experimental subchapter gives the experimental details necessary to reproduce the experimental work described in this thesis. In the results and discussion subchapter, the compatibility of different labeling strategies with porous membrane preconcentration is presented and the suitability of the integrated preconcentration and labeling for protein molecular weight determination is demonstrated. Practical challenges and troubleshooting of the microchip operation are discussed.

In Chapter three, the applicability of polysilicon-mediated anodic bonding for glass-to-glass packaging of microsystems is demonstrated. The anodically bonded glass devices were shown compatible with high field strength used for electrophoretic separations.

In Chapter four, an introduction to interfacing microfluidics with mass spectrometry is given. The design and microfabrication procedure of microfluidic system for electrophoretic separations with a monolithically integrated electrospray needle is described. A prototype microfluidic device is presented.

In conclusions Chapter five, the main results for the protein processing microsystem, anodic bonding of glass microsystems and the devices with monolithically integrated electrospray needle are summarized.

In Chapter six, possible applications of the protein processing device, anodic bonding and devices with monolithically integrated electrospray needle are discussed. Future work needed to improve the methods presented in this thesis is also speculated upon.

2 Integrated microfluidic device for protein analysis

In this chapter, the integrated microfluidic device for protein processing is presented. The protein separation, labeling and concentration methods applicable on-chip as well as the background for the molecular weight determination of proteins in gels are reviewed in the introduction subchapter on microfluidic devices for protein analysis. The experimental subchapter describes the design and microfabrication of the integrated device, the chemicals, the experimental setup, and the treatment of the collected data. The operation of the integrated microfluidic device for different labeling schemes with and without on-chip preconcentration is discussed in the results and discussion subchapter, as well as the compatibility of the labeling schemes and preconcentration with the protein molecular weight determination on the presented device. The optimization of microsystem performance (like the direction of pre-injection step) and troubleshooting of the encountered challenges (as for example the protein adhesion to the microchannel walls) are also described in the results and discussion subchapter. The main results are then summarized in the conclusions subchapter.

2.1 Microfluidic devices for protein analysis

This chapter describes protein analysis on microfluidic devices with regard to separation techniques employed on-chip, different labeling procedures to derive protein fluorescent and on-chip protein preconcentration methods. The background for protein molecular weight determination by separations in gels is also given.

2.1.1 Separation of proteins

Protein analysis typically employs electrokinetic separation, chromatographic separation, or a combination of the two. For lab-on-a-chip separations, electrokinetic separation methods are most often employed. Electrokinetic separation is one of the most powerful tools of bio-analytical chemistry, and its applications include DNA and protein separations [39-42]. To control fluid flow in the nL/s range on microfabricated devices, electrokinetic methods [43] and/or pressure can be employed. Using pressure driven flow, both charged and uncharged molecules, as well as cells, can be transported in the channels without separation. Electrokinetic transport in a microfluidic device is generated when electrodes are placed in the reservoirs at each channel end and an electric field is applied (typically in the order of 100-1000 V/cm).

Electrokinetically driven separations include free solution capillary electrophoresis (CE), capillary affinity electrophoresis (CAE), capillary isoelectric focusing (CIEF), capillary isotachophoresis (CITP), capillary electrochromatography (CEC), capillary gel electrophoresis (CGE), and capillary sieving electrophoresis (CSE) (see [44] for detailed definitions). In this work sieving electrophoresis was employed, and its mechanism is discussed in more detail together with gel electrophoresis. The theory of other separation mechanisms is described elsewhere [45-47].

In gel electrophoresis, the analyte molecules migrate in a buffer supported by a matrix material (e.g. agarose or polyacrylamide). The mobility of the analyte is determined by its charge, molecular weight, the pore size of the matrix material and the electric field strength. The pore size of the matrix can be adjusted by the choice of sieving polymer, concentration of sieving matrix and percentage of cross-linking. Sodium dodecyl sulfate assisted polyacrylamide gel electrophoresis (SDS-PAGE) [48] is widely used to separate proteins larger than 10 kDa and determine their molecular weight. A denaturant such as mercaptoethanol is often added to disrupt all disulfide bonds in proteins, so the SDS detergent can bind to all regions of the polypeptide causing additional unraveling, or denaturation of the polypeptide [49]. The negative charge from each SDS molecule (Figure 2) results in SDS-covered proteins that are highly negatively charged with a fairly constant anionic mass-to-charge ratio because SDS overwhelms the variations in charges of the proteins [50, 51]. During the electrophoretic separation the proteins experience approximately the same dragging force because of the similar mass-to-charge ratio (m/z), but they become hindered to different extents with large proteins hindered more than smaller ones [52]. As a result, the relative mobility of each anionic, denatured protein chain is a log function of its molecular weight (MW) in SDS-PAGE [48].

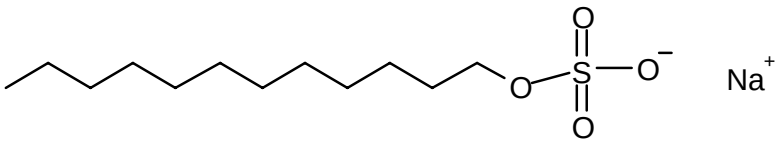

Figure 2. Structure of SDS molecule, chemical formula is $C_{12}H_{25}NaO_4S$.

A disadvantage of transferring SDS-PAGE techniques to the microchip format is the difficulty in handling of cross-linked gels in microchannels. It is challenging to fill out the separation column and, once the gel is cross-linked, it is nearly impossible to replace it when a new analysis is to be performed. This limits the microchip to a single-use device if CGE is employed.

CSE employs the same separation principle as CGE, the only difference is that the polymer matrix used for molecular sieving is not cross-linked and therefore can be easily applied and replaced [49]. The dynamic range for CSE separations is dependant on the polymer chemistry and its concentration and molecular weight. Linear polymers typically used for CSE of proteins are acrylamide, methylcellulose, polyvinyl alcohol, and dextran. Agarose gel forms strong hydrogen bonds and its handling difficulty is in between that of covalent cross-linked polymers and linear polymers. The separation efficiency in CSE can be as high as in CGE.

SDS assisted CSE has many advantages over other electrokinetic separation methods. First, the prediction of mass to charge ratio for each protein is unneeded because SDS binds to the hydrophobic regions of protein molecules in proportion to weight at ratio 1.4 and thus creates a uniform negative surface charge [50, 51]. In SDS assisted CSE, the sample proteins are therefore expected to elute only according to their molecular weight (size) and not dependent on the charge of an individual protein. Smaller proteins sieve through the matrix faster than larger ones, and the protein molecular weight can thus be determined by adding standard molecular weight markers to the sample. The negative surface charges provided by the SDS coating, also force all proteins to migrate in the same direction in the electric field with no regard to the individual pI values. Finally, the solubility of hydrophobic proteins increases when they are coated with SDS, minimizing sedimentation during the concentration step. Hydropathicity (a measure of solubility of the proteins in water) thus does not play a significant role in the SDS-assisted separation. The sieving matrix both serves for the separation and has further an advantage of suppressing the electroosmotic flow and reducing protein interactions with the glass microchannel walls.

The knowledge of protein properties such as isoelectric point (pI), grand average hydropathicity (GRAVY, by Kyte and Doolittle [1]), and mass to charge ratio (m /z) are crucial for selecting and optimizing the separation method(s) (for example, when making a decision on buffer pH value). The pI of a protein is the pH value at which the protein bears no net charge because the concentration of its cation form equals the concentration of its anion form. When a protein molecule is in a solution with a pH value higher than its pI value, it will possess a negative overall charge. Similarly, the overall charge of the protein would be positive if the pH value of the buffer is lower than the pI of the protein. Grand average of hydropathicity index (GRAVY) indicates the solubility of the protein [1]. Hydrophobic proteins possess positive GRAVY values, and hydrophilic molecules have negative hydropathicity scores.

2.1.2 Separation efficiency

The separation efficiency N can be quantified by the observed band broadening. The efficiency is dimensionless and can be determined experimentally from an electropherogram according to Equation 1 [53]:

Equation 1

$$N = 5.54\left(\frac{t_R}{w_{1/2}}\right)^2$$

where t_R is the migration time of the peak and $w_{1/2}$ is the peak width at half of its height, measured in the same units as the migration time.

In order to compare the separation efficiency of channels with different lengths, the efficiency can be expressed as the height equivalent to a theoretical plate (H) [53]:

Equation 2

$$H = \frac{L}{N}$$

where L is the separation length, and H is a distance along the length of the channel equivalent to one theoretical plate. It is also common to refer to the amount of theoretical plates per meter. A typical separation efficiency of conventional high performance liquid chromatography (HPLC) is in the range of 30,000 – 60,000 theoretical plates per meter.

Another important characteristic of separations is the resolution. The resolution for any two neighboring peaks can be calculated from electropherograms according to

Equation 3 [53]:

Equation 3

$$R = 1.177 \cdot \frac{t_b - t_a}{w_{1/2\,a} - w_{1/2\,b}}$$

where t refers to migration time and $w_{1/2}$ to the peak width at half the height in time units for peak a and peak b, respectively.

Increased resolution can be obtained either by minimizing the band broadening from injection, detection, diffusion and analyte–wall interactions, or by improving the difference in analytes mobilities. For most analytical purposes, a resolution value above 1.5 is considered satisfactory.

2.1.3 Protein molecular weight determination in gels

In 1969, Dunker and Rueckert published their “Observations on molecular weight determinations on polyacrylamide gel” [54], where they used internal calibration technique

(molecular weight markers) to construct accurate molecular weight-mobility profiles on polyacrylamide gels. Dunker et al. observed the existence of a critical low molecular weight, below which the small polypeptides would not be separated on a particular gel, and a critical high molecular weight above which the big polypeptides can not penetrate the gel. The working range (dynamic range) for several gel concentrations was determined. Apparent molecular weights determined by PAGE separations generally fell within 5 to 6% of literature values, although a few "anomalous" proteins considerably exceeded this margin of error [54]. Dunker et al. also found that adding SDS minimized the effects of intrinsic molecular charge and conformation on the separations. Apparent free mobilities of SDS-coated proteins are approximately constant, establishing a linear relationship between the log MW and the retardation coefficient (~ 1/t). The retardation coefficient was shown both empirically and theoretically to be a uniform function of molecular weight of protein-SDS complexes in specified working ranges, providing a rationale for determining molecular weight from plots of the negative log MW as a function of migration time.

2.1.4 Optical detection methods

For optical detection of proteins, both ultraviolet (UV) absorbance and laser induced fluorescence (LIF) methods can be employed. UV absorbance measurements do not require derivatization of the analyte and thus have an important advantage over laser-induced fluorescence (LIF) detection. However the sensitivity in absorbance measurements is limited by the short optical path length resulting from small channel dimensions in capillaries and microchips. LIF can be up to 1,000 times more sensitive compared to absorbance detection [55]. To employ UV detection on a chip, it requires that the chip is made out of UV transparent material like quartz, or UV transparent waveguides can be employed [56]. The increased sensitivity and compatibility with microfluidic devices makes LIF the preferred method for on-chip analysis of proteins and peptides. The drawback of LIF is that very few proteins possess a natural fluorophore. Therefore, some labeling procedure is required to render the sample fluorescent.

Fluorescence is caused by the absorption of radiation followed by nearly immediate reemission. Fluorescence ceases almost immediately when the incident radiation stops. The emission will always have a longer wavelength than that of the excitation radiation due to the loss of energy. The shift in the wavelength makes it possible to distinguish between reflected or scattered excitation background and the emitted radiation (fluorescence) by using optical filters and thereby eliminating the background signal noise coming from light source (laser).

The fluorescence of molecules is dependent on their structure and also on environmental factors such as buffer pH, viscosity, temperature, or presence of dissolved oxygen. The compatibility of the selected dye with the buffer components, its pH, and its viscosity should therefore be tested when designing and optimizing a system employing laser induced fluorescence as the detection method.

The laser power is another important parameter which needs to be optimized for the best performance of LIF. Increasing the intensity of the laser beam initially increases the fluorescence signal. However, after reaching an optimum, the fluorescence response decreases due to dye pre-dissociation and dissociation, caused by the high energy absorbed and probably also due to a local temperature increase. Pre-dissociation takes place in large molecules having bonds of lower energy than the energy used for excitation. When the excitation energy is absorbed, an internal conversion of electronic energy to vibration energy may happen, resulting in the rupture of the weak bond instead of fluorescence emission. Dissociation of a dye may take place when the absorbed energy is high enough to excite the electrons of the fluorophore directly to a higher vibration level, resulting in the rupture of the fluorophoric bond itself without internal energy conversion. Together with the loss of fluorescence efficiency due to conversion of some laser energy into the heat, these phenomena are sometimes referred to as “photo bleaching.”

2.1.5 On-chip protein labeling

Laser induced fluorescence for the detection of proteins requires a fluorophore which very few proteins possess naturally. Therefore, derivatization with a fluorescent marker molecule is necessary in order to detect the analytes. Different labeling schemes for proteins compatible with electrokinetic separations have been described in literature [57-62]. The most vital parameter for on-chip labeling of proteins is a fast reaction time between the fluorophore and the analyte. Labeling can be performed by using either covalent or non-covalent derivatization methods.

Covalent fluorescent derivatization often requires an elaborate sample preparation. Covalent labeling reactions typically have long reaction times and require pH and temperature control. Therefore, to employ a covalent labeling method on-chip, a reaction chamber has to be integrated. Unreacted covalent dye often needs to be washed off in order to reduce background level. Washing methods like dialysis or ultrafiltration are very challenging to perform on-chip and thus require derivatization and washing to be done off-chip prior to sample loading. Covalent labeling carries a high probability that molecules of the same analyte will be labeled differently from one another resulting in loss of separation efficiency [50, 63].

Non-covalent protein derivatization methods (reviewed in [64]) require less sample handling and shorter reaction times compared to covalent labeling making non-covalent methods more suitable for on-chip integration. Non-covalent interactions between dye and protein may be of electrostatic, hydrogen bonding and/or hydrophobic nature [64]. F. Welder et al. [65] performed the stability studies of non-covalent dye-protein complexes and concluded that neither hydrophobic nor electrostatic forces alone can form the strong complexes observed. Most likely, the electrostatic interaction between one site of the dye molecule and protein occurs simultaneously with intercalation or hydrophobic interaction on another site. Limits of detections in the nanomolar concentration range have been demonstrated for non-covalent labeling of proteins with fluorogenic dyes (Sypro Red®) in traditional slab gel SDS-PAGE, which is better than the sensitivity using silver staining [18].

As mentioned before high concentrations of detergent are needed to maintain denaturing of the sample molecules during molecular weight determination by SDS-assisted sieving electrophoresis. The denaturing has further the advantage for quantification that the labeling is uniform on the detergent-coated sample molecules and depends on molecular weight in contrast to the variable amount of labels per protein typical for covalent labeling methods [57]. The drawback of labeling in the presence of SDS is that non-covalent fluorogenic dyes, such as Sypro Red®, Sypro Orange®, Sypro Ruby®, Sypro Tangerine®, 5-dodecanoyl amino-, 5-hexadecanoyl amino-, 5-octadecanoyl amino fluorescein bind both to hydrophobic regions of SDS-protein complexes and to SDS micelles, thus resulting in a high background signal [66, 67]. Of special interest to on-chip protein analysis are therefore dyes which can be employed for non-covalent labeling in the presence of a detergent (for example, SDS) above the critical micelle concentration (cmc).

On-chip labeling can be performed in pre-column, on-column, or post-column formats (see Figure 3). Pre-column labeling requires integration of an on-chip reactor where protein derivatization takes place prior to injection and separation. More suitable for on-chip integration are on-column or post-column labeling, since no additional dedicated microfluidic structure is needed for labeling reaction. On-column and post-column labeling schemes require fast reaction times, which can be obtained only with non-covalent labeling.

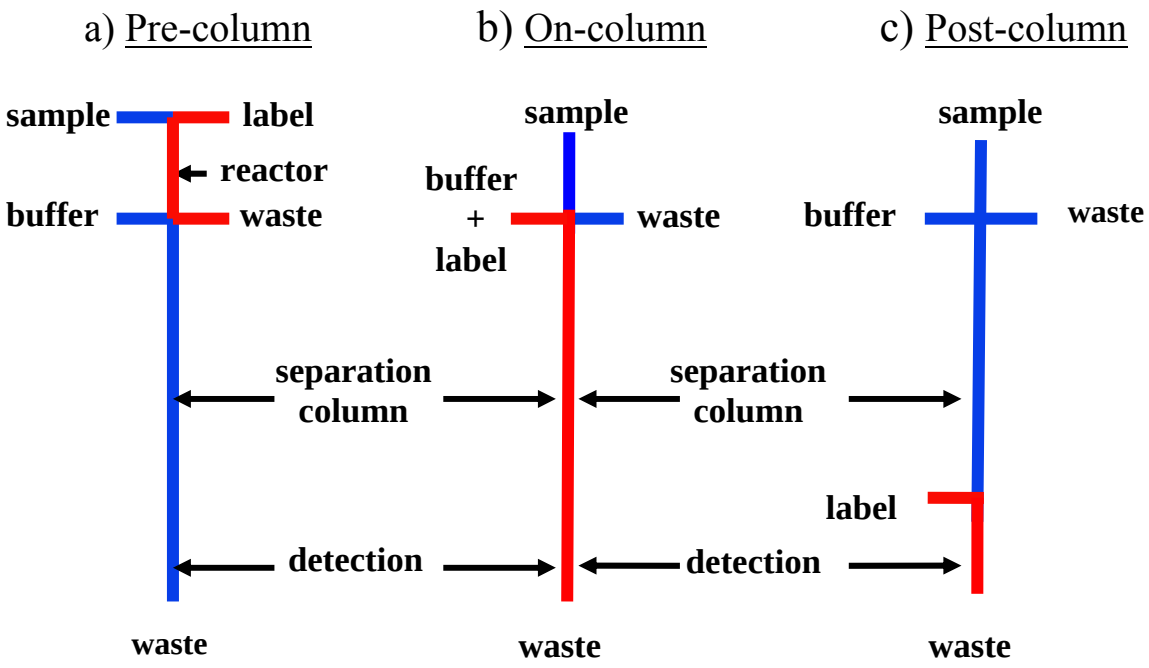

Figure 3. Schematic of different on-chip labeling modes. The solid lines outline the microchannel network. The red lines represent regions were the labeling dye is present in the channels.

Integration of post-column non-covalent labeling (Figure 3c) with on-chip CE has been demonstrated [68-70] by adding a side channel at the end of the separation column in order to electrokinetically introduce the fluorescent dye. Bousse et al. [71] demonstrated that for on-column labeling an increase in analyte signal by an order of magnitude could be obtained by introducing post-separation dilution of SDS content to the below critical micelle concentration, since dissociating micelles reduce the background fluorescence from the dye - SDS complexes. In this thesis, the compatibility of post-column labeling with post-column dilution of micelles in a single step is demonstrated, resulting in separation efficiencies slightly better and sensitivity comparable to the combination of on-column labeling with post-column dilution. For further signal enhancement, compatibility of both the on-chip labeling method with the on-chip preconcentration on a porous filter prior to separation is also successfully demonstrated.

2.1.6 On-chip protein preconcentration

The main challenge in manipulation of very small sample volumes with low concentration analytes is how to obtain a measurable signal. The sensitivity of the detection methods available is one of the main evaluation criteria for all bio-analytical techniques. Detection capabilities of nearly any method can be enhanced by sample concentration. This is where one of the unique features of microsystems, namely, the possibility for integration of different functional units becomes

advantageous. Integration of a sample preconcentration step on a microchip allows analyzing samples with low protein concentrations and is a crucial step towards the development of robust, miniaturized devices for bioanalytical applications.

Operating with both the tiny volumes inherent to electrokinetic injections on microsystems and with low analyte concentrations inherent to most proteomic applications, the situation where not a single molecule of interest would be present for detection (Figure 4) is possible.

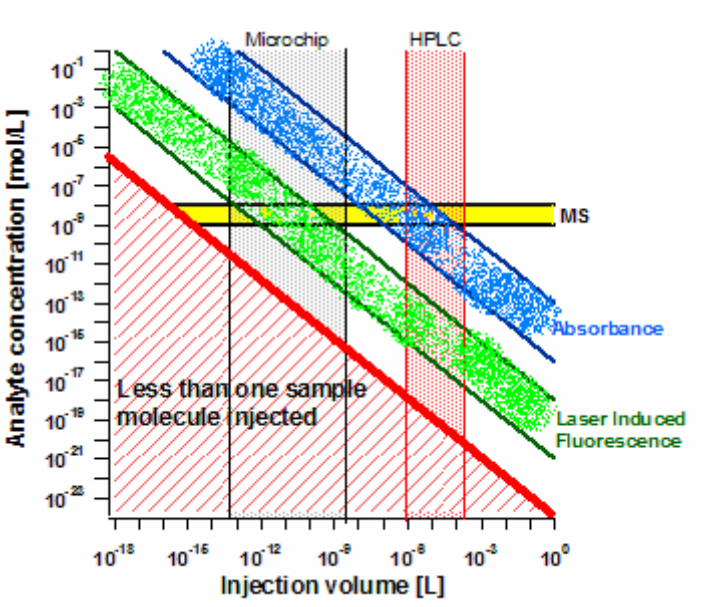

Figure 4. Typical detection limits for different detection modes used for CE [72] as well as typical injections volumes for HPLC and microchip devices.

For microchip injections, a typical volume range is from 0.06 pL to 3 nL (calculated for 25 µm wide channel with depth ranging from 50 nm up to 50 µm and an injection plug length of 50 µm to 2 mm). For comparison, typical injection volumes in High Performance Liquid Chromatography (HPLC) are in the range of 1-200 µL. The concentration level where there is only a single molecule in the injection volume can be calculated according to Equation 4:

Equation 4

$$C = \left(N_a \cdot V\right)^{-1}$$

where C is the molar sample concentration, N_a is the Avogadro constant, and V is the injection volume. For the region below the thick red line, there is in average less than a single sample molecule present for the detection due to too small injection volume or too low concentration. In order to be able to operate with sample volume and concentration in that region, an integrated sample preconcentration step is required.

Labeling of proteins at trace concentrations is also a challenge. Though there are many reports on protein labeling that demonstrate very low limits of detection (LOD), the labeling is often done with an initially high concentration of purified protein and the sample is subsequently diluted to demonstrate good sensitivity. One of the advantages of microfluidics, the extremely low volumes involved, is often exploited to report very low mass detection limits, 10^{-15} (fmol) to 10^{-21} (zmol) range. However, these low mass detection limits are due to the tiny injected volumes and not from low sample concentration, and correspond to 10^{-6} – 10^{-12} M, which is higher than the concentrations in the standard proteome analysis, down to the femtomole (10^{-15}) range.

It is extremely important to emphasize that there is a great difference between labeling a purified sample with a high protein concentration, and labeling trace levels of proteins in a complex biological fluid. The reaction rates for the labeling decrease dramatically at low protein concentrations due to the reduced number of effective collisions with the labeling reagent. A fully integrated on-chip preconcentration method then becomes essential for the microfluidic proteome analysis of native biofluids when using LIF detection.

Field amplified sample stacking (FASS), isoelectric focusing (IEF), isotachophoresis (ITP), preconcentration by solid-phase extraction (SPE), and physical traps (such as membranes or filters) are suitable concentrating methods for on-chip integration with potential further derivatization of protein sample for LIF detection. Field amplified sample stacking (FASS) can be easily integrated with electrophoretic separation techniques [73]. Sample stacking employs a difference in ionic strength between the sample and separation buffers and thereby induces a change in the local field strength between the sample and separation buffers. Providing the field strength in the sample buffer is higher than in the separation buffer (for example, if the sample buffer has a lower concentration than the separation buffer), sample ions get stacked (preconcentrated) when they enter the lower field strength in the separation buffer at the interface between the two buffers. FASS is capable of up to 3 orders of magnitude signal enhancement on-chip [74-80] but to our knowledge has not yet been demonstrated in combination with subsequent protein labeling.

The same is true for isotachophoresis (ITP) where the sample is injected in between a leading electrolyte of higher mobility and a terminating electrolyte of lower mobility as compared to the analyte. The analytes separate into zones determined by their mobilities with the fastest analyte ion moving behind the leading electrolyte in a sharp focused zone. During a single isotachophoresis experiment, it is possible to separate and concentrate either cations or anions but not both at the same time. An on-chip preconcentration of biomolecules by coupling

isotachophoresis with CE was demonstrated with a 50 [81] and a 400 [82] times increase in the detection limit compared to that of CE alone. A practical challenge of ITP is the necessity to initially fill the microchannel with the different buffers.

Solid phase extraction is a powerful method and has been demonstrated on-chip using wall coatings with C_{18} [83, 84] , with polyelectrolyte multilayers [85], polymer monolithic columns [86], or packed columns: polystyrene beads [87], nanoporous silica beads [88], and octadecylsilane (ODS) beads [89, 90]. Packing a microfluidic channel is a challenge for solid phase extraction methods. The elution of hydrophobically or electrostatically absorbed analyte also requires a buffer change. Approaches to on-chip sample preconcentration by adsorption that do not require a buffer change include the film electrode method where an analyte is captured and released electrostatically by changing the electric potential on the electrode [91]. Analytes can be absorbed and later released on surfaces that are temperature- and electric potential- sensitive [92], where binding and elution of analytes is controlled by surface modification caused by changing temperature or potential. The complicated microfabrication and chemistry of these approaches do not yet allow for their commercialization.

A completely different approach to an on-chip preconcentrator is to concentrate analytes directly at the injection intersection at the beginning of the separation column by using an integrated filter. A spin-on silicate filter [93, 94], a PDMS membrane [95], or a zwitterionic polymer membrane [96] has been demonstrated for the concentration of analytes on microfluidic devices. Electrophoretic preconcentration of the analyte on a physical filter/membrane is achieved by applying an electrical potential between a sample reservoir and a reservoir across the membrane/filter. Whereas the pore size of such a membrane or filter is large enough for small buffer ions to carry the current through the membrane, large biomolecules will accumulate in the area adjacent to the membrane/filter surface. Thus no separate release or elution buffer is needed and injection of the preconcentrated analyte is performed by simply removing the potential across the membrane/filter and applying the field strength in the separation column. Coupling of the preconcentration on porous membrane (salt bridge) coupled with injection, separation, on-chip labeling and dilution for background reduction steps is presented in experimental section below.

2.2 Protein Analysis: Experimental

In this subchapter, the layout of an integrated microsystem for preconcentration, labeling, separation and postcolumn dilution/destaining of proteins is presented. The microfabrication of this

integrated microsystem is discussed, with a separate subchapter focused on the porous preconcentrator formation. The comprehensive description of all chemicals used for the experiments follows. The subchapter for the experimental setup describes the configuration of the optical components used for the laser induced fluorescence detection, how the liquid flow control was done electrokinetically, and how the microsystem was interfaced to the world, giving details on reservoirs loading and on electrodes placement. The last subchapter is describing details of data treatment after the signal collection.

2.2.1 Layout of microsystem

A schematic of an integrated microchip for protein preconcentration, separation, and labeling is presented in Figure 5. The length of separation channel measured from preconcentrator to the dilution intersection was 6 cm. The run buffer is loaded in reservoirs 1, 2 (serves as a sample waste reservoir using the double T injections), reservoirs 4 (located on the other side of the preconcentrator structure) and 6 (serves as a waste collector during the separation, labeling, dilution and detection). Protein sample is loaded into reservoir 3. The dilution buffer is loaded into both reservoirs 5. For experiments with simultaneous dilution and post-column labeling, the dilution buffer would contain the dye. For on-column labeling, the dye was added to the run buffer prior to loading the microsystem.

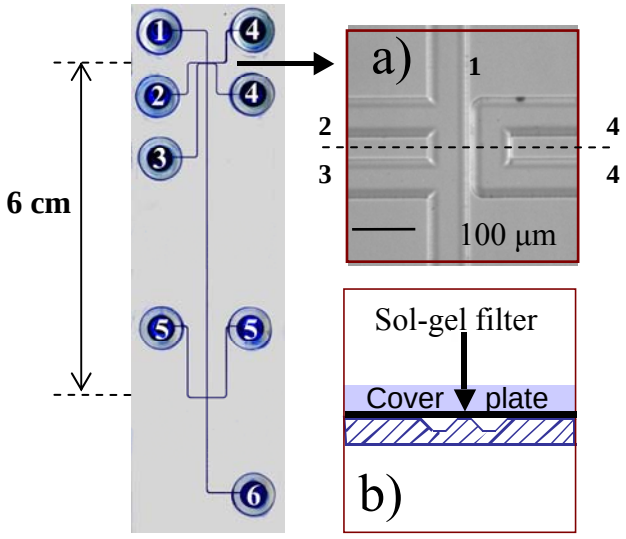

Figure 5. A schematic of microfluidic device for protein analysis is presented. Reservoirs: 1) run buffer; 2) sample waste; 3) sample; 4) pre-concentrator reservoirs, bridged with platinum wire; 5) dilution reservoirs, bridged with platinum wire; 6) waste. Insert **(a)** shows a close-up image of the preconcentrator area. Insertion **(b)** shows the cross section of the chip along the dashed line on insertion (a), not to scale. The thickness of the sol-gel layer presented by a solid black line in (b) is less than 100 nm, the width of the salt bridge (the distance between two adjacent microchannel networks) was in the range of 5 to 10 µm.

The insertion a) in Figure 5 shows a microscope image of preconcentrator area. The width of the channels is approximately 50 μm, the width of the preconcentration filter defined by the spacing between two adjacent microchannel networks (separation and preconcentrator part) is in the range from 5 to 10 μm. The insertion (b) shows a cross-sectional view of the preconcentrator along the dashed line on the insertion (a). The sketch of the insertion (b) is not to scale, it illustrates the substrate wafer where two adjacent trapezoid-shaped channels can be seen separated by the preconcentrator. The solid black line between cover plate and the substrate wafer represents the porous silicate layer with thickness of typically 30 nm.

2.2.2 Fabrication of microsystem

The application of high electrical potentials (typically up to 10 kV) restricts the choice of materials for fabricating such microsystems. Glass is a very suitable material for electrokinetic based microchips due to its electrical insulating properties [97]. Fused silica is the glass type most frequently employed in conventional capillary electrophoresis. Fused silica has the same composition as quartz but is isotropic. Fused silica is a hard material with a very low expansion coefficient. Another frequently employed glass type for microsystems is Borofloat®, which got its' name due to containing boric oxide and being formed by a special float process. The dope of boric oxide provides high chemical resistance to harsh pH compared to that of fused silica, and the float process results in superior surface finish and flatness as compared to other methods such as drawing and casting. In addition to the good electric insulating properties of glass, glass–analytes interactions are well studied and understood in conventional capillary electrophoresis and chromatographic applications where an abundance of coating protocols exists for practically any analytes type to prevent adhesion to the channel wall. Other advantages of using glass are its chemical stability, especially resistance to organic solvents compared to that of polymer materials, and mechanical stability compared to that of silicon.

Microchips were fabricated in White Crown® glass purchased pre-coated with low reflective chrome and photoresist 1518 (Telic, Santa Monica, CA, USA) using standard photolithography and wet chemical etching methods. Access holes to the channels were ultrasonically drilled (Sonic-Mill, Albuquerque, NM, USA) in the substrate with the etched channels. A closed channel network was then formed by low-temperature bonding of a glass cover plate to the etched substrate, assisted by a thin layer of potassium silicate (KASIL 2130, The PQ Corp., Valley Forge, PA, USA). The potassium silicate solution was diluted to a final concentration of 0.1 M and spun on the cover plate

at 3500 rpm for 7 s. Immediately after the spinning of silicate layer the substrate and cover plate were brought into contact and pressed together. The devices were annealed at 200 °C overnight to assist dehydration and siloxane bond formation and thereby "curing" the bond. The silicate layer functioned both as an adhesive and also formed a porous salt bridge for sample pre-concentration [93]. Cylindrical glass reservoirs were affixed with Norland optical adhesive 68 (Norland Products, Inc., Cranbury, NJ, USA).

The width of the porous membrane for preconcentration (the distance between two separate channel networks) was 5-10 μm. The channels were 14 - 16 μm deep and 47 - 51 μm wide at half depth. Dimensions were measured before bonding using a stylus-based surface profiler (P-10; Tencor, Mountain View, CA, USA). The length of the separation channel (from preconcentrator/injector to the dilution intersection) was 60 mm (see Figure 5). The length of the preconcentration cell was 100 μm measured between the centres of the sample and sample waste channels at their intersection with the separation channel.

2.2.3 Chemicals

A mixture of seven proteins (Dalton Mark VII-L for SDS gel-electrophoresis, Sigma, Saint Louis, MO, USA) was chosen as a model sample due to its commercial availability, known molecular weights and the existing sequence information for the individual proteins (see appendix 8.2 for the aminoacid sequences, which were used for theoretically estimating the pI and hydrophobicity values of the proteins as well as their mass to charge ratios presented in Table 3 on page 73). The Dalton Mark VII was considered to be a proper and representative model sample for our proof of the concept experiments since the calculated properties of Dalton Mark VII proteins represent a variety in pI values, hydrophobicity, molecular weight and overall charge-over-mass ratios at the pH = 8.3 of the separation buffer used. Molecular weights for Dalton Mark VII proteins are 14.2 kDa for α-Lactalbumin; 20.1 kDa for Trypsin inhibitor; 24 kDa for Trypsinogen; 29 kDa for Carbonic anhydrase; 36 kDa for Glyceraldehyde-3phosphate dehydrogenase, 45 kDa for Ovalbumin and 66 kDa for Bovine serum albumin. Dalton Mark VII protein sample was prepared in sample buffer BioRad CE-SDS Protein Sample Buffer (catalog number #1485033, Protein Kit 1870, Biorad Laboratories, Hercules, CA, USA). BioRad CE-SDS protein run buffer (catalog No.148-5032, the sieving range of 14-200 kDa, Protein Kit 1870, Biorad Laboratories, Hercules, CA, USA) was used for the separations. For on-column protein labeling, Sypro Orange® (472 nm excitation / 572 nm emission) or Sypro Red® (548 nm excitation / 628 nm emission) dyes

(Molecular Probes, Eugene, Oregon, USA, now Invitrogen) were added to the run buffer to the final concentration of 1x recommended by manufacturer for the gel staining of proteins. Information about formula, molecular weight and concentration of these commercial dyes is considered proprietary and is not available from manufacturer. Both dyes have initial 5000x "recommended" concentration in dimethyl sulfoxide (DMSO). "Recommended" refers to the concentration obtained by an optimization procedure performed by manufacturer for staining of proteins in conventional 2D gel electrophoresis and the actual concentration (M or mg/ml) is not available.

For commercially available protein sieving buffers, the information on polymer chemistry and concentration is often kept secret and is not available. The proprietary information is typically crucial information needed for innovation and optimization steps during the research process. The ideal dilution/postcolumn labeling buffer for our experiments would have been the exact composition of the BioRad CE-SDS Protein Run Buffer used for the separation but without SDS. Such a product could neither been obtained from the company nor prepared ourselves without the knowledge of the gel composition in the separation media.

From the material safety data sheets (MSDS) of the BioRad® run buffer for sieving electrophoresis of proteins, the composition is supposedly 400 mM Tris borate buffer containing 8.7 mM SDS and an unknown concentration of dextran serves as the sieving matrix. Therefore, after the BioRad buffer was considered the most suitable for the planned experiments, the dilution buffer was prepared to match the run buffer composition as close as possible minus SDS and sieving matrix. Dilution buffer consisting of 400 mM Tris borate buffer, pH = 8.3 was prepared by dissolving Trizma base (Sigma, St. Louis, LO, USA) and boric acid (Sigma, St. Louis, LO, USA) in deionized water. For post-column labeling, Sypro Orange® and Sypro Red® dyes were added to the dilution buffer to the final concentration of 10x and 100x of the concentration recommended by manufacturer. The Sypro dyes are commercially available at concentration of 5000x, where x is a "recommended" concentration not available to the author of this thesis. So the dye concentrations of 1x, 10x and 100x were obtained by diluting the dye solution from manufacturer 5000, 500 or 50 times respectively with the run buffer or dilution buffer depending on the labeling scheme.

2.2.4 Coating of microchannels

In this subchapter, the procedures for coating the microfluidic devices in order to prevent protein adhesion are described.

Preparation of linear polyacrylamide (LPA) solution

Reagents for 4% acrylamide solution (~15 ml):

- 0.6 g dimethyl acrylamide
- 14.4 ml of H_2O
- 37.5 µl of freshly prepared 10 % w/v ammonium persulfate in 0.5 x TBE (0.0445 M Tris base, 0.0445 M boric acid, and 10 mM EDTA, pH ~ 8.3)
- 22.5 µl of tetramethylethylenediamine (TEMED)

Procedure:

1. Prepare solution by mixing above mentioned reagents
2. Polymerize overnight
3. Precipitate the polymer in 2 volume parts of ethanol (~ 30 ml)
4. Rinse two times with ethanol using approximately the same volume as in step 3
5. Decant ethanol; let precipitate dry under vacuum to remove ethanol
6. Re-dissolve in H_2O, up to 15 ml total volume
7. Precipitation can be repeated for further purification if desired
8. Store at the room temperature covered with aluminum foil (solution is light-sensitive).

Acrylamide coating of glass channels:

1. Rinse channels with 0.1 N NaOH for 5 min with vacuum applied at each reservoir one at a time
2. Rinse channels with H_2O for at least 5 min with vacuum on each reservoir
3. Rinse channels for 30 min with 1% v/v MAPTOS (3-methacryloxypropyltrimethoxysilane) solution in H_2O with 0.4% acetic acid (pH~3.4)
4. Rinse channels with H_2O for 2 hours
5. Rinse channels with 4% acrylamide solution prepared according to the recipe above for 2 hours (or alternately, leave acrylamide solution in chip overnight; wrap chip to prevent evaporation)
6. Rinse with H_2O

Protocol for poly dimethyl siloxane (PDMS)/Pluronic® coating of glass channels:

1. Rinse channels with 0.1 N NaOH, vacuum applied for 5 min at each reservoir, one at a time.
2. Rinse channels with H_2O with vacuum at each reservoir for at least 5 min.
3. Rinse channels for 5 min on each reservoir with 20 % v/v PDMS (Sylgard, Dow Corning, Midland, MI, USA) in hexane.

4. Rinse channels with hexane for 10 min to remove excess PDMS.
5. Cure chip overnight at 65 °C.
6. Before every set of experiments, apply 30 % v/v solution of Pluronic® polymer F-127 (Sigma, St. Louis, MO) in H_2O for 20 min. Pluronic F-127 is a polyethylene oxide-polypropylene oxide-polyethylene oxide (PEO-PPO-PEO) block copolymer. Important: this Pluronic solution is only liquid at low temperatures, at room temperature it is a viscous gel. Therefore, solution should be chilled on ice before applying, and microchip should also be cooled while coating.
7. Rinse channels with DI water (1 - 5 ºC), for 5 min on each reservoir. With a longer wash, the pluronic coating will be removed from the PDMS coating.

2.2.5 Experimental setup

In this subchapter, the configuration of the optical components for dye excitation and the collection and filtering of the resulting fluorescent signal is described. Then, the description of the liquid flow control on the microsystems is given. Finally, this subchapter describes how the microfluidic systems were conditioned before loading the reservoirs with respective solutions. The electrode placement and a microsystem holder are described.

Configuration of the optic components

A sketch of the optical part of the experimental setup is presented in Figure 6. Different lasers have been coupled to this setup, depending on the optimal excitation wavelength for the labeling dyes. An Argon ion laser (Melles Griot, Carlsbad, CA, USA) was used for the excitation of Sypro Orange® dye at 488 nm. A Helium-Neon laser (Melles Griot, Carlsbad, CA, USA) was used for the excitation of Sypro Red® dye at 543 nm. Signal acquisition from the photo multiplier tube (Oriel 71260, Stratford, CT, USA) was controlled by a custom LabView® (National Instruments, Austin, TX, USA) program, created in J. Michael Ramsey's group.

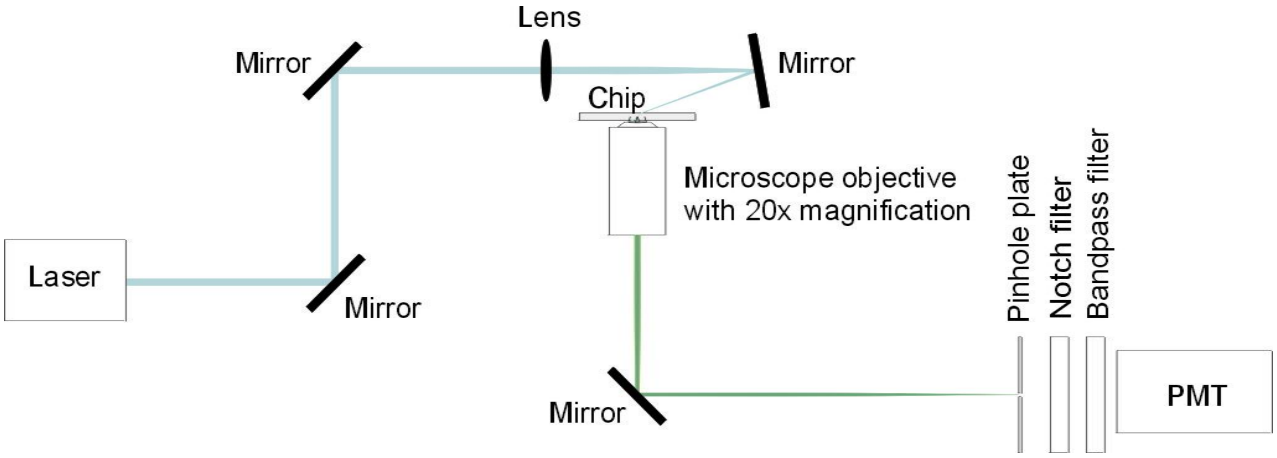

Figure 6. Configuration of the optic setup used for laser excitation and collecting the fluorescence response. After focusing the laser beam on the detection spot within the microchannel, the fluorescent signal was filtered and detected using a photomultiplier tube (PMT).

Suitable notch filters were used for each laser wavelength. The band pass filter was selected according to the emission spectra of the dye used in a specific experiment. The size of the pinhole in front of the photomultiplier tube (PMT) was 1000 μm in diameter. This pinhole size corresponded to a detection point in the micro channel having a diameter of 50 μm (approximately the channel width at half-depth), since the magnification of the microscope objective used for the collection of fluorescence signal was 20x. This was considering the optimal detection point size since the width of the detection channel was around 50 μm at half-depth.

Liquid flow control

All flows on the microchip were generated and controlled by electrokinetic means. A high voltage power supply built in-house had five independently controlled outputs each capable of delivering up to 4 kV. The integrated microchip for protein analysis (Figure 5) however had eight reservoirs, making it necessary to bridge reservoirs that could be operated with the same electrical potentials. Bridging was done between the two preconcentrator reservoirs and two dilution reservoirs (numbered 4 and 5 respectively, see Figure 5) by connecting the reservoirs with platinum wire. An electrode was then inserted in only one of the bridged reservoirs. For calculating the field strengths in the different channel segments it was assumed that the difference in the electrical potentials between such a pair of bridged reservoirs was negligible.

A specific feature of the experimental setup used for this research was a high voltage relay for each electrode. Both the high voltage power supply and the relay box were controlled by a

custom LabView® (National Instruments, Austin, TX, USA) program written in J. Michael Ramsey's group. The advantage of incorporating the relay into the circuit was the possibility of floating any electrode (by opening the relay) at any step. Without an incorporated relay system, the electric potentials would have to be optimized and controlled very precisely, even in the parts of the chip not involved in a given step, in order to prevent unwanted liquid flow. With any change of experimental conditions (partial clogging of the channel network, change of conductivity due to sample adhesion to the walls, slight variations in the channel dimensions from chip to chip, etc.), the flow balance may change. Even a very small flow rate in the wrong direction (or where no flow should be created) can be very undesirable, especially during the relatively long pre-injection step (5 min). The use of the relay box made the flow control more robust.

Microchip-to-world interface

This subchapter briefly describes how the reservoirs for liquids were affixed and filled, how the microsystem conditioning was performed prior to each set of experiments, and how the electrodes and the microchip positions were secured.

The liquid reservoirs for the microsystems were 8 mm short pieces of glass tube with an internal diameter of 3 mm. The reservoirs were affixed to the microfluidic devices using Norland optical adhesive 61 (NOA 61) from Norland, Cranbury, NJ. The glue was cured by ultraviolet light.

For a new microfluidic device, the conditioning of the microchannel walls was done by washing with 0.1 N solution of sodium hydroxide (NaOH). Higher concentration of NaOH typically used for conditioning of microchannels for other applications was proved to be harmful to the silicate preconcentrator and thus is not recommended for conditioning of silicate-bonded microsystems. After filling the whole microsystem channel network with 0.1 M NaOH, a negative pressure (vacuum line) was applied for 5 minutes on each reservoir, one at a time, in order to secure the flow of NaOH within every microchannel segment for at least these 5 minutes. Then, the reservoirs were emptied and the microchannels were filled with deionized (DI) water, then emptied and refilled with DI water again. The flow of DI water for at least 5 minutes in each channel segment was obtained by applying the vacuum on the respective reservoirs. Before loading the chemicals into the microchannels for subsequent coating of channel walls, the reservoirs and channels had been completely emptied by applying the vacuum line to the empty reservoirs.

After the end of experimental work of the day, the microsystems were emptied for sample and buffers and washed with 87 mM solution of SDS in DI water to remove all leftovers of sieving

gel buffer and any precipitated proteins. Then the microsystem was flushed out with DI water, repeatedly emptying and refilling all reservoirs after 5 min vacuum applied on each reservoir, one at a time. The microfluidic system was stored overnight in DI water. The permanently coated microsystems with acrylamide or PDMS were only flushed with SDS solution, because the NaOH solution would damage the coating.

In order to maintain the same hydrostatic pressure (equal liquid levels in reservoirs) and thus avoid a hydrodynamic flow, reservoirs with the same internal diameter were used, and equal volumes of liquids (typically 65 µl) were pipeted into the reservoirs, to assure equal height of the liquids in reservoirs. The high viscosity of the dextran-containing sieving buffer from BioRad also minimized the hydrodynamic siphoning further. For focusing the objective used for fluorescence signal collection and also for aligning the microchannel detection window with the laser beam, a microchip holder was attached to an X-Y-Z stage with micrometer positioning (Newport, Irvine, CA, USA). The chip holder had two perpendicular grooves thus allowing two possible positions for the microsystem in the holder. Depending on the selected groove for positioning the chip, an incoming laser beam could be focused either across or along the microchannel.

To avoid electrical shock and shortcuts and in order to ensure the correct electric potential outputs while operating a microsystem, a holder for electrodes (Figure 7) was designed. Vertical holes were used to insert the electrodes, and tapped holes from the sides were used to fix electrodes in place with polymer screws. The holder was designed mostly for safety reasons, enclosing the exposed ends of the electrodes, and also to facilitate service procedures like cleaning and testing. It further acted as a lid for individual reservoirs, preventing the introduction of the air born particles and reduced evaporation. The suitable material for the holder is any chemically resistive polymer with optical transparency, for convenience. For the experiments presented in this thesis the electrode holder was manufactured in polycarbonate.

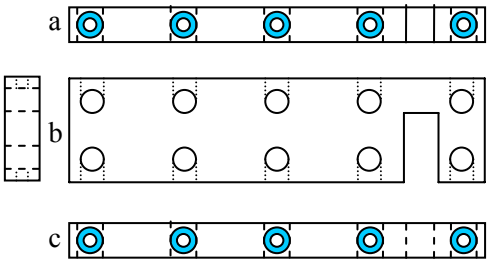

Figure 7. Projections of the designed electrode holder. The top view b) shows the non-tapped wholes for electrodes and the window for laser alignment; side views a) and c) show position of tapped holes for plastic screws to fix the electrodes in place. Tapped holes are marked with the blue doughnuts.

By standardizing the reservoir positioning on the microsystem during the design step of different photomasks, the same electrode holder could be used for all microsystems. The holder had ten holes for electrodes allowing for reconfiguration of the electrodes positions according to the actual layout for a particular experiment. The stability of the chip position in the experimental setup was secured by affixing the electrode holder to the XYZ stage holding the chip.

For analyses without preconcentration, injections were performed using the volume defined injection with a pre-run for 5 min, where the field strength of 750 V/cm between the sample (reservoir 3) and sample waste (reservoir 2) was maintained. Potential of 1.2 kV was applied at sample waste reservoir 2 and potential of 0.2 kV was applied at the run buffer reservoir 1 in order to prevent sample introduction into the run buffer reservoir during the pre-run step. All other electrodes were floated during this pre-run step. After 5 min of pre-injection, a potential of 3.1 kV was applied at the waste (reservoir 6), while run buffer electrode (reservoir 1) was grounded. Potentials of 0.3 kV were kept on reservoirs 2 and 3 in order to retract not injected sample molecules toward sample and sample waste reservoirs and thus to prevent leakage of sample into the separation channel after injection (see Figure 27, right). By varying the potential applied to the dilution buffer reservoirs (5) different dilution ratios (DR) were obtained.

2.2.6 Data treatment

All data analysis was performed in Igor Pro® (WaveMetrics, Lake Oswego, OR, USA). Between the collection of the signal from the PMT and the reporting of results there are processes of numerical calculations, some of which may involve averaging or smoothing the measured values. Decisions as to the experimental design, equipment and degree of effort in the data analysis all affect the desired quality of the analysis.

To give a realistic estimate of the uncertainty in a result, it is important that raw data is manipulated and reported correctly. The uncertainty in a result can be categorized into random errors and systematic errors. Since all data manipulations were done manually using Igor Pro® we only kept track of significant figures, without propagation-of-error methods used for more complicated calculations.

The purpose of the project was to demonstrate a highly integrated microfluidic device with good sensitivity, where for the first time the on-chip concentration is shown to be compatible with on-chip labeling and sizing. The main goal for our project was therefore to perform proof of the

concept experiments rather than collecting statistical information. The fabrication and optimization of the devices involved a high degree in chip-to-chip variations in for example length of channel segments due to variations in the placement of the access through holes (done manually by ultrasonic milling or powder blasting), quality of porous bridge for preconcentration due to the lab conditions as humidity and the temperature (see the subchapter 2.3.11 on page 80 for the troubleshooting on the porous preconcentrator performance). The electropherogram would typically only be reproduced once, to make sure that the detected signal was not an artifact. This was since only a limited number of devices were available for the experiments and the microdevices would get irreversibly clogged and wasted after typically two days of experimental work. For the best performance, a microsystem had to be rinsed and reloaded after approximately 1 hour of operation (4 to 6 separations). Only for the most optimal performances in a set of experiments the run was reproduced enough times to calculate the standard deviation and introduce the error bars to the graph. For many of the graphs representing optimization process error bars have been omitted, since experiments only were repeated/reproduced for the optimized experimental conditions.

2.3 Protein Analysis: Results and discussion

In this chapter, results for the different labeling strategies combined with preconcentration, separation and molecular weight determination are presented and discussed. Post-column labeling method combined with post-column dilution are presented and compared with results for on-column labeling combined with post column dilution. Separations showing compatibility of either labeling mode with on-chip preconcentration using a porous bridge is also demonstrated. The challenges of preventing protein adhesion to channel walls after the dilution intersection are discussed. The chemistry of the solid porous silicates is described in order to explain device-to-device variations in the performance of preconcentrator and a solution to improve the chip to chip reproducibility of the preconcentrator is suggested. Novel ways to create on-chip protein preconcentration are suggested as an alternative to the porous bridge preconcentrator.

2.3.1 On-chip labeling

Sypro Red® and Sypro Orange® dyes were selected for labeling the model proteins due to the commercial availability, ease of use, high sensitivity and suitable excitation maxima (548 nm for Sypro Red® and 472 nm for Sypro Orange® dye). The tunable argon ion laser used in the

experimental setup was capable of providing the emission at wavelength of 488 nm and 514 nm. The optimal excitation wavelength for Sypro Red® dye is however 548 nm which required the use of a different laser. The influence on sensitivity when using 488 and 514 nm as the excitation wavelength instead of 548 nm for Sypro Red® were estimated by recording fluorescence spectra of 1x concentration of Sypro Red® dye dissolved in the run buffer consisting of 50 mM Tris base, 10 mM boric acid, 8.7 mM SDS and 3% linear polyacrylamide, using respectively 488, 514 and 548 nm as the excitation wavelengths (Figure 8) using a spectrophotometer (Perkin-Elmer model 650-10, Wellesley, MA, USA). It is seen from Figure 8 that the gain in fluorescence response by using 514 nm excitation instead of 488 nm was 57 % and the gain in signal by using the optimal 548 nm compared to 514 nm was only 17 %. Since both Sypro® dyes are fluorogenic (possessing little fluorescence when free in the solution but giving a strong emission signal upon binding with a protein or an SDS micelle), the same experiments were performed with 100 nM ovalbumin protein added to the dye solution. The signal was enhanced in the presence of the protein by 7.9 % for 514 nm and 7.6 % for 548 nm wavelengths, as presented by dotted lines on Figure 8. It was concluded that the argon ion laser in experimental setup would be compatible with the Sypro Red dye without significantly reducing the sensitivity.

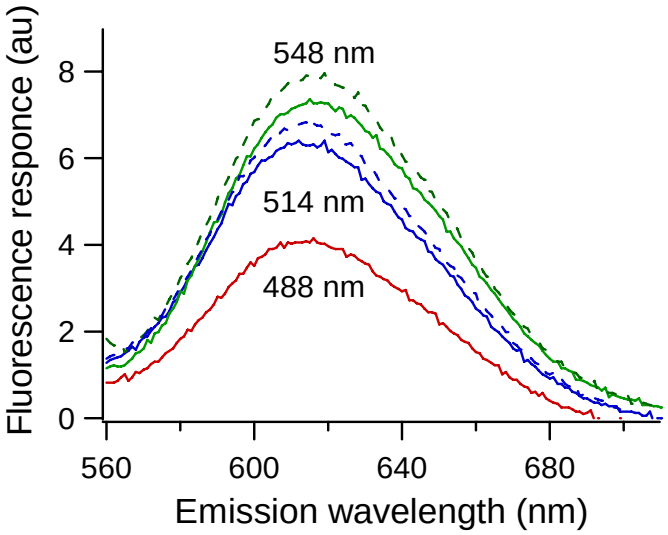

Figure 8. Emission spectra of 1x concentration Sypro Red® dye in separation media containing 50 mM Tris base, 10 mM boric acid, 8.7 mM SDS and 3% linear polyacrylamide, obtained using excitation wavelengths as indicated on the graph. The dotted lines above spectra for 514 and 548 nm demonstrate the increase of the fluorescence response with 100 nM ovalbumin present in the sample.

The similar emission spectra for 1x concentration Sypro Orange® dye in 50 mM Tris, 10 mM boric acid, 8.7 % SDS and 3 % LPA was recorded using using the 488 nm excitation wavelength (very close to 472 nm, the maximum excitation wavelength and the same gain settings

on spectrophotometer as in experiment with Sypro Red®. The fluorescence response of Sypro Orange® without protein present in the buffer was 20 times higher than that of Sypro Red® at 514 nm. This indicates that Sypro Orange® would create a significantly higher background signal in the microsystem from the dye itself compared to Sypro Red®. However, in the presence of an identical protein sample (100 nM ovalbumin), the signal enhancement using Sypro Orange® dye was more than twice that of Sypro Red®, giving an overall better signal-to-noise ratio and better limits of detection than Sypro Red® dye for the 100 nm ovalbumin sample. A dilution step just before the detection point was expected to reduce the high background level of Sypro Orange® bound to micelles and thus further improve the S/N of the proteins. Both dyes were considered suitable for testing on-chip. On-chip labeling of proteins followed by postcolumn dilution with each dye was performed to compare the experimentally obtained S/N and LOD.

2.3.2 Dilution buffer troubleshooting

Problems due to unknown buffer components were encountered when attempting to prepare optimal dilution buffers. As an example, a polymerization reaction at the dilution intersection occurred when using a self-prepared dilution buffer in combination with a protein sieving media from Beckman (Beckman Coulter, Inc., Fullerton, CA, USA).

Also post column dilution with buffer without sieving matrix and SDS could result in protein precipitation downstream after the dilution intersection. All microsystems for postcolumn dilution had to be coated to prevent/minimize this problem. There is a possibility for an improvement of the system performance by using the dilution buffer with composition of run buffer minus SDS. It was not possible to obtain such a buffer from BioRad; therefore an attempt to compose our own sieving media with known composition was undertaken. An example of a separation using a sieving buffer consisting of 50 mM Tris base, 10 mM boric acid, 8.7 mM SDS and 3% linear polyacrylamide (prepared and purified according to recipe in Appendix 2.2.4 on page 35) is presented in Figure 9.

The on-column labeling of a Dalton Mark VII protein sample was performed by adding 1x concentration of the Sypro Orange® dye to the prepared run buffer. The dilution buffer contained 50 mM Tris base, 10 mM boric acid, and 3% linear acrylamide. Shorter migration times and poorer separation of all proteins were observed compared to separations performed under the same conditions using the BioRad buffer.

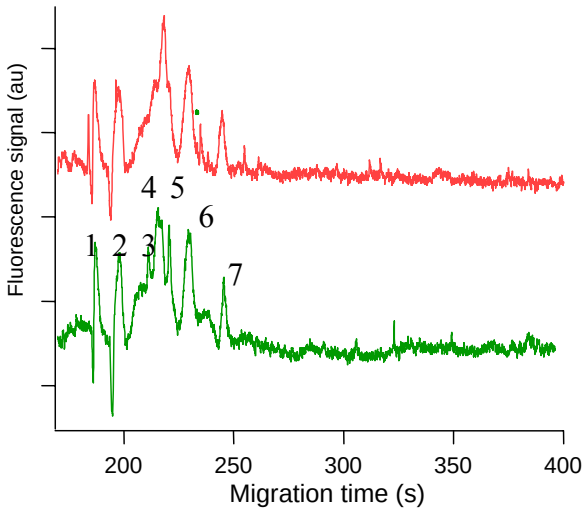

Figure 9. Separations with on-column labeling with 1x Sypro Orange® using the self-prepared separation buffer. Separation buffer composition: 50 mM Tris base, 10 mM boric acid, 8.7 mM SDS and 3 % linear acrylamide, 1x Sypro Orange®. Dilution buffer compostiton: 50 mM Tris base, 10 mM boric acid and 3 % linear acrylamide. Two electropherograms of Dalton Mark VII proteins performed under identical conditions and offset for visual clarity; the potential on both dilution reservoirs was 0.7 kV corresponding to the dilution ratio of 4.7. The detected peaks are: 1) α-Lactalbumin (9.5 μM); 2) Trypsin inhibitor (6.5 μM); 3) Trypsinogen (8 μM); 4) Carbonic anhydrase (4.65 μM); 5) Glyceraldehyde-3phosphate dehydrogenase (3.75 μM); 6) Ovalbumin (3 μM); 7) Bovine serum albumin (2.05 μM).

The shorter separation time and poorer resolution of peaks 3-5 in the middle of electropherograms suggest that the concentration and/or molecular weight of the linear polymer in our buffer was much lower than in the Bio Rad buffer. BioRad buffer was selected as the sieving matrix for the experiments presented in this thesis due to its superior separation performance. The most optimal dilution buffer tested with the BioRad CE-SDS was 400 mM Tris Borate buffer pH = 8.3 (see Figure 15 for a separation example).

2.3.3 Sample loading

This subchapter describes how the time of sample loading (also sometimes referred to as pre-run or pre-injection step) was optimized, how the loading direction has been changed in order to prevent sample molecules from entering the separation channel before the injection,

Optimizing the loading time

In order to investigate the influence of sample loading time on the signal intensity without using the preconcentrator, double-T injections (also called volume defined injections, [98]) of a fluorescein pre-labeled ovalbumin were performed with different pre-run times (Figure 10). Protein was pre-labeled off-chip to avoid influences from different injection times on the labeling and the

resulting signal. A potential difference of 1 kV was applied in between reservoirs 2 (0 kV) and 3 (1 kV) (see Figure 5) during the pre-run for all injections. All the channels were initially filled with the self prepared run buffer consisting of 50 mM Tris base, 10 mM boric acid, 3% polyacrylamide, 8.7 mM SDS. Fluorescein-conjugated protein sample with the concentration of 1 µM in run buffer was loaded into the reservoir 2 (see Figure 5). The same buffer was selected for sample preparation and as the run buffer in order to avoid possible effects of different concentrations/compositions of buffers during pre-run and injections and thus to be able to conclude on the time of the pre-run effect only.

The sample was injected and then detected at the end of 6 cm long channel. Quite surprisingly, the peak height continues to grow even after the pre-run time exceeds the estimated migration time of the protein from sample reservoir to the injection intersection (about 1.5 min). It can not be explained by stacking effects since the same buffer was used for both sample preparation and as separation buffer.

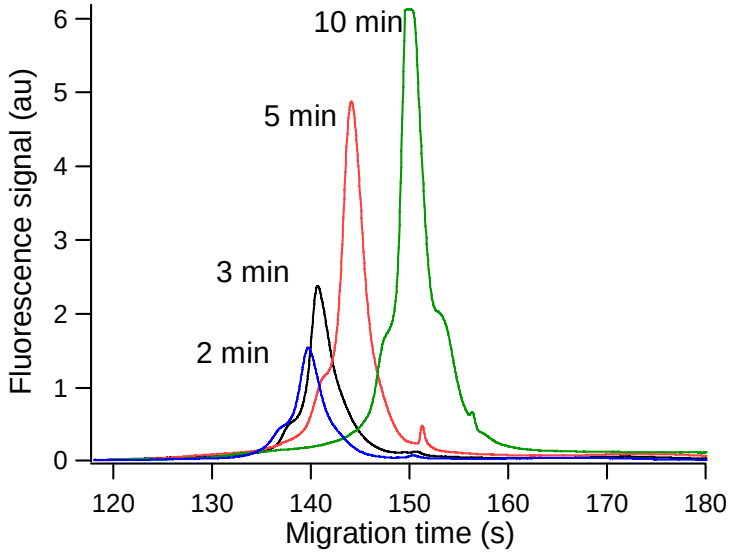

Figure 10. Influence of the pre-run time on the signal intensity. Injections of fluorescein-conjugated ovalbumin (1 µM) after different pre-run times. The sample was prepared in the run buffer consisting of 50 mM Tris base, 10 mM boric acid, 3% polyacrylamide, 8.7 mM SDS.

Possible explanations could be sample bleeding from injection intersection into the separation column during the pre-injection step. The longer the pre-run time, the more sample may be introduced into the separation channel and thus a stronger and wider signal is expected to be observed.

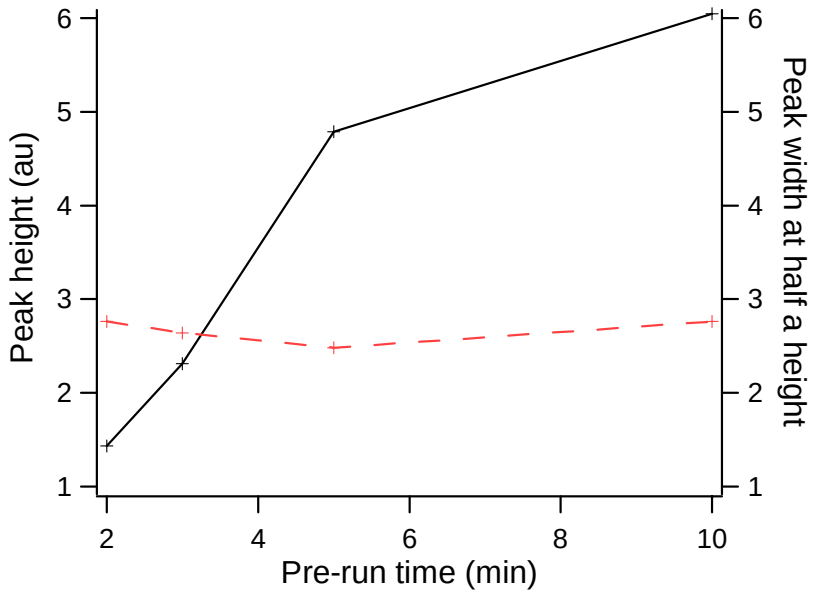

Figure 11. Effect of pre-run time on peak height and peak width. Peak height (solid line, left axis) and peak width at half height in seconds (dotted line, right axis) are presented as functions of pre-run time. The data for this graph is calculated from the electropherograms presented in Figure 10.

However as it can be seen from Figure 11, the pre-run time did not have any significant impact on the peak width at half height (right axis, dotted line), thus disapproving the hypothesis of the diffusion/bleeding origin of the signal enhancement with pre-run time. Also it is interesting to see that the migration times are increased for the longer pre-injection times. This may indicate changes in the EOF caused by protein adsorption to the wall.

The gain in sensitivity is minimal after 5 min of pre-run time compared to the high cost in the form of overall longer analysis time. The pre-run time of 5 min was thus considered optimal for the volume defined injections.

Optimizing sample loading directions

In order to minimize sample diffusion (or sample bleeding) into the separation channel during the pre-run, simulations of two possible sample loading directions using a double-T injection intersection were performed (see Figure 12 and Figure 13). The longer distance between the potential lines at the turns shows the lower field strength and its nonuniformity at the turns (Figure 12). When entering the turn some sample molecules may diffuse into the separation channel instead of following the stream lines, see Figure 12 (right). In the literature, the sample leakage on microchips is generally prevented by applying some potential to generate a small reversed flow in separation column. Such a solution to the problem can not be used with our design containing the

dilution intersection close to waste reservoir, where even a small reversed flow during the sample loading would result in a change in separation buffer composition.

To minimize unwanted sample introduction into the separation channel during the loading step, the influence of the direction of sample loading was investigated (Figure 13) combined with laminating the flow from run buffer reservoir 1. When entering the lower field strengths at the injection intersection sample molecules will than have a velocity away from the separation channel (upwards in Figure 13). Sample leaking toward the run buffer reservoir can be prevented by creating liquid flow from buffer to sample waste reservoir.

The simulations presented in Figure 12 and Figure 13 were created using codes written by Ph.D. Debashis Dutta, post-doctoral research associate at Department of Chemistry at University of North Carolina at Chapel Hill using Matlab program (The MathWorks, Inc., Natick, MA, USA). [99].

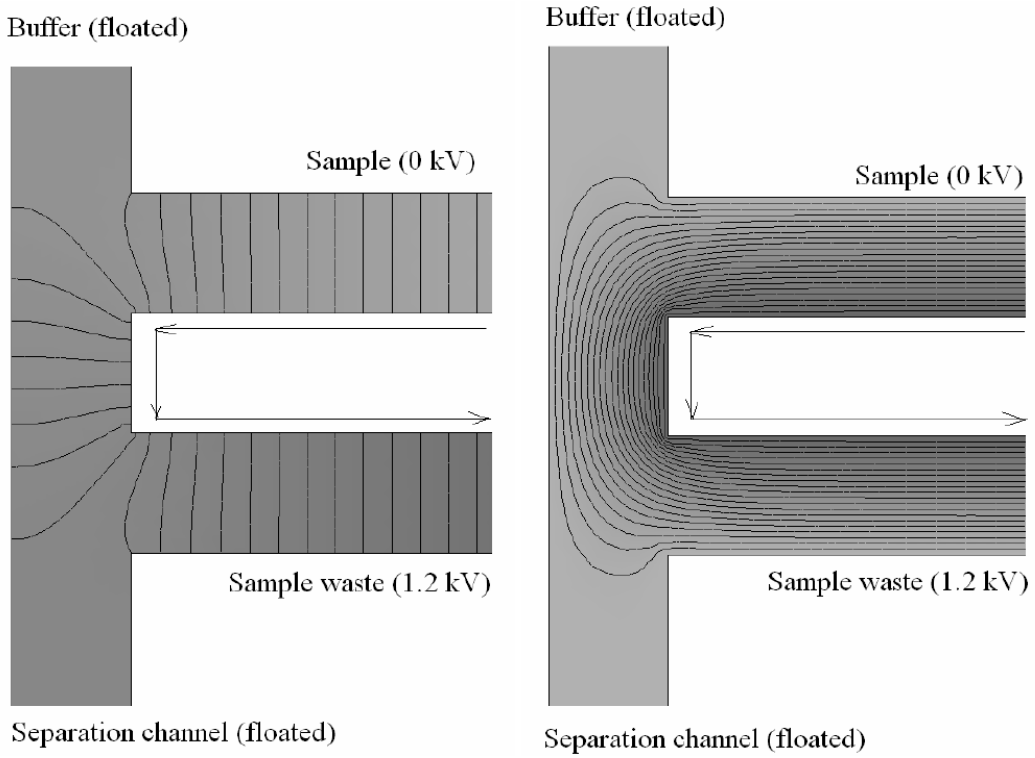

Figure 12. The equipotential fields and the stream lines distribution while electrokinetically filling the injection intersection: Standard approach. The sample loading direction in the defined volume is the same as the direction of the following injection and separation. Left: the equipotent lines; right: stream lines.

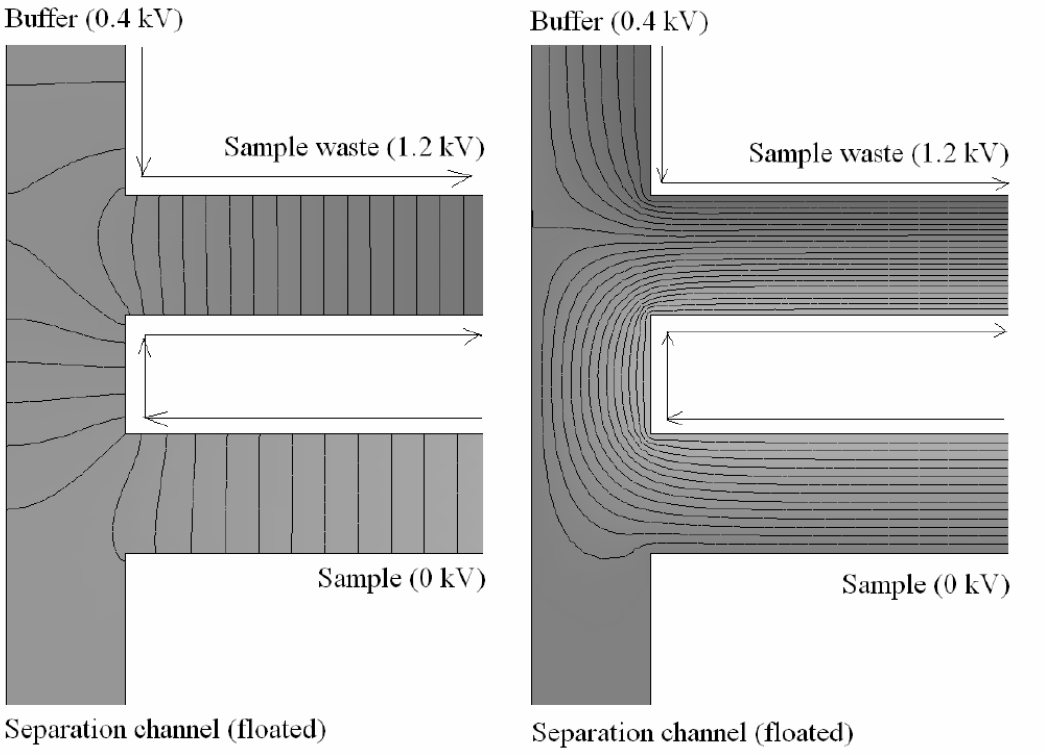

Figure 13. The equipotential fields and the stream lines distribution while electrokinetically filling the injection intersection: Reversed flow direction during the pre-run. The reversed direction of sample loading compared to that presented in Figure 12 was performed in order to prevent unwanted introduction of sample into the separation channel. A potential applied at run buffer reservoir also prevents the sample from diffusing towards the top reservoir. Left: the equipotent lines; right: stream lines.

2.3.4 Adsorption prevention strategies

A motivation for investigating different strategies to prevent protein adsorption to the glass channel is presented in Figure 14. Protein precipitation occurred in uncoated channels at the dilution intersection due to reduced detergent concentration after the dilution intersection.

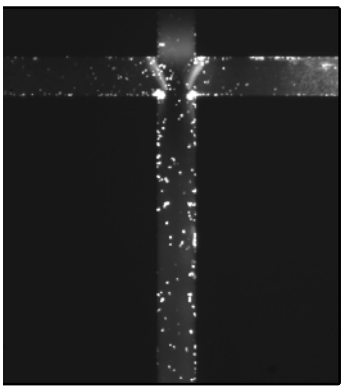

Figure 14. Protein adsorption on the microchannel walls is illustrated. A photograph of the detection channel after the dilution intersection was taken after a set of protein separation experiments; all reservoirs are floated. The bright spots are proteins adsorbed to the channel wall in the detection channel where SDS concentration is reduced. The width of the channels is 50 μm.

Adsorption of proteins on glass surfaces (channel and reservoirs) occurs due to both electrostatic and hydrophobic forces. Adsorption to the walls is the main problem for protein separations in glass devices. A surprising observation was that the problem with irreversible adsorption of the proteins increased with a decrease of total protein concentration in the sample. Problems with protein adsorption and clogging of microchannels were not encountered until the total sample content was reduced from concentrations of 0.1 – 1 mg/ml to the range of 0.01 – 0.001 mg/ml. The increase in protein adsorption with decreasing concentration may be explained through the average "residence time" on the wall. As has been shown by using isotope labeled proteins [100], protein molecules at the solution/wall interface dynamically replace each other. The higher the protein concentration is, the faster the molecules on the walls get desorbed back into solution, and replaced by other protein molecules. When the protein concentration in the solution is reduced, there are fewer competing molecules and thus the "residence time" of the proteins on the wall increases. The increased residence time results in unfolding and irreversible attachment of proteins to the wall [100].

The following strategies are typically used to prevent protein adsorption to glass channels:

- Extreme pH, since both proteins and the glass surface will have the same charge at high pH (~10) (negatively charged), and thus will electrostatically repel each other, or the glass surface will be neutral with low pH. Drawbacks of using extreme pH are possible unfolding, aggregation, deamidation, and, at high pH, hydrolysis of proteins and even dissolution of the glass chip (at pH>11).
- Protein modification by denaturing and coating with a surfactant such as urea or SDS. SDS coats protein evenly with a nearly constant SDS to protein mass ratio (1.4), thus making a uniform negative charge on the protein [51].
- Permanent wall coating in order to reduce adsorption and also to suppress the electroosmotic flow (EOF). For protein separations, channels are typically coated with polyacrylamide [101]. Permanent coating is time-consuming to apply and can be easily damaged/dissolved (for example, when rinsing the device).
- Dynamic wall coating can be applied which has the advantage of the coating agent is being present in the buffer and thus the issue of coating stability is circumvented. Buffer additives used for dynamic coating result in high ionic strength of the buffer, thus increasing Joule heating and making cooling essential if high field strengths are to be applied. Zwitterionic

salts give a minimal conductivity increase and can reduce protein interactions with walls [102].

Several coating protocols were tested to find the optimal procedure to prevent protein adsorption for the experimental work presented in this thesis. The most efficient coating was determined to be a permanent poly dimethyl siloxane (PDMS) layer with a pluronic polymer layer (polyethylene oxide-polypropylene oxide-polyethylene oxide (PEO-PPO-PEO) block copolymer) adsorbed on it as described in [103], also see the protocol described in detail in chapter 2.2.4 (page 36). While completely eliminating the protein adhesion to the walls, this coating recipe had the drawback of necessitating the application of a pluronic coating daily. Aqueous solutions of pluronic copolymers are typically liquids at low temperature and form highly viscous gels at the room temperature. Therefore, a special cooling arrangement was necessary for keeping the whole microsystem immersed under ice water (or alternatively in the thermostat) while rinsing with pluronic-containing solution. The acrylamide coating (also described in chapter 2.2.4) was less effective in preventing protein adsorption but was preferred when working with dilute samples due to the ease of maintenance once applied. The acrylamide coated microsystems were stored in the DI water and were only cleaned and conditioned using SDS buffer and DI water as described in subchapter 2.2.5. All microsystems used for generation of the results presented in this thesis have been permanently coated with acrylamide coating.

2.3.5 On-column labeling combined with post-column dilution

Run buffer containing 1x concentration of Sypro Orange® or Sypro Red® dye was loaded into reservoirs 1, 2, 4, and 6 (Figure 5 on page 32). Protein sample was loaded into reservoir 3. Reservoirs 5 were filled with dilution buffer. It should be noted that all experimental results presented in this subchapter for on-column labeling with Sypro Orange® dye were obtained using a microsystem design featuring only one dilution channel and after optimizing the chip layout an additional side channel was added as illustrated in Figure 5. For analyses without preconcentration reservoirs 4 were floated during all steps. Injections were performed by initially applying a field strength of 750 V/cm between the sample (reservoir 3) and sample waste (reservoir 2) for 5 minutes. The sieving matrix solution as well as the very high concentration of the BioRad® buffer efficiently suppressed electroosmotic flow and electrophoretic separations were performed in the so called “reversed mode” with sample molecules moving towards the anode even for the uncoated

microdevices. For the pre-injection, a potential of 400 V was applied at reservoir 1 in order to create flow from the buffer reservoir to sample waste and thus avoid sample leaking into the run buffer (Figure 13). This direction of pre-injection allowed almost no leakage of sample into the separation channel (for optimisation and simulations on pre-injection run direction, see chapter 2.3.3). All other electrodes were floated during this pre-run step. After the pre-run, an injection and separation were performed by applying a potential of 3.1 kV at waste reservoir 6 while run buffer reservoir 1 was grounded and potentials of 0.3 kV were kept at reservoirs 2 and 3 to prevent sample leakage into the separation channel after injection. By varying the potential applied at the dilution buffer (reservoirs 5), different dilution ratios (DR) were obtained. Theoretical dilution ratio (DR_t) was defined as the ratio of the current in the detection channel to the current in the separation channel. Thus, no dilution would correspond to DR = 1.

The influence of the post column dilution on sensitivity and separation is shown in Figure 15 where experiments performed with on-column labeling of 2 mg/ml total protein content with 1x concentration Sypro Orange® dye and with different post column dilution ratios is presented.

The dilution ratio was varied from run to run by varying the potential applied at the dilution channels, from 2.3 kV (DR slightly above 1) to 0.5 kV (DR = 5.6) without changing the potentials at the run buffer reservoir (0 V) and at waste reservoir (3.1 kV) during separation. The “no dilution” run was performed while floating the electrodes in the dilution reservoirs. Note that since the separations are performed in reversed mode, the higher dilution ratios are obtained with lower potentials applied at dilution reservoirs. The migration time for each protein increases with increasing dilution ratios due to decreasing field strengths in separation channel (see Figure 16).

The dilution step occurred under suppressed EOF (electroosmotic flow) conditions and resulted in a higher dilution of SDS-dye micelles compared to the proteins. The dissolution of SDS micelles containing labeling dye decreased the baseline level and increased the signal to noise by factor 10.

Post-column dilution is still possible even when EOF is suppressed. The mechanism of the dilution is different from mixing of flows using EOF. In the case without EOF, ionic streams are combined in the dilution channel. The current in the dilution channel is the sum of the current from the separation channel and from the dilution reservoirs, but the current may be carried by a different ratio of ions before and after the intersection. The dilution of the different ionic species at the dilution intersection thus depends on their apparent conductivities. More neutral analytes become less diluted than more charged and thus mobile ions. The sieving matrix in the Bio-Rad® separation

buffer is dextran, which is neutral and therefore it will not become diluted (washed out) after the dilution intersection even though it is not present in the dilution buffer. The SDS-dye complexes have a much higher mobility than the labeled proteins and therefore it is expected to become more diluted compared to the proteins. This higher mobility can be seen from the electropherograms Figure 15 where the first migrating peak is from the SDS-dye complex (sample buffer had a higher SDS concentration than the run buffer). This dilution will favor the detection limit of the proteins even before the SDS is diluted to below its cmc. Below the cmc the SDS-dye components becomes dissociated. This dissociation will give a baseline reduction for the Sypro Dyes since these non-covalent dyes are flourogenic (less fluorescent in free solution). The released dye may also bind to the proteins thereby increasing the peak height even further.

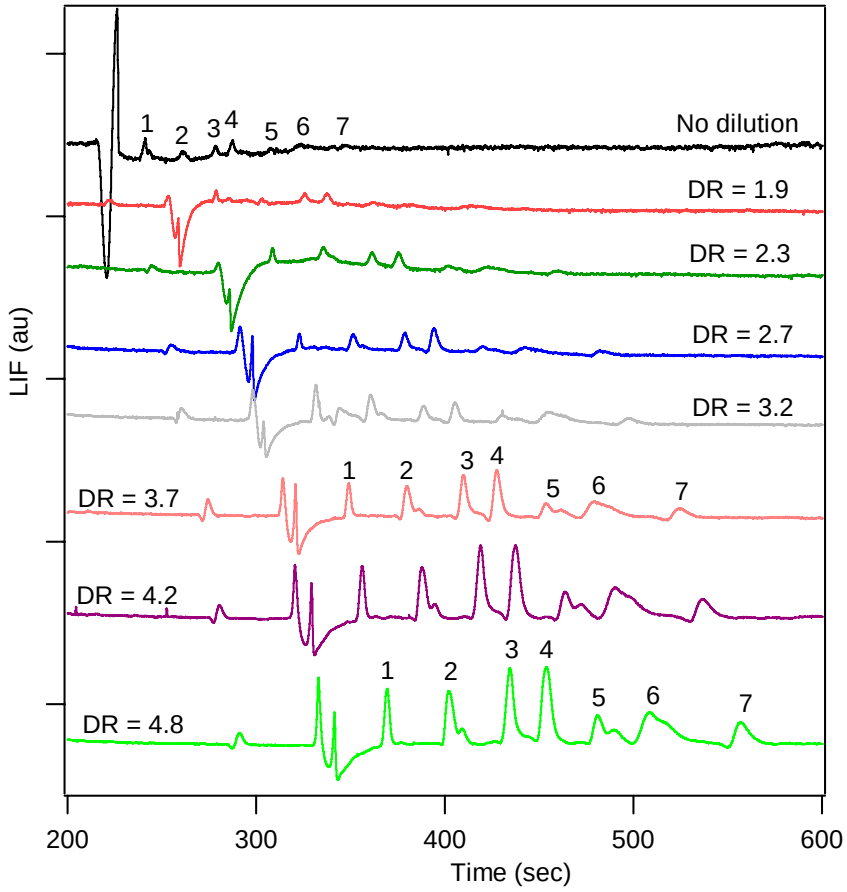

Figure 15. Effects of using different post-column dilution ratios on signal sensitivity for on-column labeling using Sypro Orange® dye. On-column labeling with 1x concentration of Sypro Orange® dye of sample containing 2 mg/ml total protein (Dalton Mark VII protein mixture) in BioRad CE-SDS buffer, with different postcolumn DR with 400 mM Tris Borate buffer, pH 8.3. Protein peaks: 1) α-Lactalbumin (19 μM); 2) Trypsin inhibitor (13 μM); 3) Trypsinogen (16 μM); 4) Carbonic anhydrase (9.3 μM); 5) Glyceraldehyde-3phosphate dehydrogenase (7.5 μM); 6) Ovalbumin (6 μM); 7) Bovine serum albumin (4.1 μM). Electropherograms has been offset for visual clarity.

Experimentally obtained dilution ratios were calculated from the baseline reduction as the baseline level of the run without dilution divided with the baseline level with dilution. For example, when applying potential of 1 kV at dilution reservoir, the background fluorescent signal became 3.6 times lower, giving an experimental DR of 3.6. This approach to estimate the experimental DR is working well at the low dilution rates (see Figure 17) where the critical micelle concentration of SDS is not approached yet.

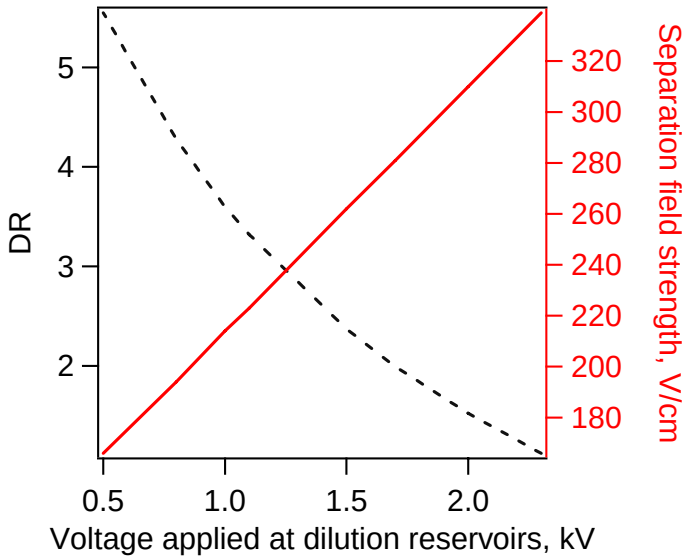

Figure 16. The dependence of the dilution ratio and separation field strength on the potential at dilution reservoirs. The field strength and DR are theoretically estimated for different electrical potentials applied at dilution reservoirs. The lower the potential at dilution reservoir is, the higher is the dilution ratio (DR) (right graph). At 2.3 kV applied on dilution reservoirs, the separation field strength is highest but the dilution is minimal and not sufficient to dilute the buffer to below critical micelle concentration for the background signal removal. Both graphs are calculated for the microsystem channel network with a layout as presented in Figure 5.

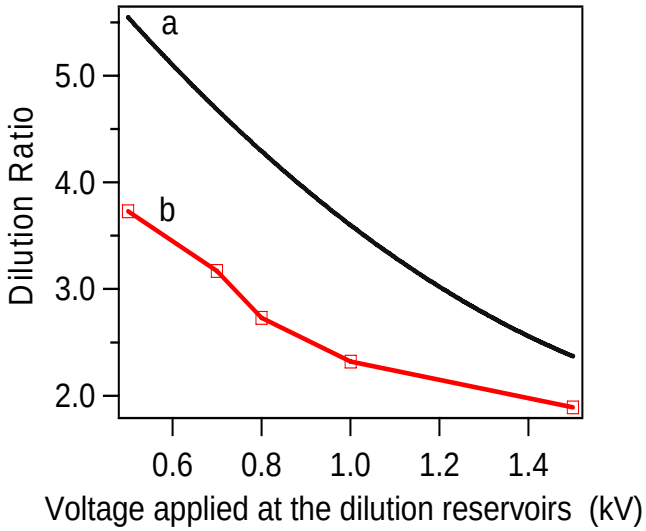

Figure 17. The experimentally and theoretically estimated Dilution Ratios versus voltage applied on dilution reservoir. Theoretically calculated values: black trace, experimentally determined: red trace.

As presented in Figure 17, the experimentally obtained dilution ratios (DRexp) were lower than theoretically estimated values for dilution ratios (DR). This can be explained by the dilution actually occurring with no EOF. The dilution is therefore more abstract and is achieved according to the conducting properties of the ions. For example, the sieving matrix (dextran in BioRad buffer) will not be diluted as it does not carry any of the current. SDS molecules are diluted to the smaller extend than the buffer ions with a higher relative conductivity.

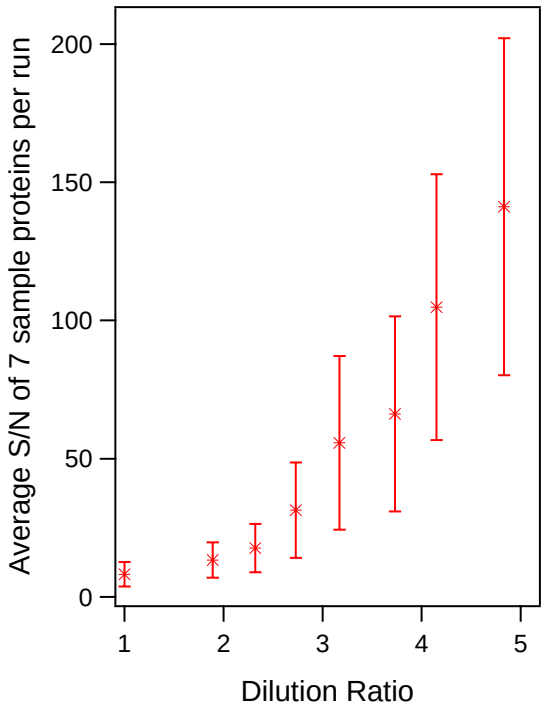

Figure 18. The average S/N of all sample proteins as a function of experimental dilution ratio. The data points are calculated from the data presented in Figure 15 where on-column labeling of sample containing 2 mg/ml total protein with 1x concentration of Sypro Orange® dye was presented. The S/N for each run is calculated as an average S/N over the 7 sample proteins (Dalton Mark VII): 1) α-Lactalbumin (19 µM); 2) Trypsin inhibitor (13 µM); 3) Trypsinogen (16 µM); 4) Carbonic anhydrase (9.3 µM); 5) Glyceraldehyde-3phosphate dehydrogenase (7.5 µM); 6) Ovalbumin (6 µM); 7) Bovine serum albumin (4.1 µM). Dilution ratios are 1.9, 2.3, 2.7, 3.2, 3.7, 4.2 and 4.8.

As seen in Figure 18, the average signal to noise ratio increases by a ten-fold from a value of 13 at dilution ratio of 1.9 to the value of 141 at the dilution ratio of 4.8. The S/N increases both because the lowering of the baseline but also from a reduction it the noise on the baseline. The noise on the baseline is strongly dependent on the background fluorescence of the buffer, this is because noise fluctuations from the laser detected at the PMT at optimal filtering will be proportional to the background fluorescence. As an example, a relative standard deviation in the laser power of 2% will manifest itself in a 2% relative standard deviation of the background (baseline) fluorescence. The higher the background fluorescence the higher the noise will appear but the relative noise is the

same. When calculating the increase in S/N by a reduction of the noise on the baseline, the relative standard deviation on the S/N is therefore also expected to be almost unchanged (2% in this example). This will manifest it self in higher variation in the measurements for the better S/N as observed in Figure 18. The relatively large standard deviation values and thus large margin of error bars in Figure 18 are also due to high variation in signal to noise enhancement for individual proteins when increasing dilution rate (see Figure 19).

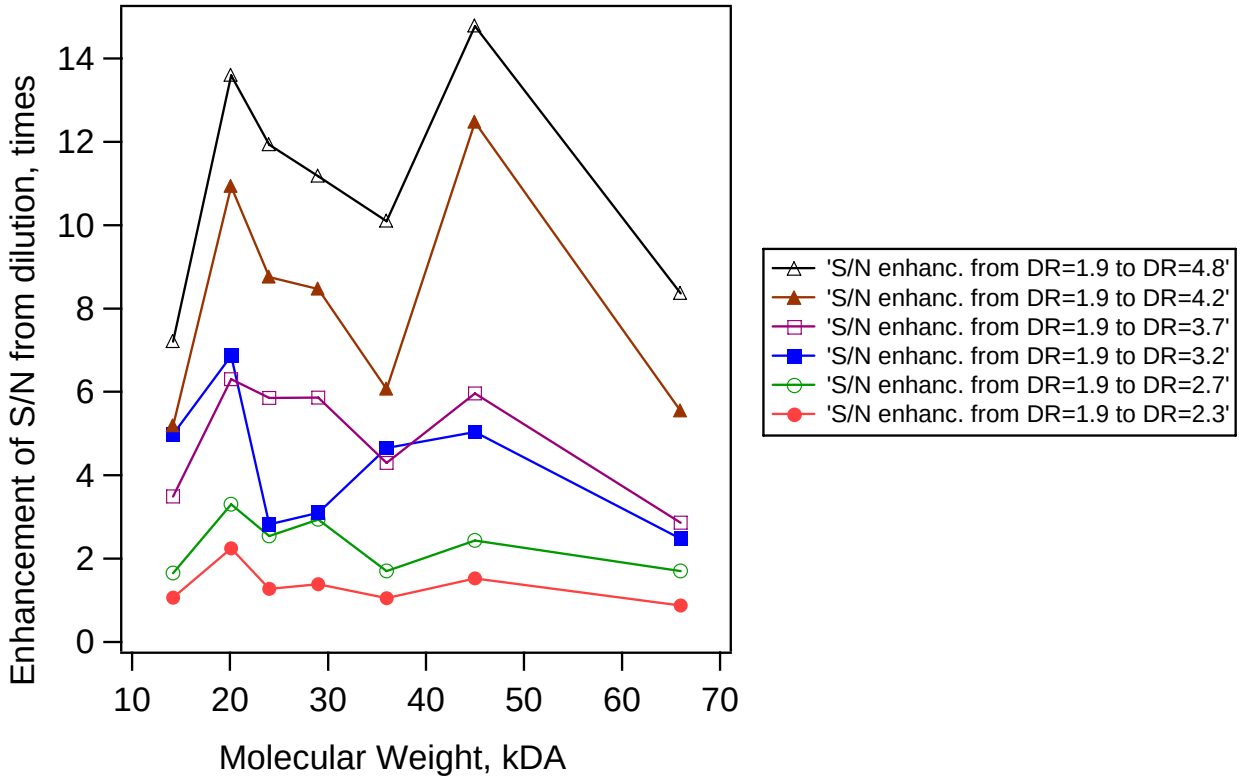

Figure 19. The enhancement of S/N for individual proteins as the result of post-column dilution. The signal enhancement is calculated as a ratio of S/N at different dilution ratios (2.3, 2.7, 3.2, 3.7, 4.2, 4.8) over the respective S/N for each protein at the dilution rate 1.9. Tha data presented on this figure is calculated from Figure 15. The seven proteins (sample: Dalton Mark VII) had molecular weights of 14.2 kDA for α-Lactalbumin (19 µM); 20.1 kDa for Trypsin inhibitor (13 µM); 24 kDa for Trypsinogen (16 µM); 29 kDa for Carbonic anhydrase (9.3 µM); 36 kDa for Glyceraldehyde-3phosphate dehydrogenase (7.5 µM); 45 kDa for Ovalbumin (6 µM); 66 kDa for Bovine serum albumin (4.1 µM).

The enhancement of S/N for individual proteins with increasing dilution did not reveal any dependence on the molecular weight of the protein. Protein peaks number 6 (45 kDa, ovalbumin) and number 2 (20.1 kDa, trypsin inhibitor) had the best signal enhancement in almost all runs, also at the low dilution rates. An intuitive explanation would be that these two proteins had a specific physical quality (for example being the most hydrophobic or possessing the highest z/m when not coated with SDS at the run buffer pH=8.3) that allowed these proteins to withheld more dye

molecules compared to the other proteins in the sample as the SDS concentration is getting diluted. Therefore, the sequences of all sample proteins was obtained and the theoretical estimation of pI, hydrophobicity and z/m values has been calculated (see Table 3 on page 73). The hydrophobicity and charge numbers obtained for the ovalbumin and trypsin inhibitor were within the values for other proteins. No dependence on the physical properties of the proteins could explain the uneven signal enhancement for different proteins with dilution.

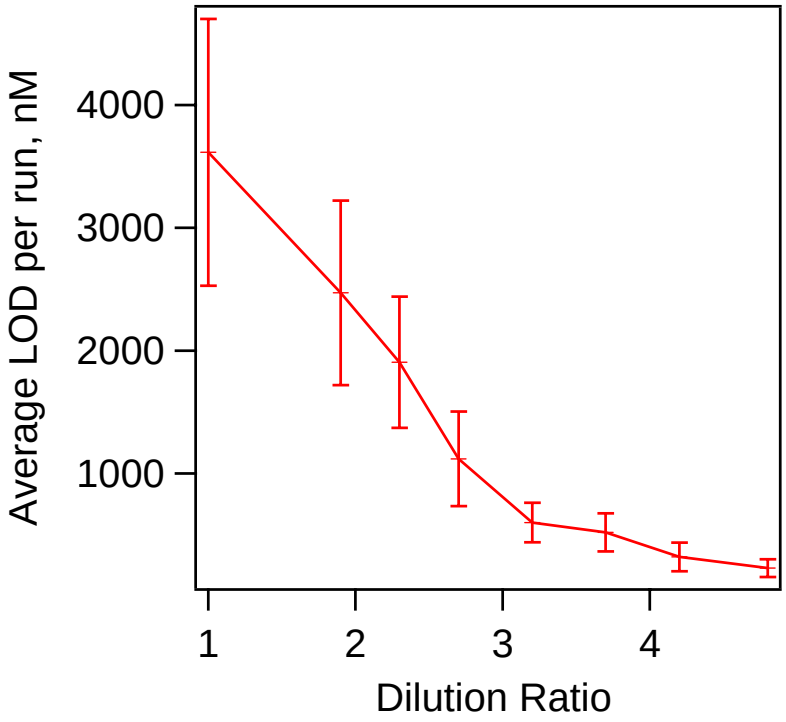

Figure 20. The average LOD of sample proteins per run in nM as a function of the experimental DR. 2 mg/ml total protein content of Dalton Mark VII sample; on-column labeling with 1x concentration of Sypro Orange® dye; experimental conditions as in Figure 15. Proteins are: 1) α-Lactalbumin (19 μM); 2) Trypsin inhibitor (13 μM); 3) Trypsinogen (16 μM); 4) Carbonic anhydrase (9.3 μM); 5) Glyceraldehyde-3phosphate dehydrogenase (7.5 μM); 6) Ovalbumin (6 μM); 7) Bovine serum albumin (4.1 μM).

The theoretical limits of detection given in Figure 20 were calculated from S/N for each individual protein as the concentration needed to give S/N = 3. The detection limit for the on-column labeling was around 300 nM when combined with post-column dilution. As can be seen from Figure 18 and Figure 20, the dilution increased the sensitivity but an optimum dilution was not achieved by using only one dilution channel. The average S/N continued to improve with higher DR, but futher increase in DR was restricted by the microsystem design. Therefore, the microsystem design was modified to include a second dilution channel to increase the DR while still maintaining acceptable field strength in the separation channel.

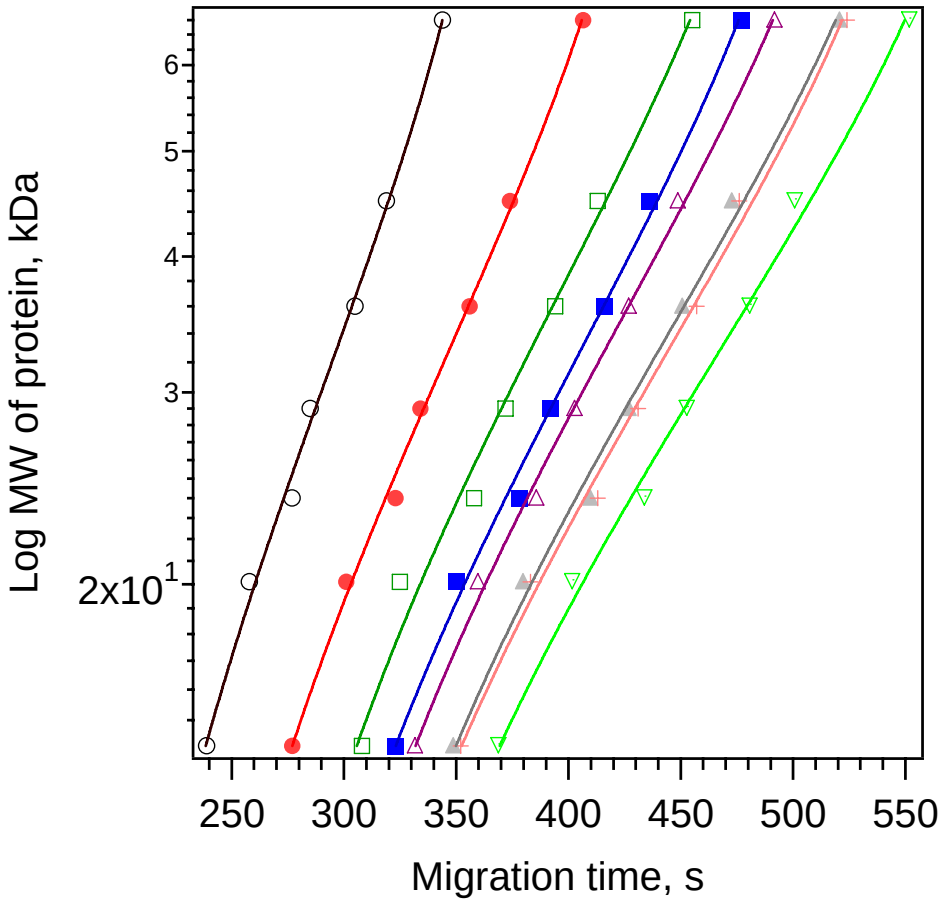

Figure 21. The log of protein molecular weight as a function of the migration time. The separations were performed with experimental conditions as in Figure 15 . Molecular weights for Dalton Mark VII proteins are 14.2 kDa for α-Lactalbumin; 20.1 kDa for Trypsin inhibitor; 24 kDa for Trypsinogen; 29 kDa for Carbonic anhydrase; 36 kDa for Glyceraldehyde-3phosphate dehydrogenase, 45 kDa for Ovalbumin and 66 kDa for Bovine serum albumin. The DR for the presented graphs from left to right: 1 (no dilution), 1.9, 2.3, 2.7, 3.2, 3.7, 4.2, 4.8. The data on this figure is calculated for the separations presented in Figure 15.

The BioRad CE-SDS buffer had a recommended dynamic range of 14 to 200 kDa given by manufacturer. This range of linearity was not necessarily expected to be valid for oncolumn or postcolumn labeling schemes tested in this work. As expected, the observed migration times is a linear function of log MW in the range of 14 to 66 kDa (see Figure 21), which allows the use of on-column labeling with sieving separations for molecular weight determination of protein samples with good accuracy (absolute standard deviation is less than 1 %). In order to determine molecular weight of an unknown protein, the presence of at least two markers with known weight in the sample is required for plotting the calibration curve. Using the linearity of log MW with migration time allows to determine the molecular weight of a protein within the dynamic range of the sieving matrix. The shift of the curves in Figure 21 is due to the differences in the electric field strength in the separation channel at the different DR (see Figure 16).

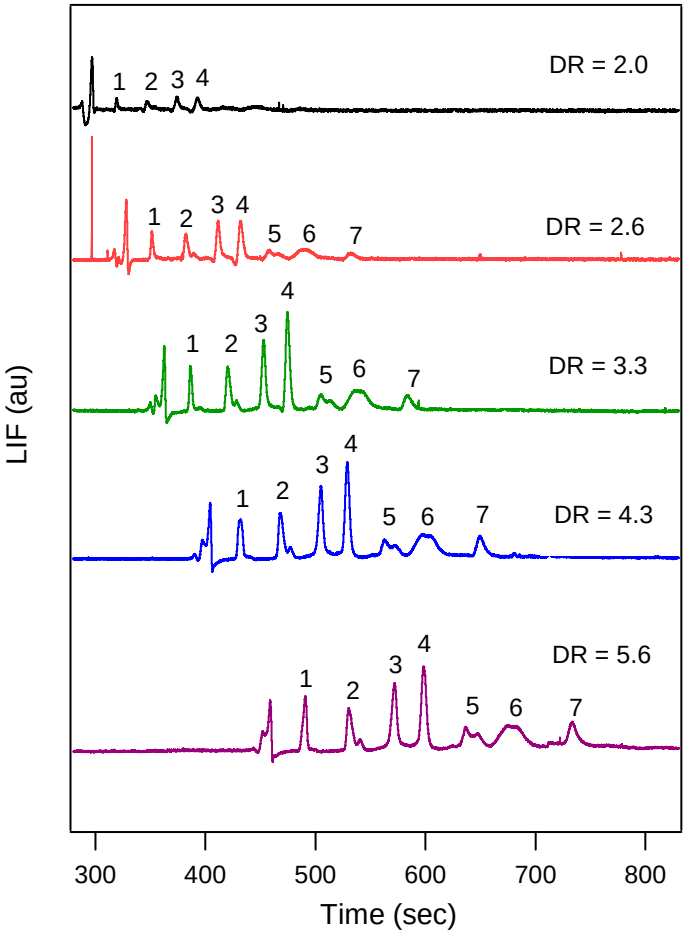

Figure 22. Effect of different post-column dilution ratios on signal sensitivity for on-column labeling using Sypro Red® dye. On-column labeling of 1 mg/ml total protein content sample (Dalton Mark VII protein mixture), protein with 1x concentration of Sypro Red® dye with different postcolumn DR with 400 mM Tris Borate buffer, pH 8.3; protein peaks are 1) α-Lactalbumin (8 μM); 2) Trypsin inhibitor (6.5 μM); 3) Trypsinogen (8 μM); 4) Carbonic anhydrase (4.7 μM); 5) Glyceraldehyde-3phosphate dehydrogenase (3.7 μM); 6) Ovalbumin (3 μM); 7) Bovine serum albumin (2 μM). Electropherograms are offset for visual clarity.

The set of experiments demonstrating different postcolumn dilution ratios using a microchip with two dilution channels for on-column labeling of 1 mg/ml total protein content sample with 1x concentration of Sypro Red® dye is presented in Figure 22.

As it can be seen in Figure 23, the signal from the protein sample when labeled with Sypro Red®, enhances rapidly at dilution ratio of 2.0 and starts to level-off at dilution ratios 3.3 and higher. Almost no gain in average signal to noise is obtained by diluting the run buffer more than 3.3 times (1.1 kV at dilution reservoirs). Further increasing the dilution ratios (by reducing the potential on dilution reservoirs) will increase the analysis time tremendously due to lower field strength in separation. Note that since the separations are performed in reversed mode, the higher dilution ratios are obtained with lower potentials applied at dilution reservoirs.

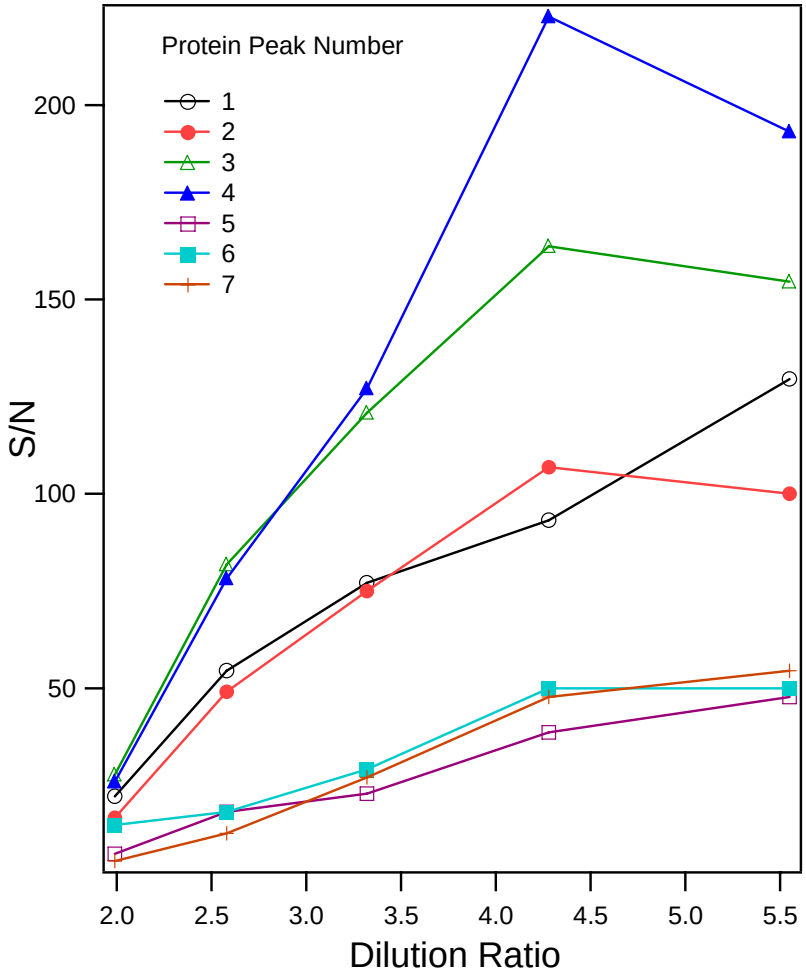

Figure 23. The S/N for proteins in each run as function of DR. On-column labeling of 1 mg/ml total protein content sample (Dalton Mark VII protein mixture), protein with 1x concentration of Sypro Red® dye with different postcolumn DR with 400 mM Tris Borate buffer, pH 8.3. Microsystem had dilution channels from both sides.

The S/N increase in Figure 23 is partially due to the decrease in the background fluorescence, resulting in decrease in the noise level. At high DR the background signal from SDS-dye complexes is reduced. This gives rise to an increased signal due to the reduction of the background noise and also due to lowered background. The theoretical limits of detection LOD for individual proteins versus DR are presented in Figure 24. The detection limits using Sypro Red® dye at the high DR are very similar to the ones obtained by on-column labeling with Sypro Orange® Dye as presented in Figure 20. The detection limits using Sypro Red® dye were not improving when going to dilution ratios higher than 3.3 (see Figure 24).

The migration time for protein separations (experiments in Figure 22) as a function of log MW for the different dilution ratios is presented in Figure 25. Using these graphs as calibration plots, the MW of an unknown protein can be easily determined from its migration time.

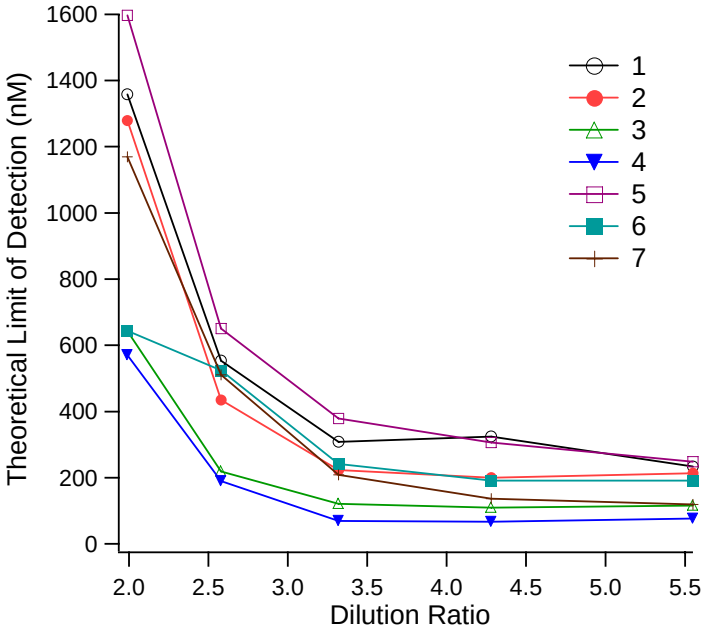

Figure 24. The LOD for each individual protein (peaks 1-7) at different DR. On-column labeling with 1x concentration of Sypro Red®; 1 mg/ml total protein content in sample. Protein concentrations were 1) α-Lactalbumin (8 μM); 2) Trypsin inhibitor (6.5 μM); 3) Trypsinogen (8 μM); 4) Carbonic anhydrase (4.7 μM); 5) Glyceraldehyde-3phosphate dehydrogenase (3.7 μM); 6) Ovalbumin (3 μM); 7) Bovine serum albumin (2 μM).

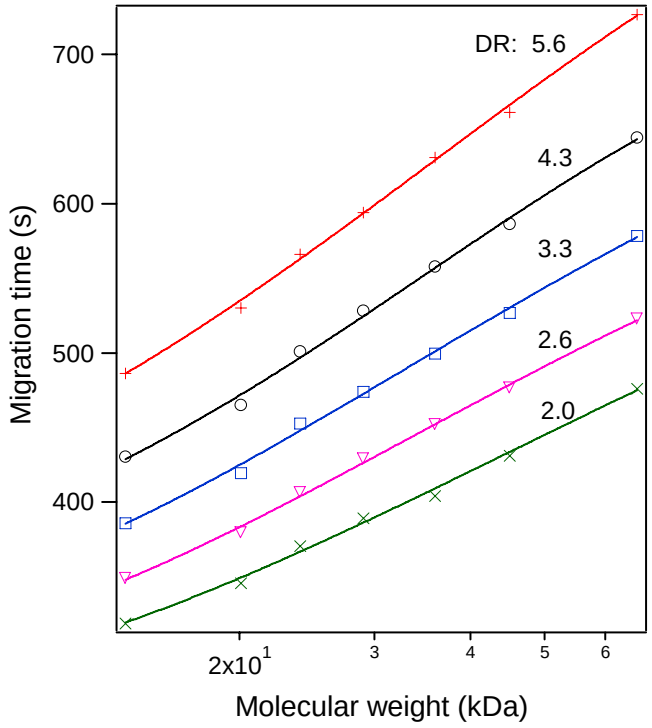

Figure 25. The migration time as a log MW for separations performed with on-column labeling with Sypro Red®. Microsystem had dilution channels from both sides. On-column labeling of 1 mg/ml total protein content sample (Dalton Mark VII protein mixture), protein with 1x concentration of Sypro Red® dye with different postcolumn DR with 400 mM Tris Borate buffer, pH 8.3; molecular weights for Dalton Mark VII proteins are 14.2 kDa for α-Lactalbumin; 20.1 kDa for Trypsin inhibitor; 24 kDa for Trypsinogen; 29 kDa for Carbonic anhydrase; 36 kDa for Glyceraldehyde-3phosphate dehydrogenase, 45 kDa for Ovalbumin and 66 kDa for Bovine serum albumin.

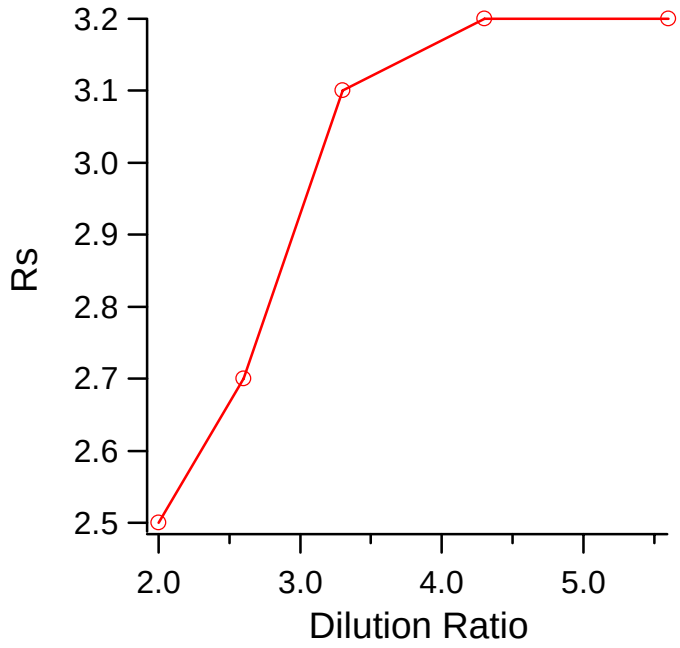

Figure 26. Peak resolution as a function of experimentally determined dilution ratio. The resolution was calculated for peaks 3 and 4 for runs with different postcolumn DR. Resolution calculated from data presented in Figure 22. On-column labeling of 1 mg/ml total protein content sample (Dalton Mark VII protein mixture), protein with 1x concentration of Sypro Red® dye with different postcolumn DR with 400 mM Tris Borate buffer, pH 8.3.

In order to select an optimal DR, the separation efficiency () also has to be considered. However, the separation efficiencies calculated according to Equation 1 on page 24 for runs obtained at different DR can not be compared without taking into account the differences in the field strengths in the separation channel and in the detection channel. This is since the detection point is located in the dilution channel, and higher field strength at the detection point (higher DR) will make the peak appear narrower compared to peak widths at lower DR. It is therefore more relevant to optimize the DR according to the resolution of the peaks *Rs* (see Figure 26). For comparing the separation performance, the resolutions between two proteins at different DR were calculated according to Equation 3 since this calculation is independent on the different velocities in the separation and detection channels. Surprisingly, an increase in resolution is observed at the higher DR.

When increasing the dilution ratio, the field strength after the dilution intersection increases and the field strength in separation channel decreases. This happens because the dilution ratio is varied by changing the potential on dilution reservoirs only and keeping the potentials applied at the run buffer reservoir 1 and the potential at overall waste reservoir 6 constant (at 0 kV and 3.1 kV respectively). From the lower separation fields, lower resolution is expected since there is more time for diffusion to take place.

2.3.6 Preconcentration with on-column labeling

For on-column labeling in combination with sample preconcentration, the preconcentration step was performed by applying a potential of 1.2 kV at the bridged reservoirs (4) while keeping sample reservoir (3) grounded (see microsystem layout in Figure 5 on page 32). All other reservoirs were kept floated during this preconcentration step. The injection/separation step was then performed exactly as described above for the volume defined injection without preconcentration.

An illustration of simultaneous sample preconcentration and on-column labeling using Sypro Orange® dye is shown in Figure 27. All microchannels shown on the image were initially filled with run buffer containing a 1x concentration of Sypro Orange® dye. Presence of the dye in the separation buffer provided the fluorescence background seen in all the channels adjacent to the preconcentration area. Upon the protein molecules arrival at the sol-gel filter, dye begins binding to the protein-SDS complex, dramatically increasing the fluorescence signal of the forming sample plug.

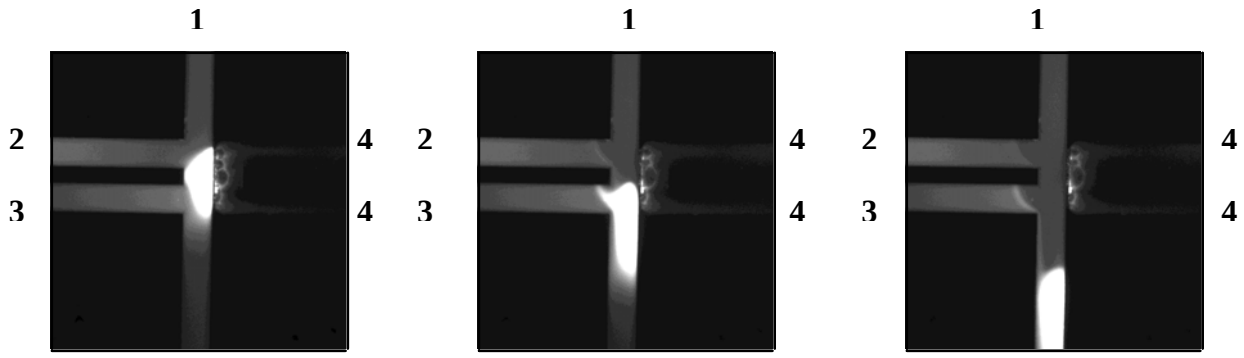

Figure 27. Simultaneous preconcentration and labeling of Dalton Mark VII protein sample for 1 minute on the porous preconcentrator followed by an injection. Buffer: 400 mM Tris-borate, pH=8.3, containing 1x concentration of Sypro Orange® dye. During the preconcentration run, a potential of 1.2 kV was applied between sample reservoir 3 and the salt bridge reservoirs 4. Left: Preconcentration and labeling of the sample for 1 minute; middle: Voltages have been changed now and the concentrated sample is being injected into the separation channel; right: Separation takes place and the sample which was not collected on preconcentrator (and thus not injected) is retracted back to sample reservoir 3 and sample waste reservoir 2 in order to avoid sample bleeding into the column during the separation run.

Figure 28 shows electropherograms of analysis performed (a) without and (b) with preconcentration for 1 minute. The on-column labeling of 2 mg/ml total protein content sample was performed with 1x Sypro Orange® dye.

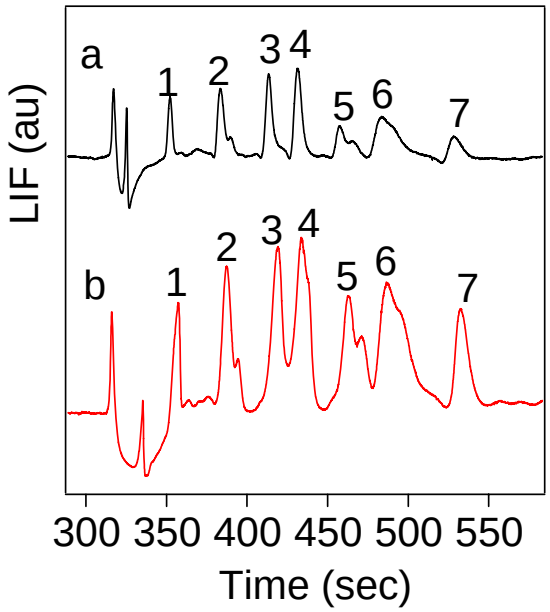

Figure 28. Comparison of analysis without and with 1 minute preconcentration combined with on-column labeling with Sypro Orange®. Data showing a) An analysis without preconcentration; b) The effect of one minute on-chip preconcentration of sample on porous preconcentrator. On-column labeling with 1x concentration of Sypro Orange® in the Bio Rad® CE-SDS run buffer for CE of proteins was followed by dilution with 89 mM Tris-borate buffer, pH 8.3, at dilution ratio of 4.2 for both experiments. Sample: Dalton Mark VII protein mixture, 2 mg/ml total protein concentration, protein peaks are: 1) α-Lactalbumin; 2) Trypsin inhibitor; 3) Trypsinogen; 4) Carbonic anhydrase; 5) Glyceraldehyde-3phosphate dehydrogenase; 6) Ovalbumin; 7) Bovine serum albumin. Electropherograms have been offset for visual clarity.

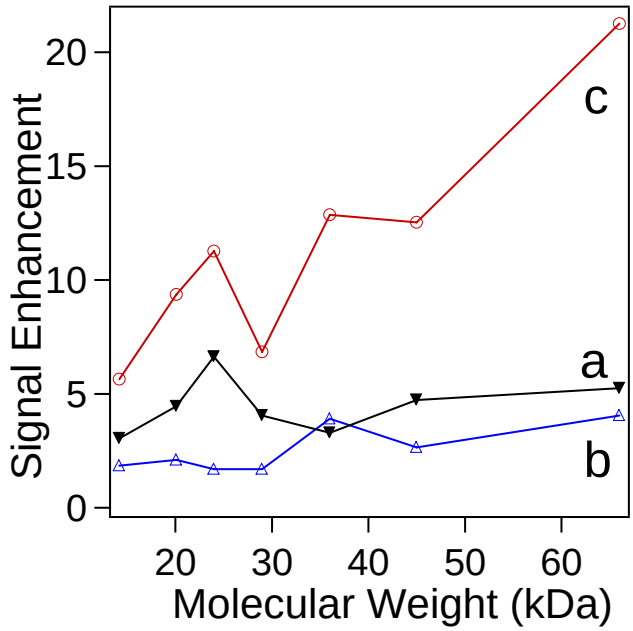

Figure 29. The signal enhancement from respectively preconcentration and dilution steps. Graph a): Increase in peak height by incorporating the dilution step (DR=4.2); Graph b): Contribution to the signal gain by the 1 min preconcentration; Graph c): Total signal enhancement (multiplying graph a by graph b). Sample: Dalton Mark VII protein mixture, 2 mg/ml total protein concentration; protein molecular weights are 14.2 kDa, 20.1 kDa, 24 kDa, 29 kDa, 36 kDa, 45 kDa and 66 kDa; on-column labeling with 1x concentration of Sypro Orange®.

The contribution to the total signal enhancement caused by respectively preconcentration and post-column dilution is shown in Figure 29c. While signal enhancement from the dilution step is nearly the same for all peaks (Figure 29a), the preconcentration step enhances the signal from the later peaks to larger extent (Figure 29b). It is seen from Figure 29 that the signal-to-noise enhancement from the preconcentration step increases with molecular weight of the proteins.

Beside the signal enhancement seen from the increase in peak height, postcolumn dilution also results in a smoother baseline, thus significantly increasing the average S/N ratio. The lower noise on the baseline can be explained by the lower background fluorescence. For separation performed with on-column labeling with 1x concentration of Sypro Orange®, average S/N for all proteins without preconcentration and dilution was approximately 10. Performing a postcolumn dilution with DR = 4.2, the average S/N is increased by ten fold to 105. Average S/N for the experiment with 1 min preconcentration and combined with the postcolumn dilution at DR = 4.2 was 304 (a further three-fold increase).

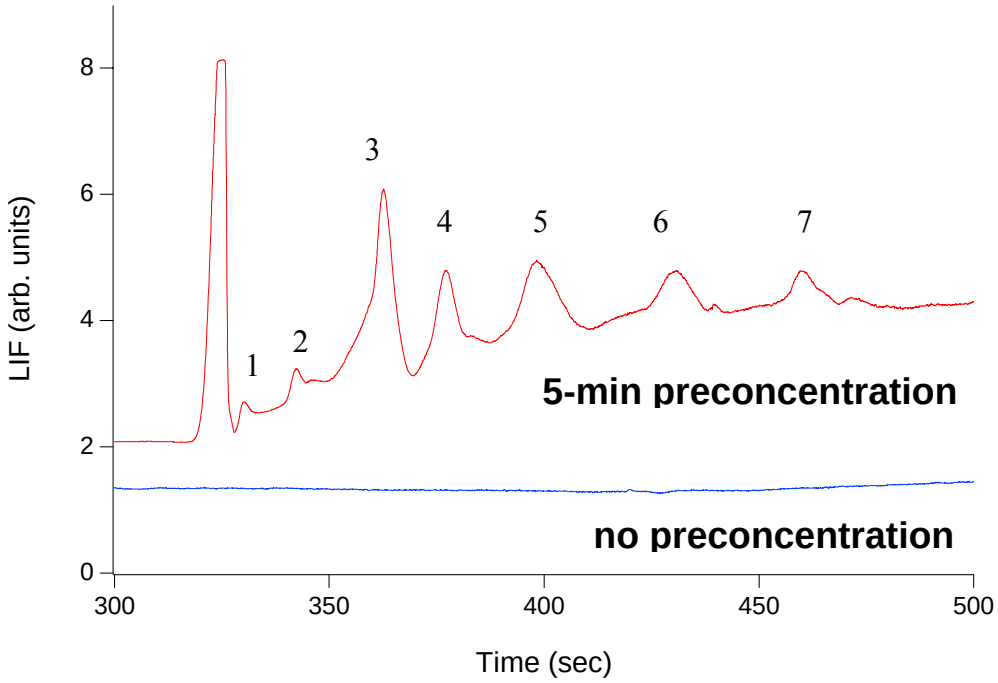

Figure 30. Effect of 5 min preconcentration for on-column labeling with 1x concentration of Sypro Orange® of 0.02 mg/ml total protein content sample. Separation in BioRad SDS-CSE buffer followed by postcolumn dilution with 89 mM Tris-borate buffer at DR = 4.2. The initial concentrations of the separated proteins were: 1) α-Lactalbumin (190 nM); 2) Trypsin inhibitor (130 nM); 3) Trypsinogen (160 nM); 4) Carbonic anhydrase (93 nM); 5) Glyceraldehyde-3phosphate dehydrogenase (75 nM); 6) Ovalbumin (60 nM); 7) Bovine serum albumin (41 nM). Electropherograms have been offset for visual clarity.

When concentrating diluted samples (see Figure 30), the non-linearity of preconcentration with protein molecular weight is even more pronounced. The low S/N for peaks 1 and 2 in Figure 30 are speculated to be due to adsorption of these faster migrating proteins to the sol-gel filter and microchannel walls. The potential sites for interactions with proteins within microchannels have a higher probability to be occupied by the faster migrating analytes on a "first come, first served" principle, thus reducing the peak height of the analyte with smallest molecular weight compared to the larger MW proteins. Also the faster migrating proteins have the smaller size and thus they have a higher probability to penetrate through the sol-gel preconcentrator.

The sol-gel filter preconcentrator demonstrates higher concentration effect with diluted samples. In the experiment presented in Figure 30, with 0.02 mg/ml total protein content, the average LOD for all 7 proteins was 16 nM, which is a 10-fold improvement compared to LOD for preconcentration of 2 mg/ml total protein content sample (seeTable 4 on page 75).

2.3.7 Post-column labeling

As described in experimental subchapter, for postcolumn labeling the CE-SDS protein run buffer from BioRad® was loaded into reservoirs 1, 2, 4, and 6 (Figure 5 on page 32). Protein sample was loaded into reservoir 3. Both reservoirs 5 were filled with the dilution buffer (400 mM Tris-borate) containing 10x or 100x concentration of Sypro Orange® dye. The higher dye concentration was used because the reaction rate can be increased by adding more labeling reagent to the dilution buffer or by increasing the flow rate from the reservoirs containing the labeling dye (Figure 34). Also, higher concentrations of the dyes were needed for postcolumn labeling when investigating the low dilution ratios, because dye was only added to the postcolumn dilution buffer. Therefore, the experiments with 100x concentration of Sypro Orange® dye in the dilution buffer were performed and compared to post-column labeling with 10x dye concentration in the dilution buffer.

A photograph of a postcolumn dilution combined with post-column labeling is presented in Figure 31. Since the labeling dye is fluorogenic, the fluorescent signal from the dye in both dilution channels becomes much stronger upon binding to the protein-SDS complexes eluting from the separation column. Visualisation of post-column labeling with 100x recommended concentration of Sypro Orange® (presented in Figure 31) was performed using 1 mg/ml total protein content sample.

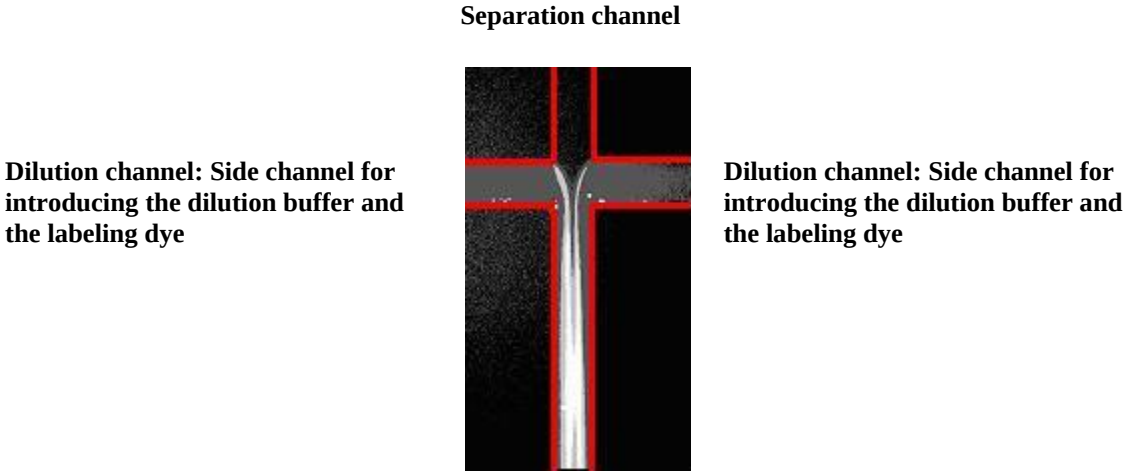

Figure 31. Postcolumn labeling and dilution is illustrated. The labeling of 1 mg/ml total protein content sample is performed postcolumn with 100x concentration of Sypro Orange® dye. Red lines are drawn on top of the image to reveal the outline of the dilution intersection.

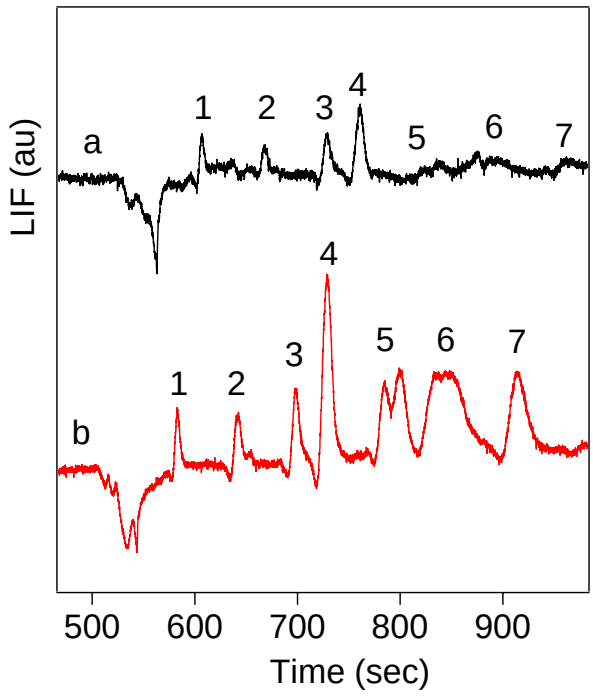

Figure 32. Separations with simultaneous post-column labeling with 10x concentration of Sypro Orange® and postcolumn dilution DR = 4.2, 1 mg/ml total protein content of Dalton Mark VII sample. a) Analysis without preconcentration; b) analysis with 1 minute preconcentration. The detected peaks had the initial concentration of: 1) α-Lactalbumin (9.5 μM); 2) Trypsin inhibitor (6.5 μM); 3) Trypsinogen (8 μM); 4) Carbonic anhydrase (4.65 μM); 5) Glyceraldehyde-3phosphate dehydrogenase (3.75 μM); 6) Ovalbumin (3 μM); 7) Bovine serum albumin (2.05 μM). Electropherograms have been offset for visual clarity.

An example of separations performed with post-column labeling with 10x concentration of Sypro Orange® dye is shown in Figure 32: a) without preconcentration; and b) with 1 min preconcentration The signal enhancement from preconcentration step (Figure 32b) for larger and thus later eluting proteins is again more pronounced than for the smaller ones as observed before.

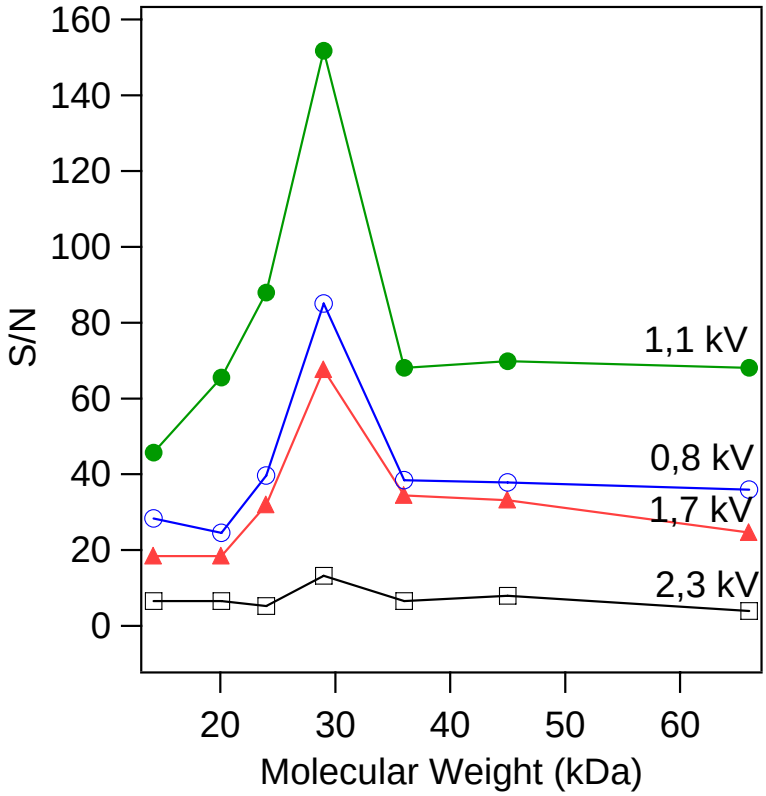

Figure 33. Average signal to noise ratios for the proteins at different potentials applied on dilution channels as a function of their molecular weight. Post-column labeling with 10x Sypro Orange®, 1 mg/ml sample. The DR is increasing with decreasing electrical potential at the labeling/dilution reservoirs since the separations are performed in the "reversed" mode, where analytes migrate towards the anode.

The effect of the postcolumn dilution and labeling step on the S/N for proteins of different sizes is shown in Figure 33. The dilution/labeling step itself results in nearly even increase in S/N for all proteins at different DR (see Figure 33). The higher signal from the 4th peak (carbonic anhydrase, 29 kDa) could probably be explained by its higher initial concentration in the sample. The Dalton Mark VII proteins are combined together to serve as MW markers and are not suitable for quantitative analysis, because the relative concentrations of each individual protein vary from sample to sample. The S/N increased while the potentials on dilution reservoirs change from 2.3 kV (black line) to 1.7 kV (red line) and to 1.1 kV (green line in Figure 33). Further increase of the dilution ratio (by further decreasing the potential at dilution reservoirs to 0.8 kV, blue line) resulted in decrease of S/N. This can again be explained by the several effects caused by changing the DR.

At higher DR more labeling is introduced but the sample also gets more diluted. Also the electric field strength changes with the DR allowing less reaction time at the higher DR.

A comparison of the calculated separation efficiency (for α-Lactalbumin, peak 1), resolution (calculated for peak 3 trypsinogen and peak 4 carbonic anhydrase, the two least separated peaks in the sample) and theoretical limit of detection (LOD) for both on-column and post-column labeling using the different labeling dyes at different concentrations is presented in Table 2. Data for different experimental modes is compared at the respective optimal DR.

Table 2. A comparison of on-column and post-column labeling modes. [a] SyR = Sypro Red®, SyO = Sypro Orange®; [b] dye concentration relative to manufacturer's recommended concentration for gel-staining; [c] total concentration of Dalton Mark VII-L proteins; [d] separation efficiency for α-lactalbumin (14.2 kDa); [e] average of individual LOD of all seven proteins in the runs. The resolution is calculated for peak 3 trypsinogen and peak 4 carbonic anhydrase, the two least separated peaks in the sample.

Dye[a]	Dye Conc.[b]	Sample conc. (mg/ml)[c]	Labeling Mode	Average S/N	N (peak 1)[d]	Resolution (peaks 3 and 4)	Theoretical LOD (average[e], nM)
SyR	1x	1	On-column	105	78,700	3.2	168
SyO	1x	2	On-column	151	76,100	2.3	320
SyO	10x	1	Post-column	8	56,000	2.1	2450
SyO	100x	1	Post-column	100	110,100	2.6	220

Data in the Table 2 is presented for the optimal DR for each labeling scheme. It is seen from Table 2 that for Sypro Orange® dye, the postcolumn labeling gave slightly better sensitivity and separations compared to on-column labeling.

2.3.8 Preconcentration combined with post-column labeling/dilution

For sample preconcentration in combination with post-column labeling, a potential of 1.2 kV was applied to the bridged reservoirs (4) while keeping sample reservoir (3) grounded. All other reservoirs were kept floating during this preconcentration step. The injection/separation step was then performed the same way as for the volume defined injection without preconcentration. Labeling dye for postcolumn labeling was added to the dilution buffer and postcolumn labeling was performed at different dilution ratios, so at high dilution ratios more labeling dye was introduced into the detection channel for labeling, with the sample and SDS being more diluted.

The effect of the labeling/dilution ratio for post-column labeling combined with the preconcentration is presented in Figure 34. All separations were performed with one minute preconcentration but with different postcolumn dilution ratios

Unlike with the on-column labeling in combination with postcolumn dilution where the signal amplitude kept increasing even at very high dilution ratios as presented in Figure 18, an optimum DR for the post-column labeling is shown in Figure 35. The observed decrease in average peak amplitude is speculated to be due to insufficient time for the dye to diffuse into the protein plug and for the labeling to take place.

When performing on-column labeling with post-column dilution, the detection point should be far enough from the dilution intersection to let the SDS micelles diffuse out and become dissociated. For post-column labeling with post-column dilution combined in a single step, the dye molecules have to diffuse from the dilution buffer into the sample plug in the direction opposite to SDS diffusion.

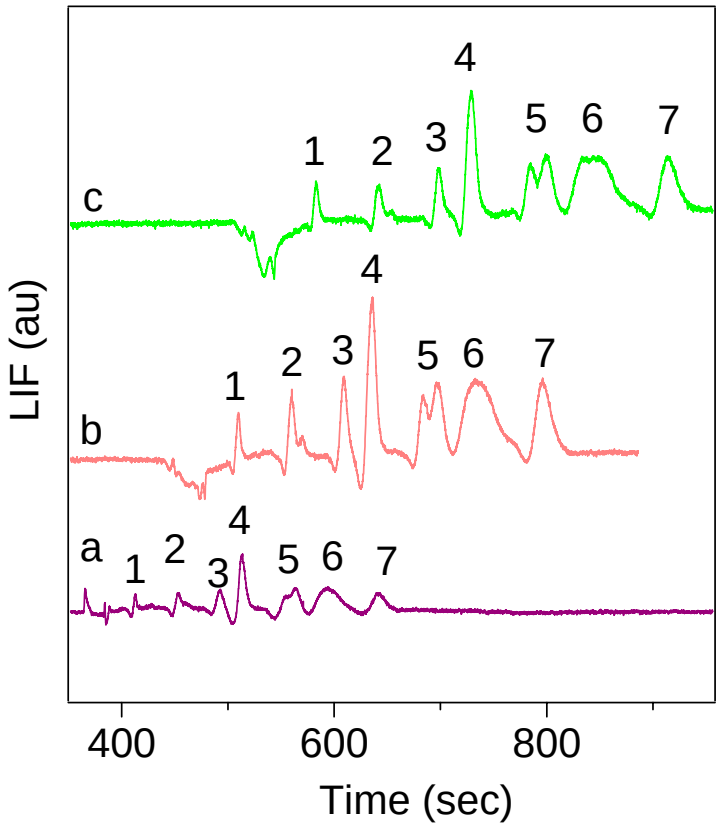

Figure 34. Preconcentration for 1 min combined with post-column dilution and labeling with 10x Sypro Orange®. a) DR=2.0; b) DR=3.3; c) DR=4.3. Initial sample: 1 mg/ml total protein content Dalton Mark VII where the initial concentrations of proteins are: 1) α-Lactalbumin (9.5 µM); 2) Trypsin inhibitor (6.5 µM); 3) Trypsinogen (8 µM); 4) Carbonic anhydrase (4.65 µM); 5) Glyceraldehyde-3phosphate dehydrogenase (3.75 µM); 6) Ovalbumin (3 µM); 7) Bovine serum albumin (2.05 µM).

When the DR is increased by decreasing the potential on dilution reservoir, the field strength in the dilution channel is increased more than the separation field strength is decreased in the separation channel (since the dilution channel is shorter than separation channel). Thus, the time available for postcolumn labeling is decreasing dramatically compared to increasing migration times for the proteins when increasing DR. The optimal sensitivity was obtained at DR = 3.3 (see Figure 34 b and Figure 35). The initial microsystem design only had one dilution channel. The optimized microsystem layout was designed with two dilution channels allowed for higher dilution rates and shorter diffusion times compared to a microsystem with one dilution channel when applying the same electrical potentials at the dilution channels.

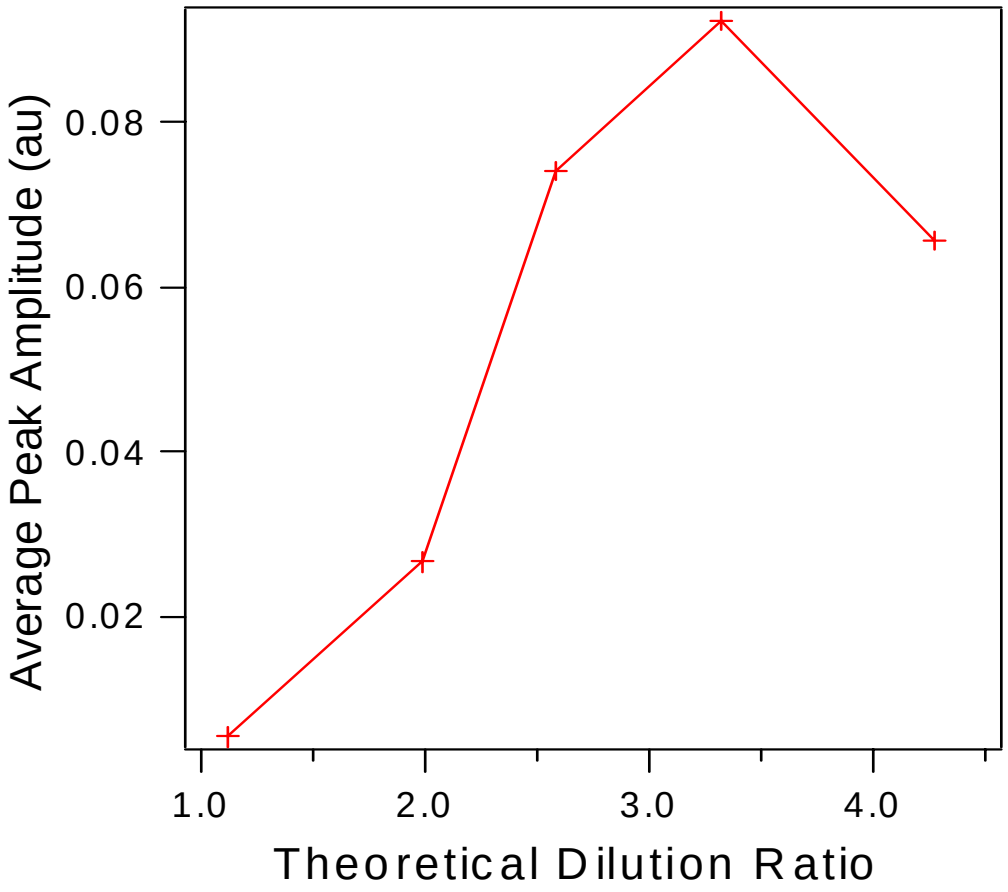

Figure 35. Influence of the dilution ratio on the average peak amplitude for 1 minute preconcentration combined with post-column labeling. Average peak amplitude for runs performed at different DR. Post-column labeling with 10x Sypro Orange®, 1 mg/ml sample (Dalton Mark VII from Sigma-Aldrich).

The signal enhancement from sample preconcentration combined with postcolumn labeling increases with increasing molecular weight of the analytes as presented in Figure 36, similar to the results obtained for on-column labeling presented in Figure 29.

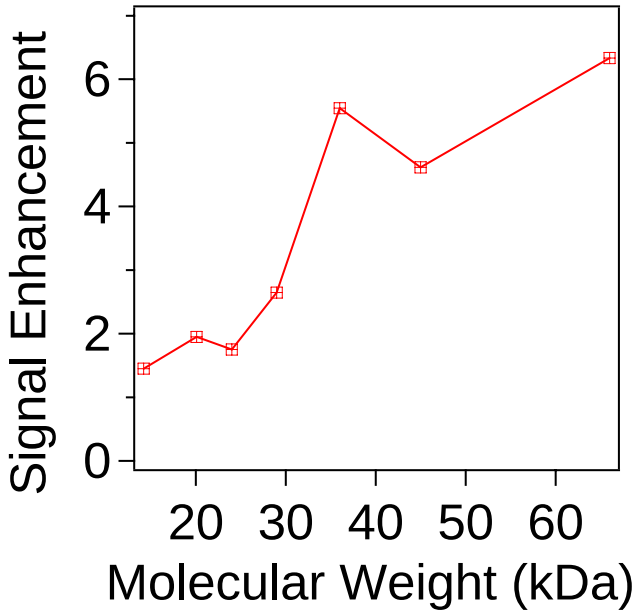

Figure 36. Signal enhancement achieved by one minute preconcentration as a function of protein molecular weight. Post-column labeling with 10x Sypro Orange®, 1 mg/ml total protein content in Dalton Mark VII sample, dilution ratio 4.3.

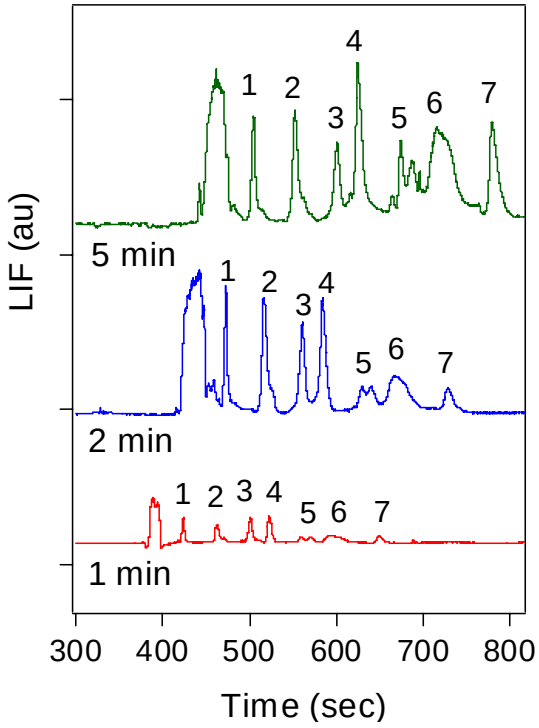

Figure 37. The effect of preconcentration time on post-column labeling with 100x concentration of Sypro Orange®. 1 mg/ml sample, using different preconcentration times (1 min, 2 min and 5 min), DR=3.3. The detected protein peaks had the initial concentrations of: 1) α-Lactalbumin (9.5 μM); 2) Trypsin inhibitor (6.5 μM); 3) Trypsinogen (8 μM); 4) Carbonic anhydrase (4.65 μM); 5) Glyceraldehyde-3phosphate dehydrogenase (3.75 μM); 6) Ovalbumin (3 μM); 7) Bovine serum albumin (2.05 μM).

Smaller proteins in the sample are found to be preconcentrated by a lesser factor when compared to large proteins. Possible reasons for non-linear preconcentration as a function of time for proteins with different molecular weight are:

1) Small proteins tend to adsorb faster to the microchannel walls than the larger proteins because they migrate faster than the large proteins and are first exposed to potential binding sites.
2) The smaller proteins can partially get through the preconcentrator filter.

The effect of different preconcentration times with postcolumn labeling and dilution is shown in Figure 37. It can be seen that larger proteins (peaks 5-7) benefit more from the increase of preconcentration time compared to smaller proteins (peaks 1-4).

To determine whether the non-linear signal enhancement from the preconcentration step with molecular weight is affected by differences in physical properties of the of sample proteins, the isoelectric points pI and GRAVY (Hydropathicity values) as well as overall charge-to-mass ratio for sample proteins were calculated. The sequences of the sample proteins in Dalton Mark VII were found in databases and are given in Appendix 8.2 [104, 105]. Predictions of pI, mass to charge, and hydropathicity values were performed using Prot Param tool at ExPASy (Expert Protein Analysis Systems) web page [104] and ChipMoST program (developed at University of Wisconsin, Madison). The values obtained for Dalton Mark VII proteins are compared in Table 3.

Table 3. The isoelectric points, hydropathicity and charge-to-mass ratios for Dalton Mark VII markers. The values were predicted by using Prot Param tool at ExPASy (Expert Protein Analysis Systems) web page [104] and ChipMoST program (developed at University of Wisconsin, Madison). Proteins are: 1) α-Lactalbumin; 2) Trypsin inhibitor; 3) Trypsinogen; 4) Carbonic anhydrase; 5) Glyceraldehyde-3phosphate dehydrogenase; 6) Ovalbumin; 7) Bovine serum albumin.

Protein	M_r kDa	ChipMoST pI	ChipMoST GRAVY	ProtParam pI	ProtParam GRAVY	ChipMoST z/m (x1000) at pH=7	ChipMoST z/m (x1000) at pH=8.3
1	14.2	4.93	- 0.433	4.80	- 0.433	- 0.456	- 0.811
2	20.1	4.74	- 0.241	4.66	- 0.241	- 0.410	- 0.560
3	25.7	8.06	0.051	8.52	0.051	0.145	- 0.062
4	29.0	6.66	- 0.555	6.40	- 0.555	- 0.048	- 0.127
5	35.7	8.11	- 0.064	8.52	- 0.064	0.105	- 0.025
6	42.9	5.21	- 0.007	5.19	- 0.007	- 0.281	- 0.395
7	69.3	5.94	- 0.424	5.82	- 0.429	- 0.178	- 0.480

It can be seen from Table 3 that neither hydropathicity nor pI and z/m values of proteins at the pH of the separation buffer used (pH = 8.3) could explain the uneven preconcentration factor. There is no obvious dependence on these physical parameters explaining the higher preconcentration rates for the larger proteins, except the molecular weight. With increase in the molecular weight, the proteins are preconcentrated to a higher extend. This finding is consistent with the physical filtering mechanism of protein retention, which would allow the escape of the smaller proteins through the preconcentrator pores. Another possible explanation is that the smaller proteins are retained at the filter surface and thus are not injected to the higher extent than the larger proteins. This hypothesis is supported by Figure 37 where it is seen that the peak height for the smaller proteins (peak 1-4) are basically unaffected by increasing the concentration time from 2 to 5 minutes which indicates that they may pass through the preconcentrator filter.

As presented in Figure 38, the protein molecular weight determination was not affected by post-column labeling/dilution alone or in combination with preconcentration. The short migration times when using DR=2.3 compared to 3.4 is because the field strength is increased in the separation channel when DR is decreased. Quite interestingly, a decrease in the migration times is observed for the run with 1 minute preconcentration as presented in Figure 38, trace a. The correlation coefficients for linear fits in Figure 38 are all ≥ 0.997. When some unknown proteins are analyzed together with the molecular weight standards, the MW of unknown proteins can be calculated from the migration times of their respective peaks using the standards for creating the calibration curve.

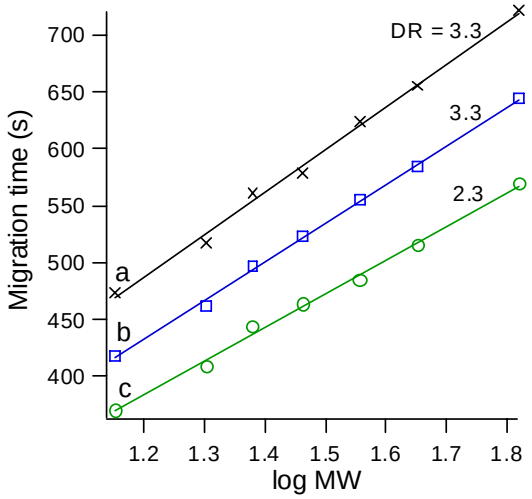

Figure 38. The migration time as a function of log MW for separations performed with postcolumn labeling with 100x SyproOrange® using different DR. Trace a: 1 minute preconcentration and DR = 3.3; Trace b: no preconcentration and DR = 3.3; Trace c: no preconcentration and DR = 2.3. Sample: 1 mg/ml of Dalton Mark VII from Sigma-Aldrich, molecular weights of 14.2, 20.1, 24, 29, 36, 45 and 66 kDa.

A comparison of separation efficiency (calculated for α-Lactalbumin peak), resolution (calculated for trypsinogen, peak 3, and carbonic anhydrase, peak 4, the two least separated peaks) and theoretical limit of detection (LOD) for preconcentration combined with both on-column and post-column labeling is presented in Table 4.

Table 4. **Comparison of on-column and post-column labeling, both combined with preconcentration.**

[a] concentration of Sypro Orange® dye relative to manufacturer's recommended concentration for gel-staining; [b] total concentration of proteins, [c] separation efficiency for α-lactalbumin (14.2 kDa); [d] average LOD for all proteins per run calculated for S/N=3. The resolution is calculated for peak 3 trypsinogen and peak 4 carbonic anhydrase, the two least separated peaks in the sample.

Dye Conc.[a]	Sample conc. (mg/ml)[b]	Labeling Mode	Precon. Time (min)	N (peak 1) [c]	Average S/N [d]	Resolution (peaks 3 and 4)	Theoretical LOD (average, nM) [d]
1x	2	On-column	1	37,900	304	1.0	104
1x	0.02	On-column	5	91,400	30	1.2	16
10x	1	Post-column	1	77,200	84	1.8	240
100x	1	Post-column	1	38,200	236	2.1	91

For the samples differing in initial concentration by hundred times (0.02 mg/ml total protein content versus 2 mg/ml), the S/N varied only by factor 10, due to the 4 minutes longer preconcentration. The resolution (calculated for the least resolved peaks 3 and 4, being trypsinogen and carbonic anhydrase) was significantly better for the postcolumn labeling compared to on-column labeling. The theoretical limit of detection (LOD) obtained for post-column labeling with 1 minute preconcentration time of 1 mg/ml sample was similar to the LOD obtained for on-column labeling with 1 min preconcentration). That allows us to conclude that the post-column labeling is a preferable scheme for the on-chip labeling combined with preconcentration. The LOD of proteins in low nanomolar range was demonstrated combining the preconcentration on porous bridge with on-chip labeling.

2.3.9 Determining the critical micelle concentration

Part of the increase in the S/N of analytes during the dilution step is due to dissociation of SDS micelles and thus minimizing the SDS-dye complexes. Without SDS micelles present in the buffer, the fluorogenic dyes had lower fluorescence efficiency and the background signal was significantly reduced. In order to determinate the cmc for SDS in a specific separation buffer, an approach to detect the light scattering values while increasing SDS concentrations was undertaken.

This was done using fluorescence spectrophotometer (from Perkin-Elmer, model 650-10, Wellesley, MA, USA). With no fluorescent dye present, the scattering values were first obtained for a 0.1 mM SDS solution (well below an expected cmc value) in buffer (50 mM Tris base, 10 mM boric acid) with different excitation wavelengths (Figure 39).

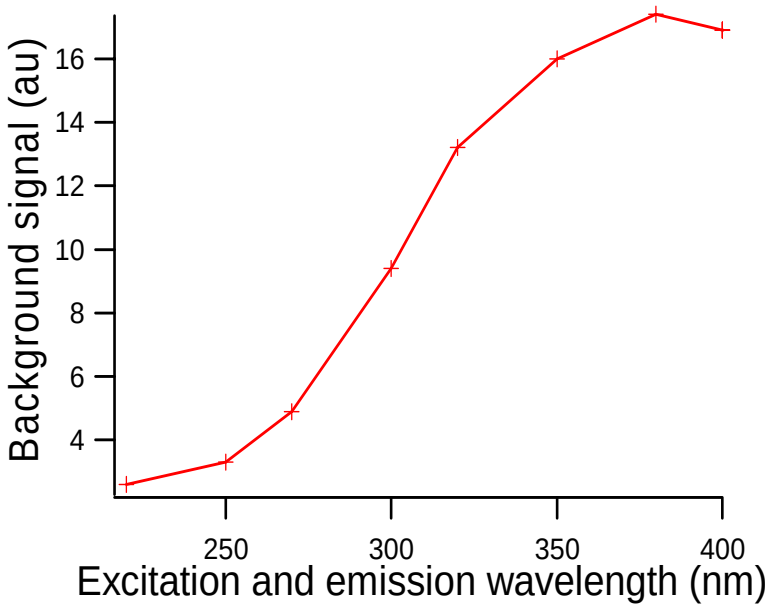

Figure 39. Scattered signal of a 0.1 mM SDS in 50 mM Tris, 10 mM boric acid buffer. The signal at different wavelengths was collected perpendicular to the excitation light in fluorescence spectrophotometer (Perkin-Elmer, model 650-10). No error bars are placed on the curve since the three times reproduced measurements on the same sample solution did not differ in three significant numbers, the deviation was less than 1 %.

A maximum background scattered signal for the 0.1 mM SDS concentration was found at 380 nm. With no fluorescent molecules present in the sample, the high background scattering is likely to be due to an increased intensity of the light source at the wavelength of the 380 nm. The goal with finding the high source intensity wavelength was to obtain the best sensitivity for the scattering measurements with different SDS concentrations. The amount of scattered light detected for different concentrations of SDS in 50 mM Tris, 10 mM boric at 380 nm is presented in Figure 40.

At concentrations higher than 4.0 mM, a significant increase in the scattered light was observed, corresponding well with the cmc found in literature for other aqueous buffers [106, 107]. This approximate cmc value for the Tris-borate buffer was used to estimate the approximate dilution ratio needed to break apart the SDS micelles. The BioRad CE-SDS buffer had an initial concentration of 8.7 mM, so a DR of 2-3 was expected to bring SDS concentration to below cmc value.

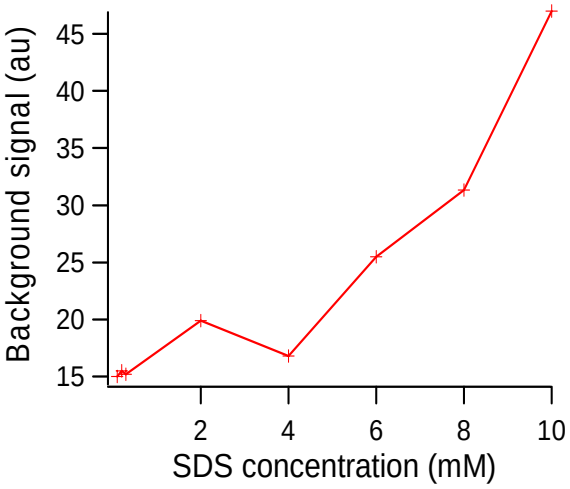

Figure 40. Scattering as a function of SDS concentration. Scattered signal for different SDS concentrations in 50 mM Tris base, 10 mM boric acid buffer; all measurements performed at 380 nm excitation and collection wavelength, the band width for the signal collection was 10 nm. The signal was collected perpendicular to the excitation light in fluorescence spectrophotometer (Perkin-Elmer, model 650-10). No error bars are placed on the curve since the three times reproduced measurements did not differ in three significant numbers.

The SDS concentration in the run buffer should be as high as possible for a successful separation but, at the same time, it should be possible to achieve dilutions below the cmc prior to the detection using the dilution capabilities intrinsic to a particular microsystem design.

2.3.10 Improving microsystem design

A next generation microsystem prototype was designed to obtain faster separations and more efficient dilution of SDS-dye complexes prior to detection compared to the design presented in Figure 5. Shorter side channels for dilution would allow the achievement of higher dilution ratios while maintaining higher field strengths in the separation channel compared to the design with longer side channels for dilution, providing for shorter overall analysis time (Figure 41). The power supply used for the experiments was only capable of providing 4 kV maximum outputs. Using twice as short side channels for dilution, 4 times higher dilution ratio can be obtained at the potential of 0.5 kV applied on the side channels (see Figure 41). Both curves presented in Figure 41 have been calculated for the long microsystem design with 6 cm long separation channel (see Figure 5 for the details). This estimation has been the motivation for changing the design to shorter side channels.

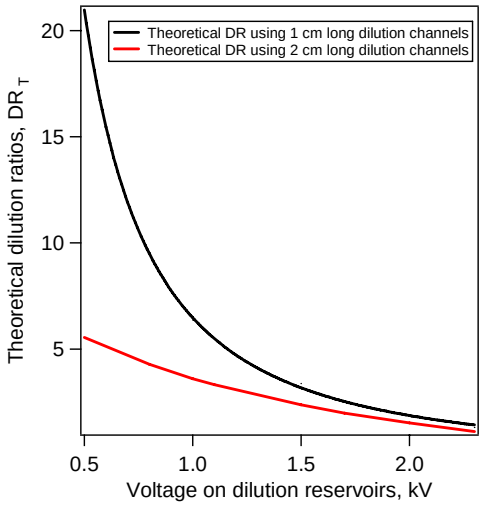

Figure 41. The theoretically estimated Dilution Ratio for the second generation microfluidic device. The comparison of the theoretical DR values demonstrates that having the dilution channels only 1 cm long (top trace, black) instead of 2 cm long (bottom trace, red), 4 times better dilution ratio can be obtained when applying the same potential of 0.5 kV at the dilution reservoirs. The calculations were performed for the microsystem layout with 6 cm long separation channel, the only different value was the length of two side channels used for dilution, 1 cm versus 2 cm.

The improved design is featuring shorter separation channel and shorter side channels for dilution (Figure 42). Shorter separation channel (1.5 cm as presented on Figure 42) further reduces the analysis time but will also degrade the separation. The shorter side channels for dilution also allow achieving higher separation field strength as the maximum output of the power supply used in this experiments was below 4 kV.

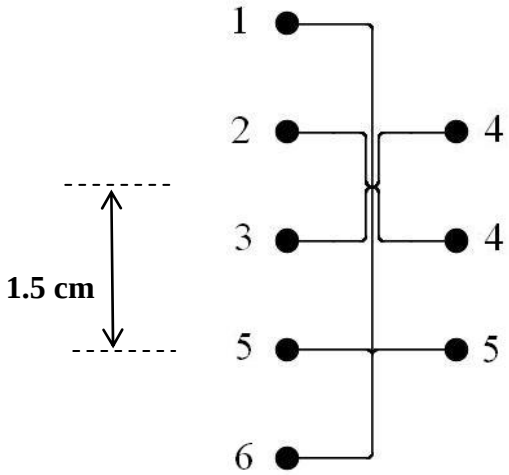

Figure 42. Schematic of a "second generation" optimized microsystem is shown. The reservoirs are: 1) run buffer; 2) sample waste; 3) sample; 4) preconcentrator reservoirs, bridged with platinum wire; 5) dilution reservoirs, bridged with platinum wire; 6) waste. The length of the separation channel is 1.5 cm compared to 6 cm in the previous design (Figure 5).

Channels leading to sample and sample waste reservoirs are coming into the separation channel only 50 μm apart, and breakthroughs of the current through the porous layer was frequently observed on the first generation design. The breakthrough would typically be observed during the pre-run for an injection without preconcentration, resulting in the sample molecules taking a "shortcut" from sample reservoir to the sample waste without passing the injection intersection, resulting in less or no sample being loaded onto the separation column. To avoid this from happening, the second generation devices were designed with rounded shapes as shown in Figure 43.

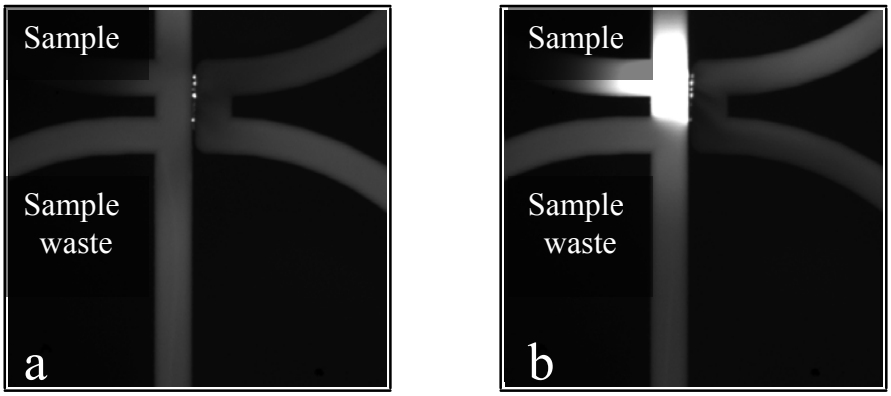

Figure 43. Preconcentration with simultaneous on-column labeling using the optimized design. a) onset of preconcentration; b) concentration and labeling of sample plug. Sample: 1 mg/ml Dalton Mark VII sample, fluorescent label: 1x Sypro Orange® in Bio Rad CE-SDS buffer for sieving electrophoresis of proteins.

The close-up picture of the preconcentrator area shown in Figure 43 illustrates simultaneous preconcentration and labeling on the porous preconcentrator at the injection intersection (Figure 43b). The channels at all intersections have been designed to part further and further away from each other immediately after intersection to prevent the possibility of current breaking through the porous silicate layer between channel parts in close proximity.

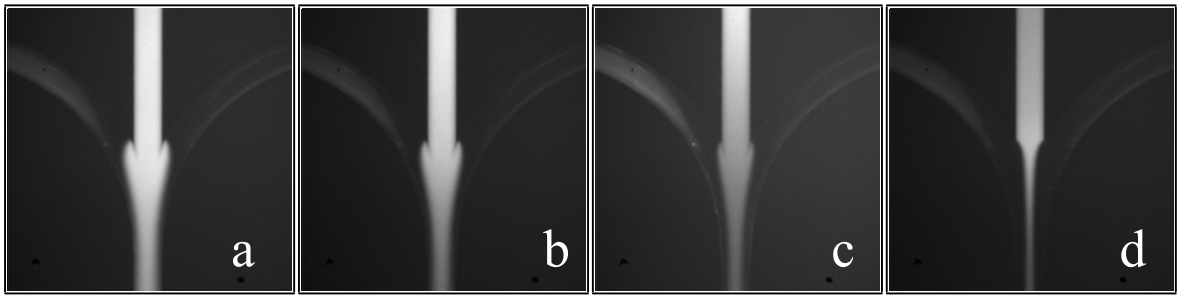

Figure 44. The dilution intersection on the second generation microsystem. Dilution of on-column labeled 1 mg/ml Dalton Mark VII sample, with 1x Sypro Orange® in Bio Rad buffer for sieving electrophoresis of proteins. Dilution buffer: 400 mM Tris-borate; see whole microsystem layout in Figure 42. Continuous sample injection was performed by applying 1 kV at the waste reservoir (6) and 0 kV at the sample reservoir (3). Potentials on the dilution reservoirs (5) are as following: a) 0.7 kV; b) 0.6 kV; c) 0.5 kV; d) 0.4 kV.

The close-up picture of the dilution intersection can be seen in Figure 44, where the continuous flow of 1 mg/ml protein sample labeled on-column with 1 x Sypro Orange® is getting diluted with DR increasing from photograph a to d.

2.3.11 Porous preconcentrator troubleshooting

Problems with device to device reproducibility of the porous preconcentrator were experienced, similar to these reported for polymer membrane preconcentrators [95]. Some devices would have no electric contact through the sol-gel bridge at all, and some would allow the protein sample to pass through. The reproducibility problem required a closer look at the silicate chemistry involved at the formation of sol-gel bridge.

KASIL® potassium silicates (PQ Corporation and National Silicates, Valley Forge, PA, USA) are routinely used as an adhesive for gluing the glass in screen/monitor applications and was used for bonding of glass devices as presented in subchapter 2.2.2 on page 33. The transparency of the coating, glass binding and ease of use make these silicates an ideal choice for a bonding layer in microfabrication. Bonding of two glass substrates can be assisted by spin coating a silicate layer on the cover glass substrate and then pressing together the two substrates [93]. Sodium and potassium silicates are composed of a mixture of silicate anions, represented by a ratio $x\ SiO_2 : M_2O$, where M is either sodium or potassium. The ratio *x* is in the range from 1.6 to 3.5 and does not accurately represent the complexity of the composition and the structure of silicate solutions. The main structural unit (monomer) of a silicate solution is a tetrahedral silicate anion (Figure 45).

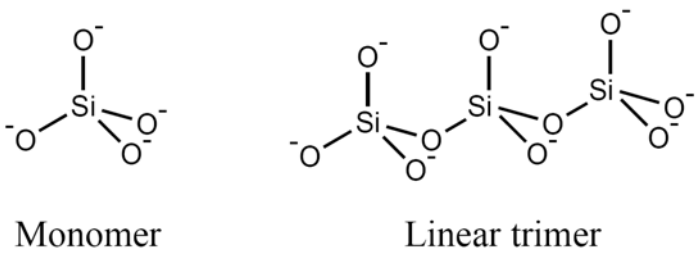

Figure 45. The structure of linear silicate anions is shown. When not linked to another silicon through tetrahedral coordination, oxygen atoms are associated with a hydrogen, potassium or sodium atom.

The tetrahedral monomers can be linked together through shared oxygen atoms and thus are represented as SiO_2 instead of SiO_4. Beside linear structures, cyclic planar and three dimensional anions can be formed as presented in Figure 46.

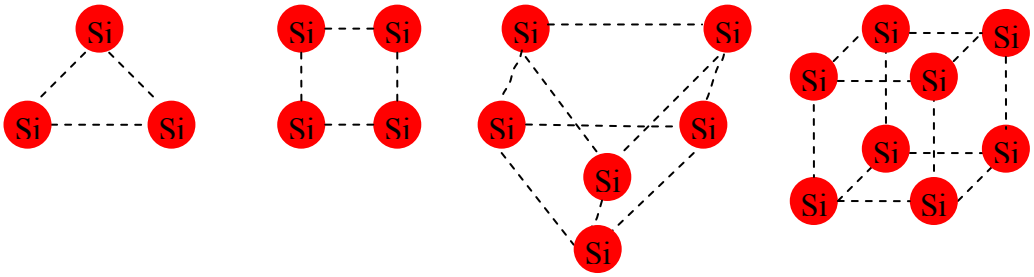

Figure 46. Schematic representation of simplest silicate anions. From left to right: cyclic trimer, cyclic tetramer, prismatic hexamer and cubic octamer. The silicon atoms are linked by oxygens atoms, which are not shown for visual clarity.

In the silicate solution, the electrical charges of the silicate anions are balanced by the sodium and potassium cations. The two major factors affecting the distribution of different anion forms presented in Figure 45 and Figure 46 are the ratio of silica to alkali and the concentration of the solid fraction in the solution [108]. When moving from high alkali content to low alkali content (see Figure 47), the amount of monomers decreases and amount of large complex structures increases, whereas the concentration of intermediate structures like those presented in Figure 46 go through a maximum (green line) and then fall after a ratio of 2.0.

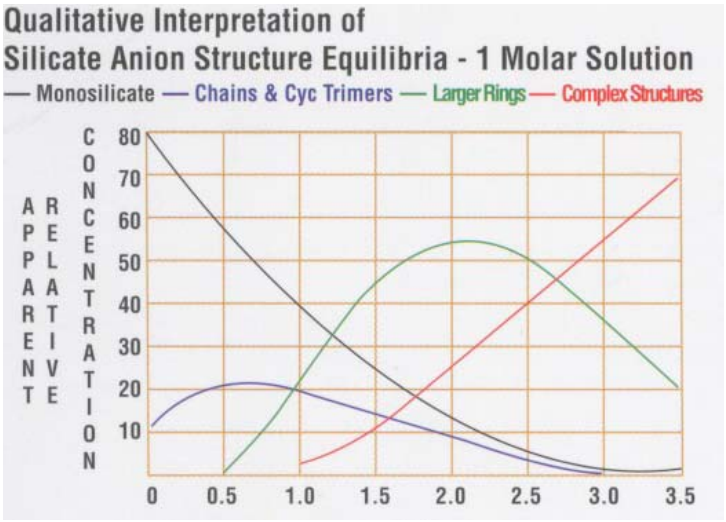

Figure 47. Apparent relative concentration of silicate anions at different molar ratios SiO_2:M_2O [108].

Above a silica to alkali ratio of 2.0, colloidal structures start to form a solid precipitant in the solution [108]. With even higher ratios, gelling of the solution will take place. When the solid fraction increases (for example by drying), redistribution of anionic forms will favor large complex structures until all the silica anions are cross-linked.

With a change in ratio of silicate to alkali content and with a change of concentration of the solid fraction in solution, the distribution of anion types (monomers, complex structures and anything in between) changes. When diluting the original solution from manufacturer, the concentration of the solid fraction is changed. According to manufacturer of KASIL® 2130 (PQ Corporation and National Silicates, Valley Forge, PA, USA), it takes more than 48 hours at room temperature with stirring in order for silicate aggregations to re-speciate. Time should be given for the solutions to rearrange, at slow stirring, instead of making the fresh dilutions and spinning the solutions right away, as was done when bonding the devices with the optimized layout described in 2.3.10 on page 77. Since the rearrangement of silica anions is a time-dependent process, it can explain why some microsystems from the same batch would sometimes work in contrast to others; the difference is probably caused by the changes in the silicate solution taking places during the time delay between bonding the different devices from the same microfabrication batch. The time from dilution of a silicate solution to its spinning on the microsystem is an important factor, responsible for the different distribution of anion species and thus the varying properties of the condensed layer.

Another important factor is the viscosity of the solution while spinning a layer of silicate for subsequent bonding. For the KASIL® 2130 potassium silicate we were using, a change of the solution temperature from 20 ºC to 25 ºC will cause the viscosity to change by almost a factor of 3 (it drops from 1050 to 370 centipoises). Daily fluctuations of the outside temperature could impact the lab temperature by a degree or two, resulting in viscosity changes and thus in a different layer thickness using the same spinning conditions.

Reproducibility of porous silicate bridge performance may be improved by using another KASIL® product with molar ratio SiO_2:M_2O close to 2 to avoid dilution. Although the etching and bonding of microsystems were carried out just in a fume hood in an ordinary chemical lab, it is advisable to the reader to use clean room conditions during the bonding step to ensure proper humidity and temperature control. It is important to allow the condensation of the silicate in the bonding layer to take place at temperatures below 100 ºC for some time to avoid boiling of the water within the forming porous sol-gel layer. After the condensation/drying step, it is important to cure the bond at above 100 ºC to ensure the stability of the resulting porous structure. For the bonding of the microsystems used for protein preconcentration presented earlier in this thesis, the first curing step was performed at 90 ºC for 2 hours and then the oven temperature was gradually ramped up to the 200 ºC and left overnight.

The current measured through the preconcentrator as a function of potential applied on preconcentrator reservoirs is shown in Figure 48. The current measurements were performed on microsystems bonded under different experimental conditions: By direct hot bonding (black trace), Using silicate solution KASIL® diluted with deionized water at the ratio 1:10 (red and blue traces) and at the ratio 1:50 (green trace). The gradually increasing voltage was applied at the preconcentrator reservoirs while the sample reservoir was grounded and all other reservoirs floated during the measurements. All the reservoirs and microchannel networks were filled with the BioRad® CE-SDS run buffer for sieving electrophoresis of proteins. The microsystems bonded with 1:50 diluted KASIL® (green trace) demonstrated slightly higher currents compared to 1:10 diluted KASIL® (blue trace) indicating that the resistance is lower in the preconcentrator created with 1:50 diluted KASIL®. The observed lower resistance of the devices bonded with 1:50 diluted KASIL® solution is speculated to be due to larger pore size or due to the presence of significant voids in silicate structure because of the 5 times higher dilution ratio of silicate (1:50 compared to 1:10 times diluted). The microsystem bonded using direct high temperature technique (black trace), demonstrated currents slightly above these measured for KASIL®-bonded microsystems, meaning even lower resistance in the preconcentrator. The interesting observation was that preconcentrators on some microsystems bonded with help of 1:10 diluted silicate solution (KASIL®), would not exhibit any conductance at applied potentials below 1 kV (see Figure 48, lower red trace). When applying an electric potential above 1 kV, the physical damage to the preconcentrator structure typically happened, where a little piece of the glass wall between the separation network and preconcentrator network would chip-off, visible under the microscope. Once such a break-through happened, the conductance of the preconcentrator is observed, through the opening in the preconcentrator wall where a defect is created. The measurement of current as a function of voltage for the same microsystem after the breakthrough damage happened is shown in Figure 48 as the upper red trace.

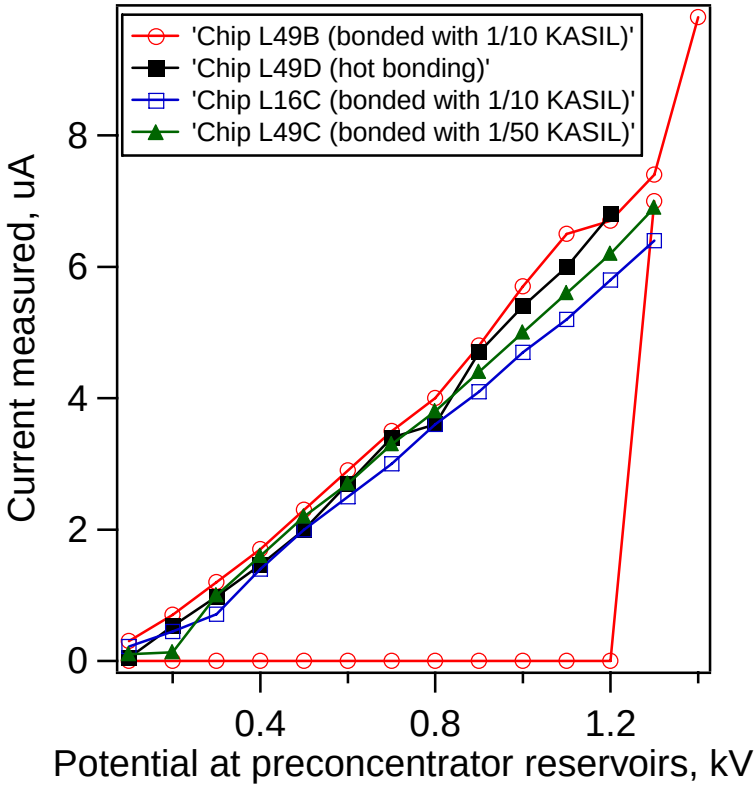

Figure 48. The current measured through the preconcentrator as a function of applied potential. The different traces represent microsystems bonded under different conditions: Hot bonding (black squares); KASIL® solution diluted 1:10 with deionized water (blue squares and red circles); KASIL® solution diluted 1:50 with deionized water (green triangles). The two traces presented with red circles are for a microsystem bonded with 1:10 diluted KASIL® which to begin with had no electrical contact over the preconcentrator (lower trace) but the breakthrough across the preconcentrator occurred at potential of 1.2 kV (see the lowest trace) and the curve measured again after the breakthrough (see the highest trace). For all microsystems, the channels were filled with BioRad® CE-SDS run buffer for sieving electrophoresis of proteins. The physical dimensions of the microfluidic channels were as presented in Figure 5.

Generally, physical damage of the silicate layer and the glass wall between adjacent channels at the preconcentrator was observed at potentials above 1.3 kV on any microsystem, independently of the bonding method and initial resistance in the preconcentrator. The damage could be observed visually and made the microfluidic system not suitable for the preconcentration of the sample. For all the preconcentration experiments presented in this work, the preconcentrator was formed using 1:10 diluted KASIL® 2130 solution since this recipe had the best overall success rate per bonding and preconcentrator performance.

2.3.12 Alternative chemistry for sol-gel filters

Due to the problems with the porous preconcentrator made using KASIL® 2130 silicate, other approaches for fabricating sol-gel filters on-chip were investigated. Silica gels were prepared

by hydrolysis and subsequent condensation of either tetraethoxysilane (TEOS) [109] or tetramethoxysilane (TMOS). Fidalgo et al. [109] suggested in their work to separate hydrolysis from condensation reaction in time by pH control. At pH =1.88, the hydrolysis is fast and condensation is slow. After completion of hydrolysis, the pH was raised by adding ammonium hydroxide in order to perform condensation of the gel.

In order to create the porous material, the initial solution with a molar ratio of TEOS (or TMOS) to H_2O and to 2-propanol of 1.0/4.0/9.2 was hydrolyzed using molar ratio of HCl to TEOS (or TMOS) of 0.003, for 60 min at 60 ºC under stirring at 140 rpm. For the condensation step, NH_3OH was added at a molar ratio to TEOS (or TMOS) of 0.7. These conditions were selected in order to achieve the porosity of 65% with an average pore diameter of about 3 nm (for TEOS) as reported by Fidalgo et al. [109]. Immediately after raising the pH, the solutions were spin coated on a glass cover plate and bonding of the microsystem devices was performed by bringing the cover plate and substrate in contact while applying pressure.

Unfortunately, the condensed nanoporous silica using either TEOS or TMOS appeared to be a very fragile material and did not provide the strong bonding between two glass substrates.

2.3.13 Micro-nano junction approach

The concept of using a junction between micro and nanochannels as a preconcentrator for large biomolecules was investigated empirically by using a microsystem where instead of the porous layer junction, an array of nano channels was created between two microchannels. The schematic of the close-up of preconcentrator area is presented in Figure 49. The nanochannels were fabricated by e-beam lithography. In the array of 8 channels, one pair had the width and depth of 500 nm, the other pair of nanochannels was 300 nm wide and 300 nm deep, the third pair had the width and depth of 100 nm, and the last two channels were 50 nm by 50 nm. The entire microsystem was filled out with the BioRad buffer with 1x Sypro Orange® dye, and the sample of 0.1 mg/ml total protein content of Dalton Mark VII was used to perform visualization of preconcentration using the array of nanochannels. Nanochannels with dimensions of 50 nm deep and 50 nm wide were preconcentrating for a limited period of time (from couple of seconds up to couple of minutes), then a break-through of sample is observed. The break-through of sample through even for the smallest nanochannel (50x50 nm) occurred even for the field strengths lower than 100 V/cm in the nanochannels. This finding was not surprising taking into account that in an unfolded state, the largest protein present in Dalton Mark VII sample (albumin) is approximately 10

nm in diameter, and the other proteins are being smaller than this. However the unfolded (denatured) protein is like a long thread where the diameter of the chain is merely the size of the amino acid residues in the sequence.

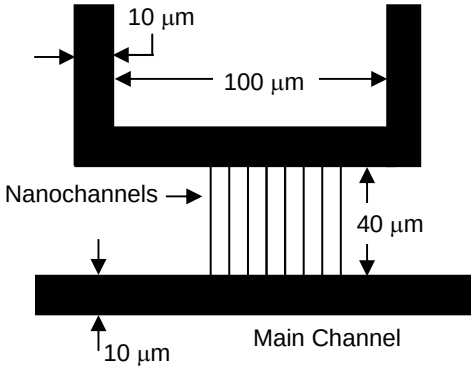

Figure 49. Nano-micro junction preconcentrator region fabricated using focused ion beam. Eight nanochannels (two with dimensions 500x500 nm, two 300x300 nm, two 100x100 nm and two 50x50 nm) were created between two adjacent microchannels with depth of 5 μm [110].

These experiments still left the hope that, with a smaller nanochannel dimension, the intersection between nano- and microchannel would function as a salt bridge, only letting the small buffer ions to get through and capturing the protein molecules.

It was decided to fabricate the smallest nanostructure possible by the means of standard glass microfabrication methods that were already available to the group, and test such a nanostructure for suitability for preconcentrating. By selecting this approach, we run into the acute question in the rapidly growing nanotechnology field, as such - what would be "traditional" glass microfabrication methods' limits for a nanosystem, without expensive instrumentation such as e-beam lithography and even without the need for a clean room? Our interest is still to work with reliable, inexpensive techniques which can be employed for high-throughput mass production. The limitations in channel depth that could be measured using the profilometer was established to be 2 nm so that the etched nanochannels still could be detected above the surface roughness. However the bonding step forced a lower limit of around 10-15 nm since the nanochannels shallower than that collapsed during the bonding step.

Microsystems with simple cross layout (Figure 50), containing both nano and micro channels were fabricated by using a single mask but with a two etching steps process.

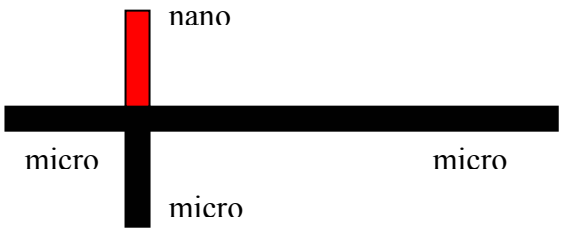

Figure 50. Nano-micro junction device for preconcentration. A simple cross microsystem is combining nano deep channel (red) and micro deep channels (black).

The whole channel network was first etched in dilute etching solution to a depth of nanometers. For this step, a 1:15 dilution of the stock Buffered Oxide Etch (BOE) (Transene, Danvers, MA, USA) in deionized (DI) water was used. The stock BOE solution consisted of 4% HF and 36% NH_4F in DI water. Etching times vary depending on the temperature and how long the solution has been used for etching other chips. The etching rate of the 1: 15 diluted BOE was 7.15 nanometers per second at 22 ºC.

To preserve the nanometer depth of one channel, it was covered by liquid photoresist up to the intersection by applying photoresist locally with a clean room swab and dragging the viscous photoresist to the very end of the covered channel creating a well-defined cut-off at the intersection. After baking the freshly deposited photoresist at 90 ºC for 30 min and then at 110 ºC for 10 min, the remaining channels were further etched to the desired micrometer depth. The access holes were then drilled through the substrate while the nanochannel was still protected by the photoresist layer. The photoresist was then stripped off in acetone and the adhesion layer (chrome) for the resist was etched away using Chrome etchant (Transene, Danvers, MA, USA). After the surface treatment of both substrate and a cover plate, bonding was performed by a novel direct bonding technique. This bonding technique was developed by Dr. Nickolaj J. Petersen and is currently being patented by Professor J. Michael Ramsey's group.

By using the nano-micro junction approach instead of a porous bridge for preconcentration of the sample, the whole microsystem including the preconcentrator can be fabricated without need for a clean room, without a device-to-device reproducibility problem. The characterization of the nano-micro preconcentrator is currently being investigated.

3 Field-assisted (anodic) bonding for glass microsystems

In order to obtain a good yield in fabricated microchips, a new fabrication process for bonding a borosilicate glass substrate to a borosilicate glass cover plate was developed at MIC. In this chapter, a successful adoption of field assisted (anodic) bonding for packaging a glass substrate with a glass cover is demonstrated. While anodic bonding is being a standard approach in silicon wafer technology, experiments presented in this thesis were the first demonstration of its applicability to glass-to-glass bonding of microfluidic systems. The presented approach involves a sputtered polysilicon layer to facilitate the anodic bonding.

First, a motivation for using glass as material for microsystems is presented in the introduction, followed by the discussion of packaging challenge. The mechanism of field-assisted bonding for concealing (often referred to as "packaging") the microsystems is described.

In the experimental part, the schematic of the necessary equipment (anodic bonder) is presented and the fabrication sequence and the experimental conditions for the anodic bonding are described. The methods used to evaluate the bond strength are presented, as well as the methods used to evaluate the performance of bonded devices.

In the results and discussion part, the bond strength is discussed. The conductivity measurements performed to ensure compatibility of semi-conductive amorphous polysilicon layer with high potentials used in electrophoretic applications of microfluidic glass devices are presented. The anodic bonding is compared to fusion bonding for glass-to-glass packaging in terms of requirements.

In conclusion, the advantages of the anodic bonding for glass-to-glass packaging are summarized. The possible applications for the developed method are suggested.

3.1 Theory for Anodic Bonding of all glass devices

The developed bonding method for glass-to-glass was adopted from the traditional silicon-to-glass anodic bonding and involves an amorphous layer of sputtered polysilicon as a mediator.
The methods for patterning and etching of glass microfluidic channels are also adapted from silicon microtechnology [111-113]. Similarly to silicon microfabrication, the layout of the channel network is defined by using photolithographic processes, as presented in Figure 51. A polysilicon or chrome layer is first deposited to enhance adhesion of the photosensitive material (photoresist) to the glass surface (Figure 51a). Photoresist is then spin coated on the substrate in a layer typically 1 – 4 μm thick (Figure 51b). After UV exposure of the photoresist through a mask, development (dissolution)

of the resist is performed (Figure 51c). The adhesion layer is then removed from the channel network (Figure 51d) defined in photoresist during the developing step. The glass substrate is etched using the photoresist and adhesive layer as an etch mask (Figure 51e). When the desired channel depth is obtained, the photoresist layer is dissolved (Figure 51f). Traditionally, the adhesion layer is then removed and bonding of substrate to a cover plate is performed by high temperature bonding which typically has a low yield of the bonded devices and requires temperatures above 550 ºC for several hours. To obtain closed channels that are used in the majority of lab-on-a-chip microfluidic devices, bonding of a cover wafer is required. Wafer bonding is thus a fundamental but also crucial part of a typical microfabrication process [114].

The novelty of the microfabrication approach presented in this thesis is that polysilicon is selected as the adhesion layer. This polysilicon layer is not removed after patterning the microchannel network but used as an assistant layer for subsequent glass-to-glass bonding (Figure 51g). This method is an adaptation of silicon-to-glass field assisted (anodic) bonding widely used for packaging of micro electro mechanical systems (MEMS). It has the advantages of being simple, reproducible, cheap and relatively fast. The developed procedure also allows avoiding the step needed to strip the adhesion layer for the photoresist, making the microfabrication procedure less complicated.

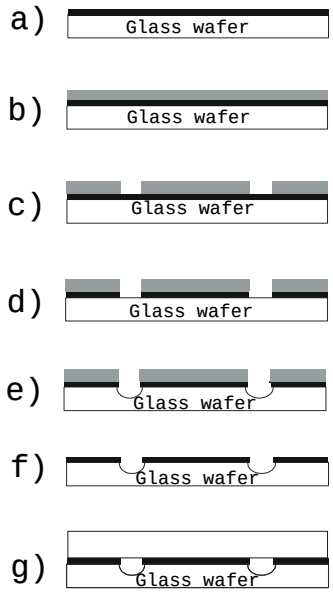

Figure 51. Schematic view of the process sequence for fabrication of anodically bonded glass microdevices. (a) Sputtering of a 100 nm polysilicon layer; (b) Spin coating layer of photoresist; (c) Exposure and development of the photoresist; (d) Etching of the channel pattern in polysilicon layer; (e) Etching of the glass; (f) Strip-off the photoresist; (g) Sealing the channels by anodically bonding with a cover plate.

Anodic (or electrostatic) bonding is a field-assisted thermal bonding technique used typically to bond a structured silicon substrate to a borosilicate glass cover plate in MEMS [115, 116]. The mechanism of anodic bonding is sketched out Figure 52. The ability to carry an electrical charge in glass is a function of the alkali concentration (sodium and potassium ions) in the glass.

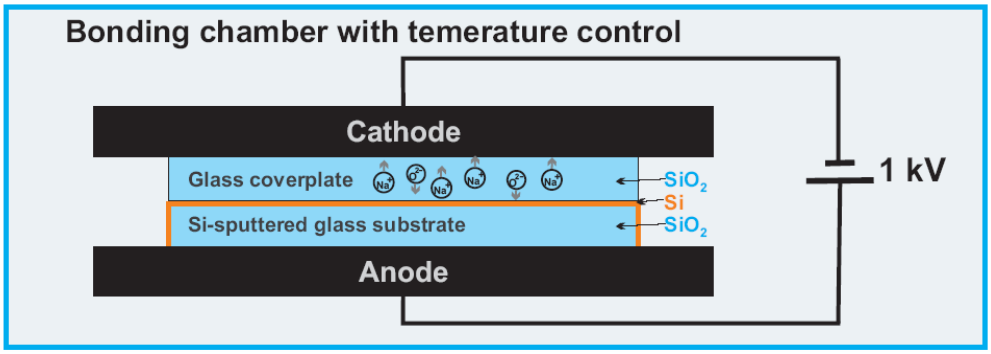

Figure 52. The basic principle of anodic bonding of two glass wafers is sketched. It is important that polysilicon is sputtered both on the top surface and the side edges of the substrate wafer, providing electrical contact with the anode.

For example, fused silica does not contain conducting impurities like potassium and sodium, which make it unsuitable for anodic bonding. The migratory effect of alkali ions in glass combined with increased mobility at elevated temperatures result in the glass being able to carry or pass a charge. Two glass substrates can not be anodically bonded without the use of an intermediate conductor or semiconductor layer.

An anodic bonder basically consists of a temperature controlled chamber and two electrodes. The assembled wafer pair is placed between the electrodes and an electrical field up to 1 kV is applied across the wafers. The cover glass is biased negatively with respect to the silicon sputtered substrate serving as the anode.

At high electrical field and raised temperature, sodium ions (Na^+) in the Borofloat® glass substrate will start to migrate towards the cathode and oxygen ions (O^{2-}) will migrate towards the anode (the Si- sputtered substrate). In the interface between the two substrates, oxidation of silicon to silicon dioxide is expected to occur and the electrons are transferred to the electrode:

$$Si + 2O^{2-} \Rightarrow SiO_2 + 4e^-$$

The oxidation of surface layer of the sputtered polysilicon thereby establishes a glass-glass bond between the two wafers.

3.2 Anodic Bonding: Experimental

The process sequence for fabricating the microfluidic structures on glass substrates was performed as sketched out in Figure 51. A polysilicon layer with a thickness of 100 nm was sputtered on the glass substrate (Borofloat® from Valley Design, Santa Cruz, CA, USA) using a cassette sputter system from Varian, Inc. (Palo Alto, CA, USA) and used as an adhesion layer for photolithographic definition of the channel network. The channels were etched in 40 % hydrofluoric acid (HF) to a depth of 12 μm and afterwards the photoresist has been removed. The polysilicon layer was left in place for the anodic bonding process.

For etching the through holes in the cover plate, the cover plate substrate was first laminated with a high chemically resistant polymer film (Cleantack Cleanroom Tape, Static Specialists Co., Inc., New York, USA). The polymer film was removed (ablated) locally by a carbon dioxide laser (DuoLase® from Synrad, Inc., Mukilteo, Wa, USA) on one side of the substrate where the desired access wholes were to be etched. The access holes were etched through the substrate in 40 % HF, and afterwards the polymer film was removed. It is not possible to use the photoresist as an etching mask for etching the through holes or more generally, for etching for extended periods of time because of the limited resistance of photoresist to HF solution. For example, to etch a through hole in 0.6 mm thick substrate at the rate of 3 micron per minute, the substrate should be immersed in HF solution for 100 minutes (when etching is done from both sides simultaneously). Typically, after 25 minutes in 40% HF, the photo resist layer would completely fall off the device, even when 4.2 micron thick layer of photo resist was applied and re-baked for higher stability.

The anodic bonding with polysilicon intermediate layer (Figure 51g) was performed in an in-house built setup sketched out in Figure 52. After the placement of both wafers between the electrodes, the chamber was hermetically sealed with the lead. To avoid an electric shortcut through the air gap in between the electrodes, and to prevent the oxidation of electrodes at elevated temperatures, the bonding chamber was purged with nitrogen twice. Then the temperature was ramped up from room temperature to the bonding temperature of 350 ºC. Once the desired bonding temperature was reached, the electrical potential applied at electrodes was gradually increased to 1 kV. After keeping 1 kV for 10 min, the electrical field was turned off and the temperature was brought back to room temperature.

The quality of the anodic bonding was tested by visual control in infrared light, where the maximum resolution of the IR camera was approximately 100 μm, allowing to see only the defects at the bonding surface large than 100 micron. The bond strength test was performed using the

razorblade technique [117, 118]. For this test (also referred to as Maszara method), a thin blade is inserted between the bonded glass wafers until cracking occurs. The length of the crack between the wafers is then evaluated using infrared camera in order to calculate the surface energy.

The compatibility of anodically bonded CE microchips with high voltages was tested by filling the reservoirs and microchannels with 10 mM tetraborate buffer (pH 9.13) prepared from disodium tetraborate decahydrate (Merck, Darmstadt, Germany). For the high voltage test, potentials have been applied between the sample and overall waste reservoirs with 500 V steps up to 4 kV while the current was monitored (Figure 53).

The numbers for surface roughness requirements in Table 5 were determined using atomic force microscope. The wafer curvature tolerance numbers were measured using a profilometer from KLA Tencor, San Jose, CA.

3.2 Anodic Bonding: Results and discussions

The bond formed by anodic bonding was typically stronger than either of the two materials and an attempt to break the bond resulted in fracture of either the glass substrates or the silicon layer. Anodic bonding was found to be more efficient than direct fusion bonding in terms of gapping over defects and particles due to the wafers being electrically pulled together during the bonding process.

With direct fusion bonding the success rate was found to be dependant on the area of the microchip. The smaller the area of the device to be bonded, the higher was the chance to get a properly bonded microsystem without leakage. No dependence on the bonding area was found for the yield of field-assisted bonding. The large wafer was as easy to bond as the smaller devices. This makes anodic bonding a favorable packaging method for especially large foot print glass wafers.

Typically, with a large particle present in between two glass plates, the area around the particle with no bond can be seen by the naked eye by the presence of Newton's rings. Newton rings are concentric rings pattern of rainbow colors produced by interference of light waves that are being reflected at glass/air and air/glass interfaces.

An inspection of the anodically bonded wafers with infrared light was performed to ensure bonding occurred without any voids. Infrared transmission is widely used for evaluating the bonding quality of a pair of silicon wafers where visual inspection can not be performed due to the non-transparency of the silicone wafers. It allows to see voids larger than 20 to 30 μm. Infrared imaging is a fast and simple way of evaluating bonding quality compared to other imaging

alternatives like ultrasonic and X-ray topography. For glass-to-glass bonding, the infrared investigation did not uncover voids others than those observed visually.

The bond strength test which was performed using the razorblade technique [117, 118]. When increasing force was applied to two glass wafers bonded anodically with polysilicon as an intermediate layer, the crack was appearing in the bulk of one or another glass substrate instead of cracking along the bonded surface. It showed that the surface energy of anodic bonding was equal to or exceeded the mechanical strength of the material. According to the manufacturer of the Borofloat® wafer, the Young's modulus (the ratio of the tensile stress in the material to the corresponding tensile strain) is 64 kN/mm^2 and the Knoop's hardness (ratio of load applied by a diamond indentation tool to the area of indentation) is 480 kg/mm^2.

For investigation of applicability of the polysilicon-mediated glass-to-glass bonded microsystems for electrophoretic separations, a breakthrough voltage test was performed (Figure 53). The voltage potential was applied between the sample reservoir and waste reservoir, the channel length between reservoirs was 7.3 cm. The channels were filled with 10 mM borate buffer.

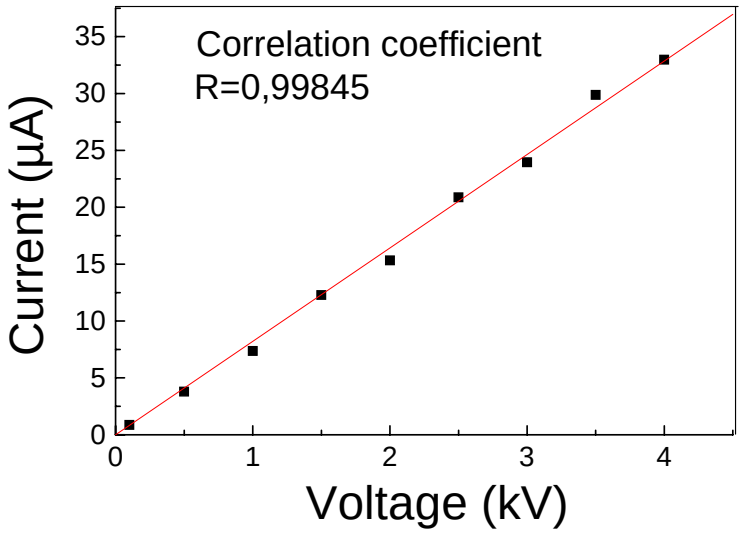

Figure 53. Current-voltage characteristic of a bonded glass microsystem with a 100 nm thick polysilicon intermediate layer. The voltage potential was applied between the sample reservoir and overall waste reservoir. The 12 µm deep microchannels were filled with 10 mM borate buffer. Channel length between reservoirs was 7.3 cm.

It can be seen that the current increased linearly with the applied potential and no electrical breakthrough happened up to 4 kV applied, which is a typical output used for most microchip separation procedures.

The sputtered polysilicon layer fulfills three requirements in preparing microchips. First, it can be successfully used as an adhesion layer for the photoresist to withstand etching in 40% HF.

Without an adhesion layer, a lift off of the photoresist starts to occur after etching to a depth of about 3 μm, causing surface defects and a severe under-etching at the top of the microchannels. Second, the polysilicon layer enables anodic bonding. Finally, it has a lower conductivity then the conductivity of the buffer solution and thus doesn't affect the separation performance of the device. Sputtering of polysilicon is furthermore a fast process that can be done in a cassette deposition system ensuring high throughput. Anodic bonding is also compatible with potential integration of metal electrodes due to the relatively low temperature used for bonding. The parameters of field-assisted anodic bonding in comparison with fusion bonding in terms of surface roughness requirement, wafer curvature, typical bonding temperature and suitability of bonding method for quartz are summarized in Table 5.

Table 5. Comparison of requirements for fusion and anodic bonding

	Fusion bonding	**Anodic bonding**
Surface roughness	< 1 nm	< 1 μm
Wafer curvature	< 10 μm	< 300 μm
Bonding temperature range	560-650 ˚C for Borofloat®	200-400 ˚C for Borofloat®
Compatible with quartz wafer	Yes	No

As can be seen from the Table 5, lower requirements on surface roughness and wafer curvature are the main advantages of anodic bonding compared to temperature fusion method. Anodic bonding tolerates particles and surface defects up to 1 μm in size, while for fusion bonding the glass surface should have very flat smooth surface with surface roughness not exceeding 1 nm. Wafer curvatures of up to 0.3 mm can be overcome by anodic bonding, where wafers are pulled together during bonding with help of an electrical potential applied, compared to the requirement of typically under 0.01 mm curvature for fusion bonding. With the identical wafer cleaning procedure, the yield rates of successfully bonded microfluidic devices were 12.5% for fusion bonding (only 1 out of 8 wafers contained a properly bonded device) and 95% for anodic bonding (19 out of 20 bonded wafers contained a properly bonded useful device).

3.3 Anodic Bonding: Conclusions

Summarizing advantages and disadvantaged on field-assisted/anodic bonding:

- Anodic bonding was successfully adopted for glass-to glass bonding, using polysilicon as an intermediate layer.
- It provided hermetic seal for the microfluidic systems.
- The anodic bonding resulted in bond strength higher than the fracture strength of the glass substrates.
- The quality of the bonded area could easily be accessed by a visual inspection.
- It was established that the presence of a semi conducting polysilicon layer does not interfere with electrokinetic operation of microfluidic system.

The main advantage of the anodic bonding for glass microsystem fabrication is its high tolerance to particle contamination and glass wafer surface roughness. The electrostatic field generates a high clamping force which overcomes these surface irregularities. In turn, surface defect tolerance results in high yield of well-bonded devices.

The additional advantage is the relatively low temperature used for the anodic bonding of 150 to 350 ºC. No measurable flow of the glass occurs at these temperatures, allowing sealing around micromachined grooves and cavities without any loss of dimensional tolerances, and keeping the original dimensions and profiles unchanged.

4 Electrophoresis chip with monolithically integrated needle for electrospray ionization

In this chapter, the introduction to ionization techniques suitable for coupling microsystems with a mass spectrometer is given. Design and fabrication of a novel monolithically integrated electrospray needle is described. In results and discussion subchapter, the monolithically fabricated needle is presented and the different aspects of needle pulling are discussed.

4.1 Introduction to ionization techniques

Ionization of analytes is required when using mass spectrometry as a detection method for on-chip processing and separation. Mass spectrometry is an attractive detection method because of its' high sensitivity and the possibility to obtain structural information about the analytes. Mass spectrometry instrumentation performs separation and analysis of gaseous ions according to their mass to charge ratio. Thus to use MS as a detection method in proteomics, it is necessary to transfer the large protein molecules into gas phase ions. Introduction of ionization methods such as electrospray ionization (ESI) [119, 120] and matrix assisted laser desorption ionization (MALDI) [11, 12] have made mass spectrometry a routine method for analysis of protein samples.

The general requirements to an optimal electrospray-MS interface are:

- It should cause no reduction in separation or mass spectrometer performance
- No uncontrolled chemical modification should occur at the interface
- Providing high sample transfer and high ionization rate, especially for analytes at trace level concentrations, polar or labile ones
- User-friendly and reliable
- Possess no chemical background interfering with analytes
- Inexpensive
- Possibility of operating in a broad range of flow rates (from tens of nanoliters to hundreds of microliters per minute).

An extended review on MALDI as an ionization method for proteins and peptides coupled with various MS instruments has recently been published by the Center of Experimental Bioinformatics in Odense, Denmark [121]. The authors [121] underline that both MALDI and ESI methods have drawbacks and strengths and are complimentary to each other in proteomic applications. MALDI is not as affected by the presence of salts and detergents in the sample as electrospray and currently MALDI allows higher throughput and automation of sample preparation.

The main application of MALDI today is identification of pre-separated proteins and peptides, with complexity of mixtures up to 10 proteins in each spot.

However, when dealing with complex samples such as cell extracts or digest products of a single cell proteome, the more laborious and lower throughput electrospray ionization (ESI) is more attractive due to the possibility of direct coupling it with a prior separation [122].

ESI produces gas phase ions at atmospheric pressure from a continuously flowing liquid stream and thus is compatible for "on-line" ionization of CE separation products in liquid phase. When an electric potential (typically in the range from 500 V to 3 kV) is applied between an electrospray tip and an orifice of a MS instrument, formation of charged droplets from the Taylor cone at the end of the tip takes place. In ESI, unlike the other ionization principles, the analyte must posess an ionizable group in order to be transferred to the gas phase ion. Less electronegative groups that are not ionized in the solution might be ionized by attaching a proton in the gas phase. In electrophoretic separations, all the analytes have an ionizable group except from neutral ions following the electroosmotic flow (EOF). By applying intense electric field strength at the spray tip, the charge distribution is introduced to the solution, and at high enough field strength, the liquid will break up into a jet of droplets. In order to stabilize the spray with high flow rate (up to 100 µl/min), a high velocity gas can be applied to assist the ESI nebulization of the solution. Due to the applied field strength, the formed droplets will possess an excessive charge and will move towards the counter electrode. Because of the charge repulsion between the droplets, the spray will expand. Evaporation of solvent leads to a shrinking of droplet size and thereby causing an increase in the surface charge density. The droplet divides or ejects charged molecules to reduce surface charge density thus yielding a stable jet of small droplets. This happens at a point called Rayleigh limit, where the Coulumbic repulsion exceed the surface tension causing the droplet to disintegrate. The process continues for the newly formed droplets until their radius has decreased to 1-8 nm as described by Kebarle in 1993 [123]. The final step, how exactly the gas-phase ions are being produced from the charged droplets, is uncertain. There are two main theories that are trying to explain the gas-phase ion formation. One theory is "single ion in the droplet" and the other one is called "ion desorption model". In the "single ion in the droplet" theory, the Coulomb explosions (called "fissions" in some literature) are assumed to proceed until there is only a single charged ion in each droplet. The "ion desorption model" is based on an assumption that a point where Coulombic repulsion exceeds the adhesion of the charged species to the surface of the droplet and

therefore the charged species are expelled from the droplet, as described by Enke et al. in 1997 [124].

Depending on polarity of the electrical potential applied at the ESI interface, the droplet can contain an excess of positive ions (positive ESI mode), resulting in protonated molecules or other positive adducts, or an excess of negative ions (negative ESI mode), resulting in de-protonated molecules.

In order for the analytes to be transformed to gas phase ions by ESI, the analyte has to have an ionizable group. Proteins produce a series of multiple charged ions, making ESI even further advantageous for proteomic applications. Multiple charged ions allow determination of compounds with molecular weights exceeding the mass to charge limit of the MS instrument. The average charge states of the proteins in ESI is observed to increase approximately linearly with the molecular weight [125] and the resulting m/z is therefore likely to be in the range of the MS detection method even for proteins with a high molecular weight [126]. In terms of quantitative measurements multiply charged ions are not favorable since the signal is spread over the wide range of tops masses, reducing the S/N ratio. This reduction of S/N can be partly compensated for by adding the ion electropherograms corresponding to the different charge states of the analyte into a single electropherogram.

ESI is a soft ionization technique, leaving protein molecular ions intact [127] although fragmentation can be achieved during transport into a MS by using a high cone voltage [128].
The interfaces for CE-ESI-MS differ in the way they provide the electric contact to the tip used for both the separation and ESI and how they stabilize the spray. Examples of the interfaces are sheath flow, liquid junction and sheathless (Figure 54).

These interfaces are “working horses” for coupling liquid chromatography and conventional capillary electrophoresis to MS. The original work demonstrating CE-ESI-MS using a sheathless interface is described in [129], where authors use etched fused silica tips with a metal coating. To overcome technical difficulties authors encountered with a sheathless design (due to an inefficient tip design), the same group combined CE with a coaxial liquid sheath flow to improve stability by increasing the flow rate [130] however at the expenses of sensitivity. In later publications, the authors returned to a sheathless interface design to improve sensitivity [131], where they presented a novel type of sheathless interface with electrical contact provided through a piece of micro dialysis tubing, which also gives an opportunity for post-column chemistry modification.

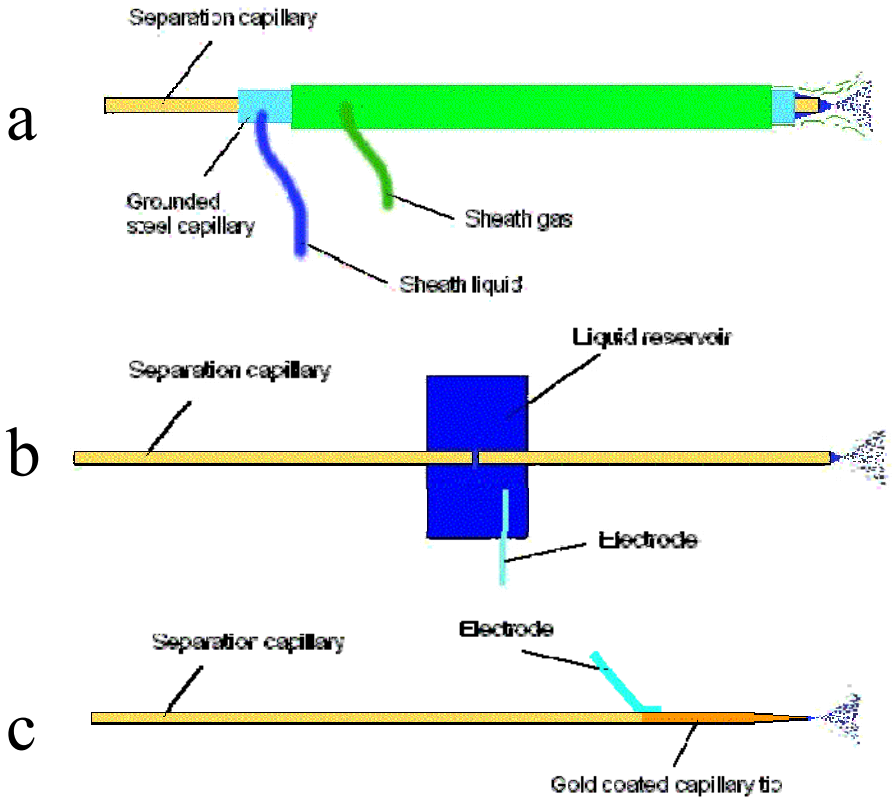

Figure 54. Different CE-ESI-MS interfaces: a) sheath flow; b) liquid junction; c) sheathless. On figure a), the metal capillary is working both to supply a coaxial flow of the sheaf liquid and also as the electrode.

Different fabrication approaches of microchip needles/nozzles are reviewed in [2]. The approaches can be categorized into three main groups: Spraying directly from the edge of a chip at the channel outlet, Using an inserted tip, or Spraying from microfabricated nozzles. The main problems with most methods in creating an on-chip electrospray tip are dead volume formed at the needle joint and stability of the spray. A dead volume along the microflow increases band broadening and decreases separation efficiency [132, 133]. Dead volume is especially problematic for microchip analysis because channel dimensions and respectively the injection volumes are very small. Spray stability depends on the electric field at the tip of the needle, which in turn depends on the sharpness of the needle edge and the geometry of the channel and its opening radius. Using a direct spray from the channel outlet, it is challenging to prevent the Taylor cone from expanding and moving across the edge of a chip, even with hydrophobic materials applied around the outlet. This problem with confining the Taylor cone inspires the second approach, to insert/attach a capillary at the channel outlet. However an extra dead volume issue is introduced by this approach and the ways to attach the spray tip are generally not suitable for mass production of microfabricated devices. Microfabricated nozzles for the electrospray integrated onto microfluidic

system are also reported. DiagnoSwiss and Girault's [134] group use microchannels that are plasma-etched or photoablated in a tip shape cut PET (Polyethylene Terephthalate) or polyimide foils. Other groups have demonstrated microfabricated integrated nozzles, using Poly Dimethyl Siloxane (PDMS) [135], silicon/parylene [136], silicon dioxide [137] or silicon wafer [138]. The comparison of microfabricated monolithically integrated nozzles with conventional pulled silica capillaries demonstrated matching [137] or even a slightly better performance [138] of microfabricated nozzles in terms of sensitivity and spray stability for the peptides. It has to be noticed that both silicon and silicon dioxide nozzles were fabricated by using deep reactive ion etching (DRIE) technology. It is interesting to note that even though a stable spray has been demonstrated on chip, it is still remains a challenge to couple an efficient separation on a microsystem with the ESI-MS interfaces.

4.2 Design and fabrication of monolithically integrated electrospray needle

In this work, a novel design and microfabrication procedure for monolithically integrating a spray tip in connection with the separation channel by pulling is presented, offering the advantages of a pulled capillary but avoiding the dead volume inherited to the inserted tip approach and avoiding the use of DRIE. At the end of the separation channel, a thin glass string with a microchannel inside was pre-formed using standard photolithography and etching. The bonding was performed utilizing the novel field-assisted (anodic) bonding technique, described earlier in this thesis. The needle was then formed by pulling while heating in a manner similar to pulling the needle out of a capillary. An electric contact to the needle tip was created by depositing gold on a titanium adhesion layer. The fabrication procedure for this integrated electrospray tip for sheathless and liquid junction interface to MS was optimized and prototypes were tested [139].

The microchips for sheathless electrospray were designed featuring a simple injection cross, straight separation channel and the integrated ESI needle. The microfluidic device for liquid junction electrospray (shown in Figure 55). The side channels were placed at the end of the separation channel to create an electrical contact close to the spray tip similar to the liquid junction interface and in order to be able to adjust the electrospray by controlling the flow to the spray tip and/or adding spray modifiers to the stream. For sheathless spraying, an electric contact was provided by gold layer deposited at the outer sufrace of the ESI spraying tip, using a titanium adhesion layer.

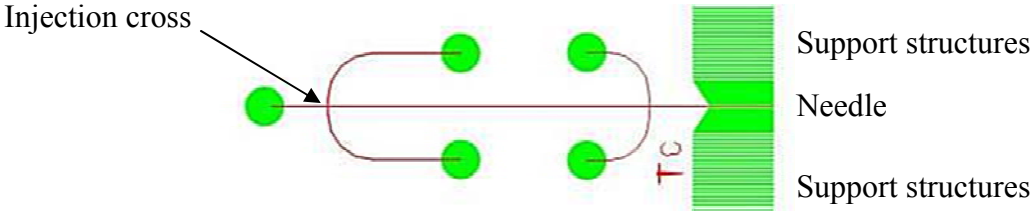

Figure 55. The layout used for the microchip with integated ESI interface and a liquid junction intersection to provide an electrical contact. The channel network was etched in two steps. First the microchannels were etched to the depth of about 20 µm. In green, the areas etched during the second etching step are shown. During the second etching, the channel network was protected by a new photoresist layer. The green pattern was etched on both the bottom substrate and the lid wafer to the depth of around 100 µm, and the microsystem wafer and the cover plate were aligned prior to bonding.

Borofloat® glass was chosen as the substrate material due to its chemical resistance and electrical insulation properties. The devices were fabricated according to the recipe presented in Appendix 8.1. Briefly, the fabrication method is sketched out in Figure 56.

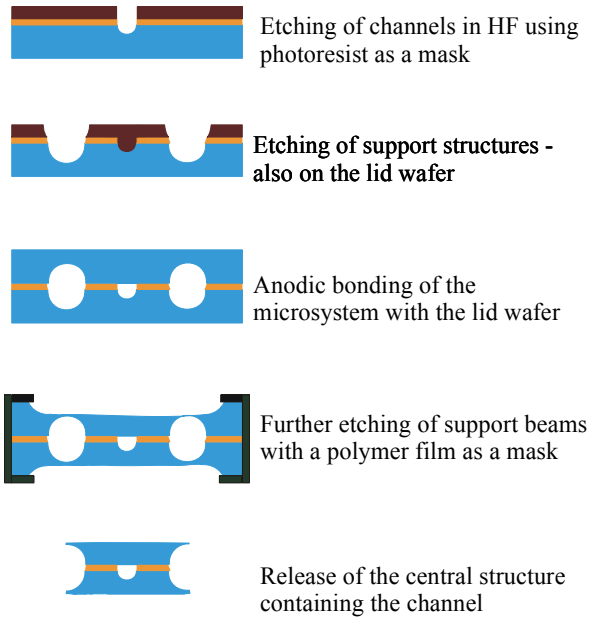

Figure 56. Fabrication sequence for a glass microsystem with integrated electrospray needle. Cross sectional drawing is shown for the area where the electrospray needle is being formed.

Two photolithography steps were involved (see Appendix 8.1). After exposure through the first mask containing the microchannel network layout, the first etching step was performed to obtain a depth of around 20 µm. The photoresist layer was then stripped off and a new resist spun on. A second photolithographic exposure was performed using a mask design containing an array of parallel channels in the area where the spray tip was to be formed. The cover plate was patterned

with the same mask containing support structures in a one-step photolithography process (see Appendix 8.1). After anodically bonding the cover plate to the substrate, further etching was performed in order to release the support structure strings according to steps 25 through 31 in appendix 8.1. The microsystems were wrapped with a polymer film (Cleantack Cleanroom Tape, Static Specialists Co., Inc., New York, USA). This polymer was then removed by CO_2 laser ablation in the areas adjacent to the future needle on both sides of the microsystem. Using the remaining polymer film as an etch mask, bulk glass around the future needle and support strings were removed by etching from the top and bottom surfaces of the chip until the needle string was released as a free standing structure. Needles were then pulled by using three different approaches described in Figure 57.

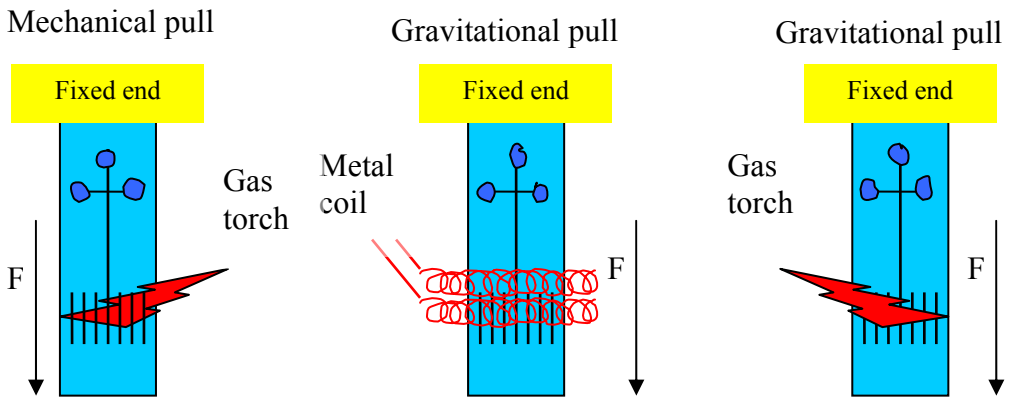

Figure 57. Three different approaches to the simultaneous heating of the support structures and pulling the needle. Left: Constant mechanical pulling by mounting the chip on a syringe pump, heating was provided by using a gas torch; middle: Pull by gravity force, heating by applying electric potential to a coil, wrapped around the support structure; right: Pull by gravity with an additional weight attached while heating with a gas torch.

The glass string used for pulling the ESI needle was designed to be 100 µm x 100 µm in cross-section and containing a 20 µm deep separation channel. Support structures after the final etching were designed to be 100 µm wide with a spacing of 400 µm with the nearest support structures positioned 3.2 mm away from the electrospray needle [140].

4.3 Monolithically Integrated Electrospray Needle: Results and Discussions

Figure 58 shows an image of the microfabricated glass string which is subsequently pulled to create the electrospray needle. The proper alignment of the substrate and cover wafer was crucial for the successive pulling of the needle. The alignment was performed using an aligner from Electronic Visions (EV), Schärding, Austria as if the cover plate was the mask. After the fine

alignment using alignment marks incorporated in the mask design, the substrate and the cover plate were pressed together in the aligner as if contact mode lithography was performed.

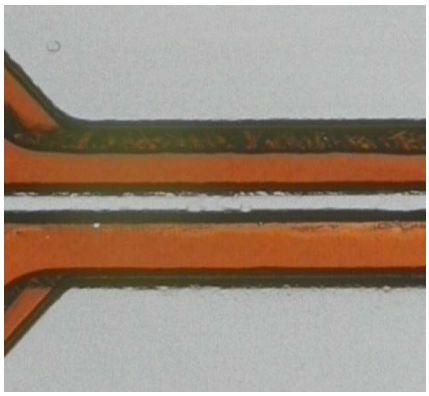

Figure 58. A photograph of the microfabricated glass string at the end of the chip is shown, from which a needle later is formed by pulling at melting temperature. In the center of the structure, a separation channel is seen. The glass string containing the separation channel is 100 µm wide. The non-transparent brown color is due to the 100 nm thick polysilicon layer used for the anodic bonding.

The temporary support structures parallel to the needle dummy (see Figure 58) provide the mechanical stability of the glass string during handling. These support structures are heated and pulled simultaneously with the glass string and then broken off after formation of the needle, as illustrated in Figure 59.

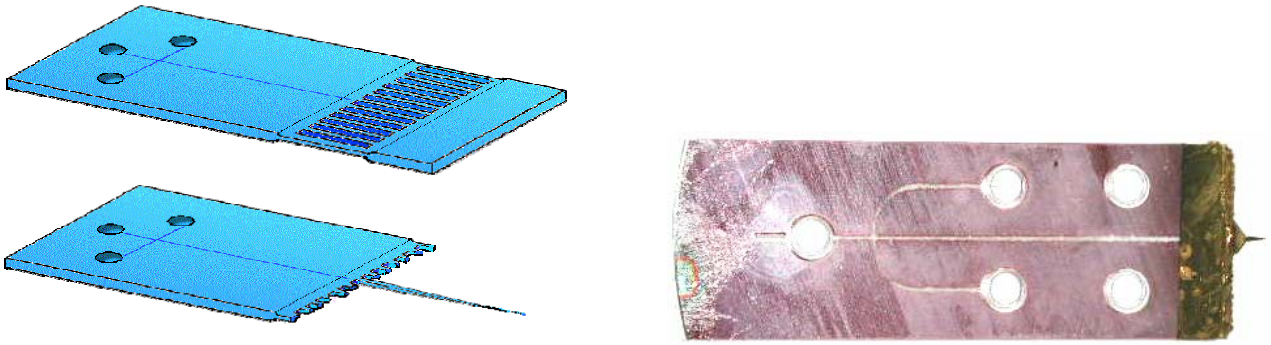

Figure 59. Sketch of the microchip with the temporary support structures (left top), after release of the tip (left bottom), and a photograph of an actual device (right) are presented.

Different approaches for pulling a needle were investigated (Figure 57). Mechanical pull (Figure 57 left) has the advantages of being reproducible and controllable. The pulling force was applied in controlled way by using a syringe pump. The drawback is the necessity to synchronize the onset of pulling with heating of the pre-formed glass string and support structures to the melting point. Pulling mechanically before reaching the melting point resulted in ruptures of the glass string, whereas a delay in initiating pulling resulted in collapsing of the channel inside the needle due to melting.

Gravitational pull with a load (Figure 57 middle) or without a load (Figure 57 right) did not apply the initializing stress and thus resulted in better yields. It was also easier to optimize the applied force in gravitational pull by adjusting the weigh load. Gravitational pull was thus preferred over the mechanical pull. Heating with a torch (Figure 57 left and right) was more efficient than heating with the metal coil (Figure 57 middle) although it required precise distance and flame size control.

After pulling the needle, the microchip was visually inspected to ensure the needle end was not sealed by melted glass. When necessary, the needle tip was etched open by insertion of the tip into hydrofluoric acid. To prevent the acid from entering and thus etching the microchannel, the microsystem was filled with water and a pressure is applied using the syringe pump, thus creating an outgoing flow when the needle is etched open. A layer of gold was then deposited on the needle and surrounding area in order to provide an electric contact with the needle tip. A photograph of a prototype device with monolithically integrated needle is presented in Figure 60.

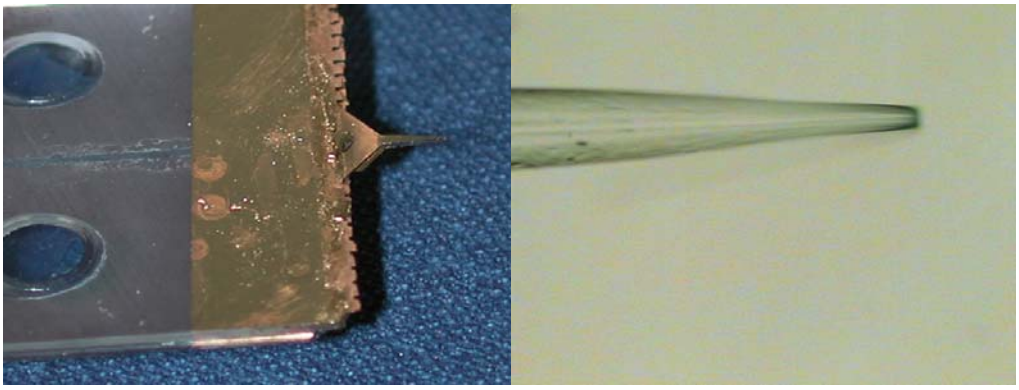

Figure 60. The photographs of the monolithically integrated electrospray needle. Photographs of an integrated needle with a close-up photograph of the gold-coated end of the microsystem (left) and a close-up picture of the needle tip taken under the microscope (right), focused on the channel seen inside the tip. Gold was deposited at the spray tip and adjacent area in order to provide for an electric contact for both electrophoresis and electrospray.

Spray stability was tested, and test separations coupled with a Bruker Data Analysis Esquire-LC 1.5I MS at Helsinki University [141].

5 Conclusions

The work presented in this thesis comprises of three different projects: “Integrated microfluidic device for protein analysis”, “Anodic bonding as a novel packaging method”, and “Electrospray needle with no dead volume monolithically integrated on microchip for capillary electrophoresis”. For clarity, the conclusions in this chapter are listed separately for each project.

5.1 Integrated microfluidic device for protein analysis

The main advantage of miniaturized analytical systems is the possibility to integrate different analytical procedures on the same device. Therefore, the main goal for this project was to perform the proof of the concept experiments to demonstrate that the non-covalent labeling of proteins can be integrated with on-chip preconcentration of proteins on the same device in a single run. This goal has been successfully achieved. A fully integrated glass microsystem for protein analysis was developed and optimized. This microsystem combines preconcentration, labeling, separation, dilution/destaining, and detection steps. To my knowledge, this is the first demonstration of compatibility of on-chip protein preconcentration on a sol-gel filter with on-chip non-covalent labeling. Furthermore, from investigation of on-column versus post-column protein labeling modes integrated with protein separation by capillary sieving electrophoresis, dilution/destaining, and detection steps on the same chip, the following results have been concluded:

- Non-covalent labeling can be performed simultaneously with preconcentration and separation of proteins (on-column mode) or after the preconcentration and separation has taken place (post-column mode).
- On-chip protein labeling with Sypro Orange® shows detection limits similar to those obtained by labeling with Sypro Red® dye.
- Integration of post-column labeling in one step with post-column dilution (destaining) was successfully demonstrated, with sensitivity similar to that of on-column labeling combined with postcolumn dilution and a slightly better separation performance.
- Integrating the labeling and dilution steps simplified the operation of the microsystem.
- Preconcentration was shown to improve the limit of detection (LOD) by more than 15 times.

5.2 Anodic bonding as a novel method for bonding all-glass devices

When the experimental work for this project began, the bonding of all-glass microsystems was a main challenge on microfabrication part at our laboratories at MIC. Therefore, the main goal of this project was to develop a new method for glass-to-glass bonding which would give at least 50% yield of well-bonded devices.

A new method for packaging of glass microfluidic devices for capillary electrophoresis was developed. The method employs polysilicon as an adhesion layer for the photoresist first, allowing the etching of 25 μm deep channels without the photoresist layer falling off. Subsequently, the same polysilicon layer is used as a mediator for anodic bonding. Using polysilicon for both adhesion and bonding purposes reduces the number of microfabrication steps compared to use of another material as an adhesion layer. In addition, anodic bonding gave a higher yield of well bonded devices (19 out of 20 bonded wafers contained a properly bonded useful device, or 95% success rate) compared to direct bonding technique (only 1 out of 8 wafers bonded by direct fusion bonding contained a properly bonded device, giving a 13% success rate). This difference in device yield is due to less stringent requirements on surface roughness and cleanliness for anodic bonding compared to direct fusion bonding. Furthermore, the semi-conducting polysilicon layer was shown compatible with the typical electrical potentials required for operation of electrically driven microfluidic systems. Microsystems, bonded by polysilicon-mediated bonding, have exhibited stable performance in electrophoretic separations (Appendix 8.3).

5.3 Monolithically integrated electrospray needle

The most powerful method for the rapid automated detection and identification of biological analytes is mass spectrometry. Therefore, the main goal for this project was to design, fabricate and test a prototype of a microfluidic device which monolithically integrates a separation and an electrospray interface to a mass spectrometer. The microfabrication recipe for such a device has been developed and optimized. The fabricated prototypes showed a stable electrospray and are still to be tested for coupling with a protein separation.

6 Future work

In this chapter, I will discuss possible applications for the devices and methods presented in this thesis. Furthermore, I will sketch out some ideas about the possible experimental work which could be performed in order to improve the fabrication and analytical aspects of the presented microsystems, separately for each project.

6.1 Integrated microfluidic device for protein analysis: Outlook

Besides sample preconcentration, the salt bridge of the integrated device presented in this thesis can be potentially used for on-chip protein digestion and labeling of the resulting peptides (Figure 61, left). In the first step, both sample and enzyme solution can be trapped on the salt bridge in order to simultaneously preconcentrate and digest the sample proteins. The utilization of the salt bridge would allow achieving fast reaction times typical for enzymes immobilized on solid supports without the necessity of laborious immobilization protocols. The reaction products could then be injected for separation, labeling and detection.

Another possible application of the demonstrated integrated microfluidic device is performing a highly selective antibody assay (Figure 61, right), capable of giving either positive or negative result on a few particular proteins. Several antibodies labeled individually with dyes of the same excitation wavelength but detected at different emission wavelengths could provide an immediate answer whether the proteins in question are present in the sample. A single peak detected at the emission wavelength of the dye conjugated with a specific antibody would mean that no protein matching the antibody was present and in the case of two peaks (one for the protein-antibody complex and one for the unreacted antibody) a positive test would be given.

The ultimate goal beyond the two above mentioned possible applications would be integrating the system for protein processing demonstrated in this thesis with on-chip cell analysis and lysis. On such an integrated device, cells could be presorted, the desired cells could be lysed [103, 142], and their protein content could be then concentrated, labeled and analyzed in the protein processing unit as presented in this work in a single run/operation within minutes.

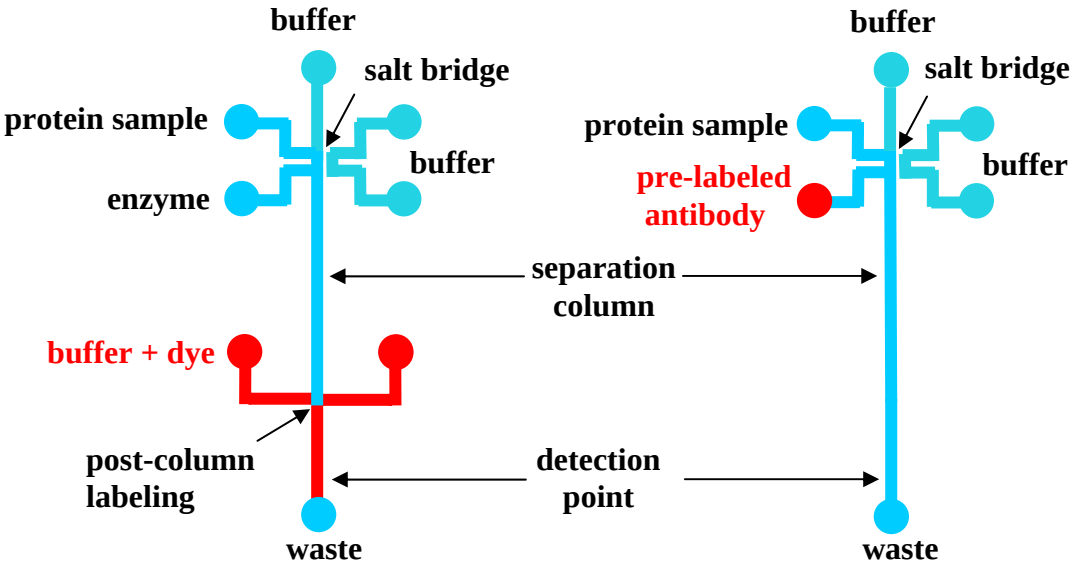

Figure 61. Possible future applications for on-chip preconcentrator are sketched. Left: a schematic of device for simultaneous preconcentration and digest of proteins, with following separation and post-column labeling of resulting peptides. Right: a schematic of a highly selective diagnostic device. Simultaneous preconcentration of biological sample with a pre-labeled antibody could give an immediate answer to whether a specific protein is present in the sample or not.

The necessity to dilute the SDS concentration to below cmc to reduce the background level could be avoided if a detergent with higher cmc could replace SDS in our separation media. One approach would be to find a surfactant, which could assist the separation and prevent absorption to the walls by coating the protein molecules at concentrations below cmc. Another approach is to add an organic additive to the SDS containing buffer to prevent the formation of micelles thus allowing an excess of SDS in the solution without a high background. This approach has to my knowledge not been used with protein separations yet. The possible challenges and complications of such an approach would be: a) organic additive may dissolve sieving polymer in a separation media, thus affecting the separation efficiency to some extend; b) high concentrations of organic solvent may dissociate the dye from SDS-protein complex; c) precipitation of proteins may occur; d) though no reduction of separation efficiency is expected from low organic content in the buffer, additional experiments will be necessary to investigate it.

Potential advantages of using organic additives could be: a) eliminating the need for the dilution step would mean simpler setup and thus a more reproducible and universal method; b) higher sensitivity since dilution of sample is avoided; c) organic additives have been shown to prevent protein-wall interactions, thus eliminating the need for wall coating; d) denaturing of proteins could probably be done on-chip by mixing the sample with an organic solvent instead of heating prior to loading onto the chip; e) organic additives would reduce the surface tension of the

separation media and thus facilitate electrospray stability for potential coupling of molecular weight determination with structural analysis by MS.

6.2 Glass-to-glass anodic bonding: Outlook

The first reported commercial application of field-assisted glass-to-glass bonding utilizing the intermediate polysilicon layer [143] employs the anodic bonding technique for a new plasma display panel packaging method.

Anodic bonding with a polysilicon intermediate layer can not be used for all types of glass. It is not possible to anodically bond a pure silica substrate (quartz) or fused silica to an intermediate layer due to the low concentration of conducting ions in these materials.

Low temperature of anodic bonding allows more design flexibility, for example, for the future integration of metal/polymer features into glass microfluidic systems. Additionally, the sealing process can readily be performed in vacuum, allowing hermetically sealed reference cavities to be formed (or the sealing in of special gas mixtures).

6.3 Monolithically integrated electrospray needle: Outlook

A high-resolution microchip separation followed by an electrospray from the same device is still remaining a challenge. In order to improve the yield of successfully pulled needles and to increase chip-to-chip reproducibility, the conventional equipment for pulling optical fibers might be used. Such instruments have a controllable local heating with a laser beam and a controllable pulling force.

7 References

1. Kyte, J., Doolittle, R., *A simple method for displaying the hydropathic character of a protein.* J. Mol. Biol., 1982(157): p. 105-132.
2. Lion, N., et al., *Microfluidic systems in proteomics.* Electrophoresis, 2003. **24**(21): p. 3533-3562.
3. Gygi, S.P., et al., *Quantitative analysis of complex protein mixtures using isotope-coded affinity tags.* Nature Biotechnology, 1999. **17**(10): p. 994-999.
4. Hoogland C., M.K., Sanchez J.-C., Hochstrasser D.F., Appel R.D., *SWISS-2DPAGE, ten years later.* Proteomics, 2004. **4**(8): p. 2352-2356.
5. Kurien, B.T. and R.H. Scofield, *Western blotting.* Methods, 2006. **38**(4): p. 283-293.
6. Wehr, T., *Multidimensional liquid chromatography in proteomic studies.* Lc Gc North America, 2002. **20**(10): p. 954-+.
7. Patton, W.F., *A thousand points of light: The application of fluorescence detection technologies to two-dimensional gel electrophoresis and proteomics.* Electrophoresis, 2000. **21**(6): p. 1123-1144.
8. Tabb, D.L., W.H. McDonald, and J.R. Yates, *DTASelect and contrast: Tools for assembling and comparing protein identifications from shotgun proteomics.* Journal Of Proteome Research, 2002. **1**(1): p. 21-26.
9. Delahunty, C. and J.R. Yates, *Protein identification using 2D-LC-MS/MS.* Methods, 2005. **35**(3): p. 248-255.
10. Tanaka K, W.H., Ido et al, *Protein and polymer analyses up to m/z 100,000 by laser ionization time-of-flight mass spectrometry.* Rapid Communications In Mass Spectrometry, 1988. **2**(151).
11. Fenn, J.B., et al., *Electrospray Ionization For Mass-Spectrometry Of Large Biomolecules.* Science, 1989. **246**(4926): p. 64-71.
12. Fenn, J.B., et al., *Electrospray Ionization-Principles And Practice.* Mass Spectrometry Reviews, 1990. **9**(1): p. 37-70.
13. Kaiser, J., *Proteomics - Public-private group maps out initiatives.* Science, 2002. **296**(5569): p. 827-827.
14. Gustafsson, M., et al., *Integrated sample preparation and MALDI mass spectrometry on a microfluidic compact disk.* Analytical Chemistry, 2004. **76**(2): p. 345-350.
15. Issaq, H.J., et al., *Methods for fractionation, separation and profiling of proteins and peptides.* Electrophoresis, 2002. **23**(17): p. 3048-3061.
16. Wagner, K., et al., *An automated on-line multidimensional HPLC system for protein and peptide mapping with integrated sample preparation.* Analytical Chemistry, 2002. **74**(4): p. 809-820.
17. Patton, W.F., *Detection technologies in proteome analysis.* Journal Of Chromatography B-Analytical Technologies In The Biomedical And Life Sciences, 2002. **771**(1-2): p. 3-31.
18. Harvey, M.D., D. Bandilla, and P.R. Banks, *Subnanomolar detection limit for sodium dodecyl sulfate capillary gel electrophoresis using a fluorogenic, noncovalent dye.* Electrophoresis, 1998. **19**(12): p. 2169-2174.
19. Evans, C.R. and J.W. Jorgenson, *Multidimensional LC-LC and LC-CE for high-resolution separations of biological molecules.* Analytical And Bioanalytical Chemistry, 2004. **378**(8): p. 1952-1961.
20. Goh, L.T. and M.G.S. Yap, *Determination of interferon-gamma in Chinese hamster ovary cell culture supernatant by coupled-column liquid chromatography.* JOURNAL OF SEPARATION SCIENCE, 2005. **28**(16): p. 2104-2110.

21. Wolters, D.A., M.P. Washburn, and J.R. Yates, *An automated multidimensional protein identification technology for shotgun proteomics.* Analytical Chemistry, 2001. **73**(23): p. 5683-5690.
22. Ru, Q.H.C., et al., *Proteomic profiling of human urine using multi-dimensional protein identification technology.* Journal Of Chromatography A, 2006. **1111**(2): p. 166-174.
23. Kislinger, T., et al., *Multidimensional protein identification technology (MudPIT): Technical overview of a profiling method optimized for the comprehensive proteomic investigation of normal and diseased heart tissue.* Journal Of The American Society For Mass Spectrometry, 2005. **16**(8): p. 1207-1220.
24. Zhu, H., et al., *Global analysis of protein activities using proteome chips.* Science, 2001. **293**(5537): p. 2101-2105.
25. Mircean, C., et al., *Robust estimation of protein expression ratios with lysate microarray technology.* Bioinformatics, 2005. **21**(9): p. 1935-1942.
26. Hultschig, C., et al., *Recent advances of protein microarrays.* Current Opinion In Chemical Biology, 2006. **10**(1): p. 4-10.
27. Rocklin, R.D., R.S. Ramsey, and J.M. Ramsey, *A microfabricated fluidic device for performing two-dimensional liquid-phase separations.* Analytical Chemistry, 2000. **72**(21): p. 5244-5249.
28. Ramsey, J.D., et al., *High-efficiency, two-dimensional separations of protein digests on microfluidic devices.* Analytical Chemistry, 2003. **75**(15): p. 3758-3764.
29. Marshall, A., *HGS launches "first" genomics product in clinic.* Nature Biotechnology, 1998. **16**(2): p. 129-129.
30. Marshall, A. and J. Hodgson, *DNA chips: An array of possibilities.* Nature Biotechnology, 1998. **16**(1): p. 27-31.
31. *www.gene-chips.com*. [cited.
32. Culbertson, C.T., S.C. Jacobson, and J.M. Ramsey, *Microchip devices for high-efficiency separations.* Analytical Chemistry, 2000. **72**(23): p. 5814-5819.
33. Figeys, D. and D. Pinto, *Proteomics on a chip: Promising developments.* Electrophoresis, 2001. **22**(2): p. 208-216.
34. Marko-Varga, G.A., J. Nilsson, and T. Laurell, *New directions of miniaturization within the biomarker research area.* Electrophoresis, 2004. **25**(21-22): p. 3479-3491.
35. Liang, J.G. and Z. He, *Recent advances in protein chip and its application in analytical chemistry.* Chinese Journal Of Analytical Chemistry, 2004. **32**(2): p. 244-247.
36. Schasfoort, R.B.M., *Proteomics-on-a-chip: the challenge to couple lab-on-a-chip unit operations.* Expert Review Of Proteomics, 2004. **1**(1): p. 123-132.
37. Seong, S.Y. and C.Y. Choi, *Current status of protein chip development in terms of fabrication and application.* Proteomics, 2003. **3**(11): p. 2176-2189.
38. White, C.N., D.W. Chan, and Z. Zhang, *Bioinformatics strategies for proteomic profiling.* Clinical Biochemistry, 2004. **37**(7): p. 636-641.
39. A. van den Berg, T.S.J.L., *μ-TAS: Microfluidics aspects, integration concept and applications*, in *Microsystem technology in chemistry and life sciences*, H.B. A. Manz, Editor. 1997. p. 21-49.
40. Spiering, V.L. *Technologies and microstructures for separation techniques in chemical analysis*. in *SPIE*.
41. Ache, H.J., *Chemical analytical systems: objectives and latest developments.* Fresenius J Anal Chem, 1996. **355**: p. 467-474.
42. J. M. Ramsey, S.C.J., M. R. Knapp, *Microfabricated chemical measurement systems.* Nature Medicine, 1995. **1**: p. 1093-1096.

43. Bousse, L. *Electrokinetic microfluidics systems*. in *SPIE*. 1999.
44. Riekkola, M.L., J.A. Jonsson, and R.M. Smith, *Terminology for analytical capillary electromig ration techniques - (IUPAC recommendations 2003).* Pure and Applied Chemistry, 2004. **76**(2): p. 443-451.
45. Landers, J.P., *Handbook of Capillary Electrophoresis, 2nd Ed.* 1997, Boca Raton, Fl: CRC Press.
46. Khaledi, M.G., *High Performance Capillary Electrophoresis*. 1998, New York: John Wiley&Sons.
47. Weinberger, R., *Practical Capillary Electrophoresis, 2nd Ed.* 2000, San Diego: Elsevier.
48. Weber, O., *Reliability of Molecular weight determinations by Dodecyl-Sulfate-polyacrylamide gel electrophoresis.* J. Biol. Chem., 1969. **244**: p. 4406.
49. Ganzler, K., et al., *High-Performance Capillary Electrophoresis Of Sds Protein Complexes Using Uv-Transparent Polymer Networks.* Analytical Chemistry, 1992. **64**(22): p. 2665-2671.
50. Craig, D.B., et al., *Sodium dodecyl sulfate-capillary electrophoresis of proteins in a sieving matrix utilizing two-spectral channel laser-induced fluorescence detection.* Electrophoresis, 1998. **19**(12): p. 2175-2178.
51. Reynolds, J.A. and C. Tanford, *"Binding Of Dodecyl Sulfate To Proteins At High Binding Ratios - Possible Implications For State Of Proteins In Biological Membranes."* Proceedings Of The National Academy Of Sciences Of The United States Of America, 1970. **66**((3)): p. 1002-&.
52. Heiger, D.N., *High Performance Capillary Electrophoresis*. 1997: Hewlett Packard Company.
53. Poole, C.F.P.a.S.K., *Chromatography Today*. 1991, Amsterdam: Elsevier.
54. Dunker, A.K. and R.R. Rueckert, *Observations On Molecular Weight Determinations On Polyacrylamide Gel.* Journal Of Biological Chemistry, 1969. **244**(18): p. 5074-&.
55. Skoog, D.A., F.J. Holler, and T.A. Nieman, *Principles of Instrumental Analysis*. Fifth Edition ed. 1998: Harcourt Brace College Publishers.
56. Petersen, N.J., K.B. Mogensen, and J.P. Kutter, *Performance of an in-plane detection cell with integrated waveguides for UV/Vis absorbance measurements on microfluidic separation devices.* Electrophoresis, 2002. **23**(20): p. 3528-3536.
57. Krull, I.S., et al., *Labeling reactions applicable to chromatography and electrophoresis of minute amounts of proteins.* Journal of Chromatography B, 1997. **699**(1-2): p. 173-208.
58. Bardelmeijer, H.A., et al., *Pre-, on- and post-column derivatization in capillary electrophoresis.* Electrophoresis, 1997. **18**(12-13): p. 2214-2227.
59. Bardelmeijer, H.A., et al., *Derivatization in capillary electrophoresis.* Journal of Chromatography A, 1998. **807**(1): p. 3-26.
60. Banks, P.R., *Fluorescent derivatization for low concentration protein analysis by capillary electrophoresis.* Trac-Trends in Analytical Chemistry, 1998. **17**(10): p. 612-622.
61. Waterval, J.C.M., et al., *Derivatization trends in capillary electrophoresis.* Electrophoresis, 2000. **21**(18): p. 4029-4045.
62. Zhang, X., J.N. Stuart, and J.V. Sweedler, *Capillary electrophoresis with wavelength-resolved laser-induced fluorescence detection.* Analytical and Bioanalytical Chemistry, 2002. **373**(6): p. 332-343.
63. Liu, H.J., et al., *Derivatization of peptides and small proteins for improved identification and detection in capillary zone electrophoresis (CZE).* Analytica Chimica Acta, 1999. **400**: p. 181-209.

64. Colyer, C., *Noncovalent labeling of proteins in capillary electrophoresis with laser-induced fluorescence detection.* Cell Biochemistry and Biophysics, 2000. **33**(3): p. 323-337.
65. Welder, F., et al., *Symmetric and asymmetric squarylium dyes as noncovalent protein labels: a study by fluorimetry and capillary electrophoresis.* Journal of Chromatography B-Analytical Technologies in the Biomedical and Life Sciences, 2003. **793**(1): p. 93-105.
66. Jin, L.J., B.C. Giordano, and J.P. Landers, *Dynamic labeling during capillary or microchip electrophoresis for laser-induced fluorescence detection of protein-SDS complexes without pre- or postcolumn labeling.* Analytical Chemistry, 2001. **73**(20): p. 4994-4999.
67. Kang, C., et al., *Highly sensitive and simple fluorescence staining of proteins in sodium dodecyl sulfate-polyacrylamide-based gels by using hydrophobic tail-mediated enhancement of fluorescein luminescence.* Electrophoresis, 2003. **24**(19-20): p. 3297-3304.
68. Jacobson, S.C., et al., *Microchip Capillary Electrophoresis with an Integrated Postcolumn Reactor.* Analytical Chemistry, 1994. **66**(20): p. 3472-3476.
69. Fluri, K., et al., *Integrated capillary electrophoresis devices with an efficient postcolumn reactor in planar quartz and glass chips.* Analytical Chemistry, 1996. **68**(23): p. 4285-4290.
70. Liu, Y.J., et al., *Electrophoretic separation of proteins on a microchip with noncovalent, postcolumn labeling.* Analytical Chemistry, 2000. **72**(19): p. 4608-4613.
71. Bousse, L., et al., *Protein sizing on a microchip.* Analytical Chemistry, 2001. **73**(6): p. 1207-1212.
72. Norberto A. Guzman, R.E.M., *New directions for concentration sensitivity enhancement in CE and Microchip technology.* LCGC, 2001. **19**(1).
73. Mikkers, F.E.P., Everaerts, F.M., and Verheggen, Th.P.E. M., *Concentration Distributions in Free Zone Electrophoresis.* Journal of Chromatography A, 1979. **169**: p. 1-10.
74. Kutter, J.P., et al., *Determination of metal cations in microchip electrophoresis using on-chip complexation and sample stacking.* Journal Of Microcolumn Separations, 1998. **10**(4): p. 313-319.
75. Li, J.J., et al., *Rapid and sensitive separation of trace level protein digests using microfabricated devices coupled to a quadrupole-time-of-flight mass spectrometer.* Electrophoresis, 2000. **21**(1): p. 198-210.
76. Quirino, J.P. and S. Terabe, *Sample stacking of cationic and anionic analytes in capillary electrophoresis.* Journal Of Chromatography A, 2000. **902**(1): p. 119-135.
77. Lichtenberg, J., E. Verpoorte, and N.F. de Rooij, *Sample preconcentration by field amplification stacking for microchip-based capillary electrophoresis.* Electrophoresis, 2001. **22**(2): p. 258-271.
78. Palmer, J., et al., *Electrokinetic injection for stacking neutral analytes in capillary and microchip electrophoresis.* Analytical Chemistry, 2001. **73**(4): p. 725-731.
79. Yang, H. and R.L. Chien, *Sample stacking in laboratory-on-a-chip devices.* Journal Of Chromatography A, 2001. **924**(1-2): p. 155-163.
80. Jung, B., R. Bharadwaj, and J.G. Santiago, *Thousandfold signal increase using field-amplified sample stacking for on-chip electrophoresis.* Electrophoresis, 2003. **24**(19-20): p. 3476-3483.
81. Vreeland, W.N., et al., *Tandem isotachophoresis-zone electrophoresis via base-mediated destacking for increased detection sensitivity in microfluidic systems.* Analytical Chemistry, 2003. **75**(13): p. 3059-3065.
82. Wainright, A., et al., *Sample pre-concentration by isotachophoresis in microfluidic devices.* Journal Of Chromatography A, 2002. **979**(1-2): p. 69-80.
83. Kutter, J.P., S.C. Jacobson, and J.M. Ramsey, *Solid phase extraction on microfluidic devices.* Journal of Microcolumn Separations, 2000. **12**(2): p. 93-97.

84. Broyles, B.S., S.C. Jacobson, and J.M. Ramsey, *Sample filtration, concentration, and separation integrated on microfluidic devices.* Analytical Chemistry, 2003. **75**(11): p. 2761-2767.
85. Ro, K.W., et al., *Capillary electrochromatography and preconcentration of neutral compounds on poly(dimethylsiloxane) microchips.* Electrophoresis, 2003. **24**(18): p. 3253-3259.
86. Yu, C., et al., *Monolithic porous polymer for on-chip solid-phase extraction and preconcentration prepared by photoinitiated in situ polymerization within a microfluidic device.* Analytical Chemistry, 2001. **73**(21): p. 5088-5096.
87. Sato, K., et al., *Determination of carcinoembryonic antigen in human sera by integrated bead bed immunoasay in a microchip for cancer diagnosis.* Analytical Chemistry, 2001. **73**(6): p. 1213-1218.
88. Singh A.K., T.D.J., Kirby B.J., Thompson A.P. in *MicroTAS*. 2002.
89. Jemere, A.B., et al., *An integrated solid-phase extraction system for sub-picomolar detection.* Electrophoresis, 2002. **23**(20): p. 3537-3544.
90. Oleschuk, R.D., et al., *Trapping of bead-based reagents within microfluidic systems: On-chip solid-phase extraction and electrochromatography.* Analytical Chemistry, 2000. **72**(3): p. 585-590.
91. Lin, Y.C., et al., *A poly-methylmethacrylate electrophoresis microchip with sample preconcentrator.* Journal Of Micromechanics And Microengineering, 2001. **11**(3): p. 189-194.
92. Huber, D.L., et al., *Programmed adsorption and release of proteins in a microfluidic device.* Science, 2003. **301**(5631): p. 352-354.
93. Khandurina, J., et al., *Microfabricated porous membrane structure for sample concentration and electrophoretic analysis.* Analytical Chemistry, 1999. **71**(9): p. 1815-1819.
94. Khandurina, J., et al., *Integrated system for rapid PCR-based DNA analysis in microfluidic devices.* Analytical Chemistry, 2000. **72**(13): p. 2995-3000.
95. Kim S.M., H.E.F. *Electrokinetic preconcentration of proteins on thin PDMS membranes*. in *MicroTAS*. 2003.
96. Song, S., A.K. Singh, and B.J. Kirby, *Electrophoretic concentration of proteins at laser-patterned nanoporous membranes in microchips.* Analytical Chemistry, 2004. **76**(15): p. 4589-4592.
97. Y. Fintschenko, A.v.d.B., *Silicon microtechnology and microstructures in separation science.* J. Chromatography A, 1998(819): p. 3-12.
98. Effenhauser, C.S., A. Manz, and H.M. Widmer, *Glass Chips For High-Speed Capillary Electrophoresis Separations With Submicrometer Plate Heights.* Analytical Chemistry, 1993. **65**(19): p. 2637-2642.
99. Dutta, D., *Dispersion reduction on microchip geometrics*, in *chemical engineering*. 2003, University of Notre Dame: Notre Dame. p. 206.
100. Doherty, E.A.S., et al., *Microchannel wall coatings for protein separations by capillary and chip electrophoresis.* Electrophoresis, 2003. **24**(1-2): p. 34-54.
101. Jacobson, S.C., A.W. Moore, and J.M. Ramsey, *Fused Quartz Substrates For Microchip Electrophoresis.* Analytical Chemistry, 1995. **67**(13): p. 2059-2063.
102. Liu, Y.J., et al., *Electrophoretic separation of proteins on microchips.* Journal of Microcolumn Separations, 2000. **12**(7): p. 407-411.
103. McClain, M.A., et al., *Microfluidic devices for the high-throughput chemical analysis of cells.* Analytical Chemistry, 2003. **75**(21): p. 5646-5655.
104. Swiss Institute of bioinformatics, S., *http://www.expasy.org/; http://us.expasy.org/*.

105. Protein data base, P., <http://www.rcsb.org/pdb/index.html>.
106. Cifuentes, A., J.L. Bernal, and J.C. DiezMasa, *Determination of critical micelle concentration values using capillary electrophoresis instrumentation.* Analytical Chemistry, 1997. **69**(20): p. 4271-4274.
107. Orfi, L., M.F. Lin, and C.K. Larive, *Measurement of SDS micelle-peptide association using H-1 NMR chemical shift analysis and pulsed field gradient NMR spectroscopy.* Analytical Chemistry, 1998. **70**(7): p. 1339-1345.
108. PQ, *Quantitative Interpretation of Silicate Anion Structure Equilibria - 1 Molar solution*.
109. Fidalgo, A., M.E. Rosa, and L.M. Ilharco, *Chemical control of highly porous silica xerogels: Physical properties and morphology.* Chemistry Of Materials, 2003. **15**(11): p. 2186-2192.
110. J.P. Alarie, A.B.H., S.C. Jacobsen, A.P. Baddorf, L. Feldman and J.M. Ramsey. *Fabrication and evaluation of 2D confined nanochannels*. in *Micto Total Analysis Systems*. 2003. Squaw Valley, CA, USA.
111. Madou, M., *Fundamentals of Microfabrication*. 1997, Boca Raton, FL: CRC Press LLC.
112. Oliver Geschke, H.K.a.P.T., *Microsystem Engineering of Lab-on-a-Chip Devices*, ed. K. Geschke, Telleman. 2004.
113. Harrison, D.J., et al., *Micromachining A Miniaturized Capillary Electrophoresis-Based Chemical-Analysis System On A Chip.* Science, 1993. **261**(5123): p. 895-897.
114. S. C. Jakeway, A.J.d.M., E. L. Russell, *µ-TAS for biological analysis.* Fresenius J Anal Chem, 2000(366): p. 525-539.
115. Anthony, T.R., *Anodic Bonding Of Imperfect Surfaces.* Journal Of Applied Physics, 1983. **54**(5): p. 2419-2428.
116. Anthony, T.R., *Dielectric Isolation Of Silicon By Anodic Bonding.* Journal Of Applied Physics, 1985. **58**(3): p. 1240-1247.
117. Andreas Plößl, G.K., *Wafer direct bonding: tailoring adhesion between brittle materials.* Materials Science and Engineering, 1999. **R25**: p. 1-88.
118. Weichel, S., *Silicon to Silicon Wafer Bonding for Microsystems Packing and Formation*, in *MIC*. 2000, DTU: Kgs. Lyngby.
119. Karas, M. and F. Hillenkamp, *Laser Desorption Ionization Of Proteins With Molecular Masses Exceeding 10000 Daltons.* Analytical Chemistry, 1988. **60**(20): p. 2299-2301.
120. Hillenkamp, F. and M. Karas, *Matrix-assisted laser desorption/ionisation, an experience.* International Journal Of Mass Spectrometry, 2000. **200**(1-3): p. 71-77.
121. Rappsilber, J., et al., *Experiences and perspectives of MALDI MS and MS/MS in proteomic research.* International Journal Of Mass Spectrometry, 2003. **226**(1): p. 223-237.
122. Wilm, M., et al., *Femtomole sequencing of proteins from polyacrylamide gels by nano-electrospray mass spectrometry.* Nature, 1996. **379**(6564): p. 466-469.
123. Kebarle, P. and L. Tang, *From Ions In Solution To Ions In The Gas-Phase - The Mechanism Of Electrospray Mass-Spectrometry.* Analytical Chemistry, 1993. **65**(22): p. A972-A986.
124. Enke, C.G., *A predictive model for matrix and analyte effects in electrospray ionization of singly-charged ionic analytes.* Analytical Chemistry, 1997. **69**(23): p. 4885-4893.
125. Smith, R.D., et al., *Collisional Activation And Collision-Activated Dissociation Of Large Multiply Charged Polypeptides And Proteins Produced By Electrospray Ionization.* Journal Of The American Society For Mass Spectrometry, 1990. **1**(1): p. 53-65.
126. Schnier, P.D., D.S. Gross, and E.R. Williams, *On The Maximum Charge-State And Proton-Transfer Reactivity Of Peptide And Protein Ions Formed By Electrospray-Ionization.* Journal Of The American Society For Mass Spectrometry, 1995. **6**(11): p. 1086-1097.

127. Rohner, T.C., N. Lion, and H.H. Girault, *Electrochemical and theoretical aspects of electrospray ionisation.* Physical Chemistry Chemical Physics, 2004. **6**(12): p. 3056-3068.
128. Severs, J.C. and R.D. Smith, *Characterization of the microdialysis junction interface fcr capillary electrophoresis microelectrospray ionization mass spectrometry.* Analytical Chemistry, 1997. **69**(11): p. 2154-2158.
129. Smith, R.D., et al., *Capillary Zone Electrophoresis Mass-Spectrometry Using An Electrospray Ionization Interface.* Analytical Chemistry, 1988. **60**(5): p. 436-441.
130. Smith, R.D., C.J. Barinaga, and H.R. Udseth, *Improved Electrospray Ionization Interface For Capillary Zone Electrophoresis - Mass-Spectrometry.* Analytical Chemistry, 1988. **60**(18): p. 1948-1952.
131. Severs, J.C., A.C. Harms, and R.D. Smith, *A new high-performance interface for capillary electrophoresis electrospray ionization mass spectrometry.* Rapid Communications In Mass Spectrometry, 1996. **10**(10): p. 1175-1178.
132. M. Lazar, R.S.R., Stephen C. Jacobson, Robert S. Foote, J. Michael Ramsey, *Novel fabricated device for electrokinetically induced pressure flow and electrospray ionization mass spectrometry.* Journal of Chromatography A, 2000. **1-2**(892): p. 195-201.
133. Qifeng Xue, F.F., Yurij M. Dunaevskiy, Paul M. Zaracky, Nicol E. McGruer, Barry L. Karger, *Multichannel Microchip Electrospray Mass Spectrometry.* Anal. Chem., 1997. **69**: p. 426-430.
134. Lion, N., J.O. Gellon, and H.H. Girault, *Flow-rate characterization of microfabricated polymer microspray emitters.* Rapid Communications In Mass Spectrometry, 2004. **18**(14): p. 1614-1620.
135. Kim, J.S. and D.R. Knapp, *Miniaturized multichannel electrospray ionization emitters on poly(dimethylsiloxane) microfluidic devices.* Electrophoresis, 2001. **22**(18): p. 3993-3999.
136. Licklider, L.J., M.T. Davis, and T.D. Lee, *Development of novel microfluidic devices for on-line mass spectrometry analysis.* Abstracts Of Papers Of The American Chemical Society, 1997. **214**: p. 94-ANYL.
137. Sjodahl, J., et al., *Characterization of micromachined hollow tips for two-dimensional nanoelectrospray mass spectrometry.* Rapid Communications in Mass Spectrometry, 2003. **17**(4): p. 337-341.
138. Schultz, G.A., et al., *A fully integrated monolithic microchip electrospray device for mass spectrometry.* Analytical Chemistry, 2000. **72**(17): p. 4058-4063.
139. Oliver Geschke, D.P., Sami Varjo, Marja-Liisa Riekkola and Jörg P. Kutter. *'Glass CE Microfluidic Devices with Monolithically Integrated Electrospray Tip for Coupling to MS'*. in *ITP*. 2002.
140. Yuen, P.K., et al., *Microchip module for blood sample preparation and nucleic acid amplification reactions.* Genome Research, 2001. **11**(3): p. 405-412.
141. Petersen, D., Varjo, S. Geschke, O., Riekkola, M.L.,Kutter, J.P. *A new approach for fabricating a zero dead volume electrospray tip for non-aqueous microchip CE-MS* . in *Micro-TAS*. 2002. Nara, Japan.
142. Ramsey, C.R.P.a.J.M. *On-chip single cell lysis integrated with microflow cytometry*. in *Micro Total Analysis Systems*. 2004. Malmo, Sweden.
143. Duck-Jung Lee, J.-W.J., Young-Cho Kim, Yun-Hi Lee, Byeong-Kwon Ju, Tae-Seung Cho, Eun-Ha Choi, Jin Jang, *New plasma display panel packaging technology using electrostatic bonding method.* J. Vac.Sci. Technol. B, 2001. **19**(4).
144. Jacobson, S.C., et al., *High-Speed Separations on a Microchip.* Analytical Chemistry, 1994. **66**(7): p. 1114-1118.

8 Appendix

8.1 Fabrication procedure for devices with integrated needle for CE-ESI-MS

The microfluidic substrate

Step #	Step description	Comments	Illustration
1	Rinse glass substrate in a detergent solution and water using a rotating polishing disk	10 s on each side; detergent: Triton X100 (t-Octylphenoxypolyethoxyethanol) from Soltec Ventures, Beverly, MA, USA	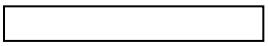
2	Chemical polishing	5 parts H_2SO_4, 2 parts H_2O_2, for 10 min. H_2O bath for 5 min	
3	Sputtering of polysilicon adhesion layer	Cassette sputtering system from Varian (Palo Alto, CA, USA); 100 nm thick layer of amorphous silicon	
4	Preparation of the surface for photo resist deposition	Hexamethyldisilazane (HMDS) oven for 30 min to improve resist adhesion to the polysilicon surface. Wafers should cool down before the next step.	
5	Spinning of photoresist	4.2 µm thick resist (AZ 4562, Shipley Company, LLC, Marlborough, MA, USA)	
6	Humidity equilibration	Wait 30 min for the resist to obtain the right humidity before UV exposure	
7	Exposure with UV light through a mask (aligner from EVG, Schärding, Austria)	16 s exposure time, proximity mode 20 µm, separation 20 µm. Mask for microchannel network is used.	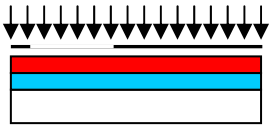
8	Development of resist pattern	3 min 20 s at 22 ºC in developer	
9	Hard baking of the resist	5 min at 90 ºC to improve adhesion during the etching	
10	Etching of polysilicon	Polyetch: 2800 ml H_2O, 2800 ml HNO_3, 140 ml BHF at 35-38 ºC for about 40 s, visual control, N_2 bubbles, bubbler bath for 5 min	
11	Etching of microchannels	Etchant: 40 % HF. Etching time should be calculated from etch rate of 3.34 µm/min at 22 ºC	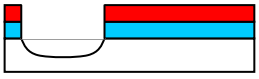
12	Removal of photoresist	Acetone for 40 s, clean acetone with ultrasound for 10 min, H_2O bath 1 min	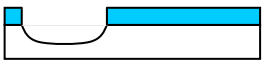
13	Measurement of channel depth	Tencor profilometer (KLA Tencor, San Jose, CA, USA)	

14	Deposition of the second adhesion layer	Cassette sputtering system from Varian (Palo Alto, CA, USA); 100 nm thick layer of polysilicon	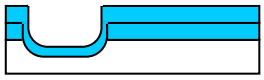
15	Preparation of the surface for photo resist deposition	HMDS (hexamethyldisilazane) oven for 30 min Wafers should be allowed tocool down before the next step	
16	Spinning of photoresist	Track 1 spinner, 4.2 µm thick resist	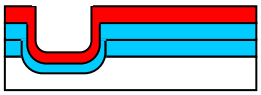
17	Exposure with UV light through a second mask on EV aligner	16 s exposure time, proximity mode 20 µm, separation 20 µm. Mask for needle support structure is used in this step.	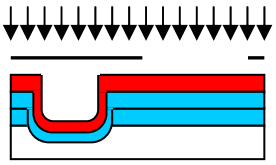
18	Development of resist pattern	3 min 20 s at 22 ºC in developer	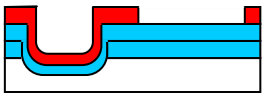
19	Hard baking of the resist	5 min at 90 ºC	
20	Etching of polysilicon	Polyetch: 2800 ml H_2O, 2800 ml HNO_3, 140 ml BHF at 35-38 ºC for about 40 s, visual control, N_2 bubbles, bubbler bath for 5 min	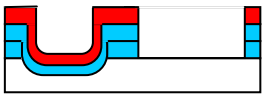
21	Etching of needle support structure	Etchant: 40 % HF Etching time should be calculated using etching rate of 3.34 µm/min	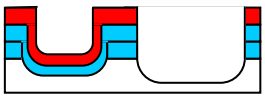
22	Removal of photoresist	Acetone for 40 s. Acetone with ultrasound for 10 min, bubbler bath for 1 min	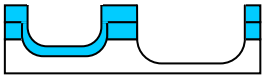
23	Measurement of channel depth	Tencor profiler	
24	Anodic bonding	350 °C in nitrogen at atmospheric pressure, 1 kV, 30 min	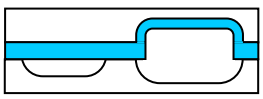
25	Dice into individual microsystems		
26	Polymer wrap	Cleantack Cleanroom Tape (Static Specialists Co., Inc., New York, USA)	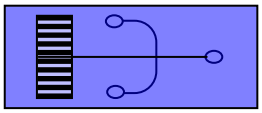
27	Laser patterning on both sides	low power CO_2 laser ablation	

28	Etching of the support structure and the needle	Etchant: 40 % HF. Etching time should be calculated from etch rate of 3.34 µm/min	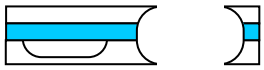
29	Pull the needle	Different approaches are presented in (Figure 57 on page 102)	
30	Gold deposition	With Ti as adhesion layer (10 nm), 300 nm gold was deposited by evaporation at the tip area in thin-film deposition system fra Leybold (Germany)	
31	Attach reservoirs	Polyurethane, various epoxy, UV-curable optical adhesives can be used	

The cover plate

Step #	Description	Comments
1	Rinse substrate in a detergent solution and water using a rotating disk	10 s on each side
2	Chemical polishing	5 parts H_2SO_4, 2 parts H_2O_2, 10 min Bubbler washing for 5 min
3	Sputtering of polysilicon adhesion layer	Varian sputtering system, 100 nm thick layer
4	Preparation of the surface for photolithography	HMDS oven for 30 min Wafers should cool down before the next step
5	Spinning of photoresist	Track 1 spinner, 4.2 µm thick resist
6	The resist gets the right humidity before UV exposure	Wait 30 min.
7	Exposure with UV light through a mask on EVC aligner	16 s. exposure time, proximity mode 20 µm, separation 20 µm
8	Development of resist pattern	3 min 20 s at 22 ºC in developer
9	Hard baking of the resist	5 min at 90 ºC
10	Etching of polysilicon	Polyetch: 2800 ml H_2O, 2800 ml HNO_3, 140 ml BHF at 35-38 ºC for about 40 s. Visual control, N_2 bubbles, bubbler bath for 5 min
11	Etching of support structures	Etchant: 40 % HF Etching time should be calculated from etch rate of 3,34 µm/min
12	Removal of photoresist	Acetone for 40 s Acetone while sonicating for 10 min, bubbler bath for 1 min
13	Measurement of channel depth	Tencor profiler
14	Etching the rest of polysilicon layer	Polyetch: 2800 ml H_2O, 2800 ml HNO_3, 140 ml BHF at 35-38 ºC for about 40 s, visual control, N_2 bubbles, bubbler bath for 5 min
15	Polymer wrap	PVC film with acrylate adhesive
16	Laser patterning for the access holes	low power CO_2 laser ablation
17	Etching of the through holes	Etchant: 40 % HF Etching time should be calculated from etch rate of 3.34 µm/min
18	Remove of the PVC film	
19	Chemical polishing	5 parts of H_2SO_4, 2 parts of H_2O_2, 10 min. Bubbler washing for 5 min.
20	Anodic bonding	350 °C in nitrogen at atmospheric pressure, 1 kV, 30 min

8.2 Amino acid sequences of proteins in Dalton Mark VII sample

1) Alpha lactalbumin (fragment), ID: Q28049, MW = 14156 Da, pI = 5.2

EQLTKCEVFRELKDLKGYGGVSLPEWVCTAFHTSGYDTQAIVQNNDSTEYGLFQINNKIWCKDDQNPHSSNIC
NISCDKFLDDDLTDDIMCVKKILDKVGINYWLAHKALCSEKLDQWLCEKL

2) Trypsin inhibitor B, ID: ITRB_SOYBN, P01071, MW = 20040 Da, pI= 4.6

DFVLDNEGNPLSNGGTYYILSDITAFGGIRAAPTGNERCPLTVVQSRNELDKGIGTIISSPFRIRFIAEGNPLRLKF
DSFAVIMLCVGIPTEWSVVEDLPEGPAVKIGENKDAVDGWFRIERVSDDEFNNYKLVFCTQQAEDDKCGDIGI
SIDHDDGTRRLVVSKNKPLVVQFQKVDKESL

3) Chymotrypsinogen, ID: CTRA_BOVIN P00766**,** MW = 25666 Da**,** pI = 9.3

CGVPAIQPVLSGLSRIVNGEEAVPGSWPWQVSLQDKTGFHFCGGSLINEN
WVVTAAHCGVTTSDVVVAGEFDQGSSSEKIQKLKIAKVFKNSKYNSLTINNDITLLKLSTAASFSQTVSAVCLP
SASDDFAAGTTCVTTGWGLTRYTNANTPDRLQQASLPLLSNTNCKKYWGTKIKDAMICAGASGVSSCMGDS
GGPLVCKKNGAWTLVGIVSWGSSTCSTSTPGVYARVTALVNWVQQTLAAN

4) Carbonic anhydrase II, ID: CAH2_BOVIN P00921, MW = 28982 Da, pI = 5.4-5.9

SHHWGYGKHNGPEHWHKDFPIANGERQSPVDIDTKAVVQDPALKPLALVY
GEATSRRMVNNGHSFNVEYDDSQDKAVLKDGPLTGTYRLVQFHFHWGSSDDQGSEHTVDRKKYAAELHLV
HWNTKYGDFGTAAQQPDGLAVVGVFLKVGDANPALQKVLDALDSIKTKGKSTDFPNFDPGSLLPNVLDYWT
YPGSLTTPPLLESVTWIVLKEPISVSSQQMLKFRTLNFNAEGEPELLMLANWRPAQPLKNRQVRGFPK

5) Glyceraldehyde 3-phosphate dehydrogenase, G3P_RABIT P46406, MW = 35688 Da, pI = 6.6-9.6

VKVGVNGFGRIGRLVTRAAFNSGKVDVVAINDPFIDLHYMVYMFQYDSTHGKFHGTVKAENGKLVINGKAIT
IFQERDPANIKWGDAGAEYVVESTGVFTTMEKAGAHLKGGAKRVIISAPSXDAPMFVMGVNHEKYDNSLKIV
SNASCTTNCLAPLAKVIHDHFGIVEGLMTTVHAITATQKTVDGPSGKLWRDGRGAAQNIIPASTGA
AKAVGKVIPELNGKLTGMAFRVPTPNVSVVDLTCRLEKAAKYDDIKKVVKQASEGPLKGILGYTEDQVVSCD
FNSATHSSTFDAGAGIALNDHFVKLISWYDNEFGYSNRVVDLMVHMASKE

6) Ovalbumin, ID: Q804A4, MW 42903 Da, pI=4.6

MGSIGAASMEFCFDVFKELKVHHANENIFYCPIAIMSALAMVYLGAKDSTRTQINKVVRFDKLPGFGDSIEAQ
CGTSVNVHSSLRDILNQITKPNDVYSFSLASRLYAEERYPILPEYLQCVKELYRGGLEPINFQTAADQARELINS
WVESQXNGIIRNVLQPSSVDSQTAXVLVNAIVFKGLWEKAFKDEDTQAMPFRVTEQESKPVQMMYQIGLFRV
ASMASEKMKILELPFASGTMSMLVLLPDEVSGLEQLESIINFEKLTEWTSSNVMEERKIKVYFPRMKMEEKYN

LTSVLMAMGITDVFSSSANLSGISSAESLKISQAVHAAHAEINEAGREVVGSAEAGVDAASVSEEFRADHPFLF
CIKHIATNAVLFFGRCVSP

7) Bovine Serum Albumin, ID: ALBU_BOVIN P02769, MW 69293 Da, pI = 4.9

MKWVTFISLLLLFSSAYSRGVFRRDTHKSEIAHRFKDLGEEHFKGLVLIAFSQYLQQCPFEHVKLVNELTEFAK
TCVADESHAGCEKSLHTLFGDELCKVASLRETYGDMADCCEKQEPERNECFLSHKDDSPDLPKLKPDPNTLC
DEFKADEKKFWGKYLYEIARRHPYFYAPELLYYANKYNGVFQECCQAEDKGACLLPKIETMREKVLASSARQ
RLRCASIQKFGERALKAWSVARLSQKFPKAEFVEVTKLVTDLTKVHKECCHGDLLECADDRADLAKYICDNQ
DTISSKLKECCDKPLLEKSHCIAEVEKDAIPENLPPLTADFAEDKDVCKNYQEAKDAFLGSFLYEYSRRHPEYA
VSVLLRLAKEYEATLEECCAKDDPHACYSTVFDKLKHLVDEPQNL
IKQNCDQFEKLGEYGFQNALIVRYTRKVPQVSTPTLVEVSRSLGKVGTRCCTKPESERMPCTEDYLSLILNRLC
VLHEKTPVSEKVTKCCTESLVNRRPCFSALTPDETYVPKAFDEKLFTFHADICTLPDTEKQIKKQTALVELLKH
KPKATEEQLKTVMENFVAFVDKCCAADDKEACFAVEGPKLVVSTQTALA

8.3 Article drafts

**"Field-assisted glass-to-glass bonding
for microfabrication of capillary electrophoresis devices"**

Daria Petersen, Klaus B. Mogensen, Nickolaj J. Petersen and Jorg P. Kutter

Mikroelektronik Centret, MIC, Technical University of Denmark

Abstract

In this paper we present a fabrication process based on field-assisted bonding of two borofloat glass wafers with sputtered-on polysilicon as an intermediate layer. Furthermore, the polysilicon layer was also used as an adhesion layer for the photolithography, reducing the number of microfabrication steps. It is shown that the polysilicon layer doesn't affect the stability of the fabricated microsystems for electrophoretic separations. An exemplary electrophoretic separation of a mixture of rhodamine 110, dichlorofluroscein, fluroscein and 5-carboxyfluroscein in borate buffer was performed. A mechanism of field-assisted anodic bonding is discussed. This bonding scheme is superior in terms of process yield compared to direct bonding methods such as fusion bonding, because due to electrostatic attraction involved it reduces the requirements on wafer cleanliness and surface roughness.

1. Introduction

Electrokinetic separations are one of the most powerful tools of analytical chemistry, and their applications include DNA separations, enzyme assays, and cell biology [1-4]. To drive systems with channel dimensions in the tens of microns and flow rates in the nanoliter per second range, electrokinetic methods are also the favored ones [5]. The application of high voltage potentials in electrokinetics restricts the choice of materials for such a microsystems. Glass is a suitable material for fabrication of electrophoresis microchips due to its insulating properties [6].

To obtain closed channels that are used in the majority of lab-on-chip devices, especially for microliquid handling, the bonding of two wafers is required. Wafer bonding is thus a fundamental, but also crucial part of a typical microfabrication process [7].

Two most frequently used bonding methods are anodic bonding and thermal fusion bonding. In this paper we discuss the field-assisted bonding parameters and make a comparison with fusion bonding in terms of process yield and microfabrication complexity and compatibility. Anodic (or electrostatic) bonding is a field-assisted thermal bonding, used typically to bond a structured silicon substrate to a borosilicate glass cover plate. Two glass substrates can not be anodically bonded without the use of at least one intermediate layer. The principle behind the bonding mechanism is sketched in figure 1. A set-up for anodic bonding consists of a vacuum chamber, two electrodes and heat plates for temperature control. The assembled wafer pair is placed between the electrodes and an electrical field ranging from 200 to 1000 V is applied over the wafers. The glass substrate is biased negatively (cathode) with respect to the silicon sputtered substrate (anode). The temperature is typically 200-450^{o} C. Sodium ions (Na^{+}) in the borofloat glass substrate migrate towards the cathode and oxygen ions (O^{2-}) migrate towards the anode, due to the presence of the high electrical field. This results in a negative space charge region in the glass interface towards the silicon intermediate layer and the two wafers will thus be electrically attracted to each other, because of the positive potential applied to the substrate

sputtered with polysilicon. This attraction takes place locally at the wafer interfaces and is thus more efficient in terms of gapping over defects and particles than pressing the two wafers together with an external load.

The presence of oxygen ions at the wafer interface results in oxidation of the bottom substrate with sputtered polysilicon and hence establishes a bond between the two wafers. The bond is stronger than either of the two materials and an attempt to break the bond would result in fracture of either the glass substrates or the silicon layer.

2. Methods and Materials

2.1 Fabrication of microsystems

The layout of the microfabricated devices for capillary electrophoresis separations is presented on Figure 2. The separation channel is 3.5 cm long.

In order to obtain good yield in the bonding step, a new fabrication process has been developed. The process sequence for fabricating of microfluidic structure on the buttom substrate is sketched out in Figure 3. A polysilicon layer with a thickness of 100 nm was sputtered and used as an adhesion layer for photolithographic definition of the channel network. After the etching of the channels in glass to a depth of 12 μm and removing of the photoresist, the polysilicon layer was remained for the later anodic bonding process.

The cover plate substrate was laminated using a polymer film with a high chemical resistance. At the places for the access holes, the polymer film was burned by a laser on one side of the substrate. Then the access holes were etched through the substrate in the 40 % HF, and the polymer film was removed.

2.2 Bonding

The anodic bonding of two substrates with polysilicon intermediate layer (step g on Fig.3) was performed in the in-house built setup. To achieve a bonding, the 1 kV was applied for 10 min at 350 ˚C, atmospheric pressure. The quality of the anodic bonding was checked by visual control in infrared light, where the maximum resolution of the IR camera was approximately 100 μm. The bond strength test was performed using the razorblade technique [8, 9]. A picture of the injection cross of an anodically bonded microsystem is presented on Figure 4.

2.3 Setup for electrophoretic separations

A power supply unit, based on individually controllable high-voltage modules (10A12-P4; Ultravolt Inc., Ronkonkoma, NY, USA) was built in-house. The high-voltage power supply was controlled by software written in LabView 6i (National Instuments, Austin, TX, USA). The same setup was used for the breakthrough measurement test (Fig. 5).

The free-space optic system was used to focus argon ion laser (model T543R-AP-A01; Melles Griot, Carlsbad, CA, USA) into the detection cell. The emitted light was detected by a photomultiplier tube (PMT) (model No. 77348; Oriel Instruments, Stratford, CT, USA). The signal from the PMT was sent to a low noise current amplifier (model SR570; Standford Research Systems, Inc., CA, USA) and was sampled at 50 Hz using an analog-to-digital board (SS420; Beckman Instruments, Fullerton, CA, USA).

2.4 Chemicals

A 10.0 nm tetraborate buffer (pH 9.13) was prepared from di-sodium tetraborate decahydrate (Merck, Darmstadt, Germany). Deionized water (18 MΩ cm) was obtained from an Ultra-Q water system (USFilter IonPURE, Palm Desert, CA, USA). Fluorescein (lot. no. F-1300) was purchased from Molecular Probes (Leiden, Holland). 5-Carboxyfluorescein (lot. no. C-0537) and 2,7-dichlorofluorescein (lot. no. D-6665) were obtained from Sigma (St.

Louis, MO, USA). Phodamine 110 chloride (lot. no. 83695) was obtained from Fluka Chemie (Buchs, Switzerland). Stock solutions were prepared with concentrations of 0.5 mM of the different fluorescent dyes dissolved in 10 mM borate buffer (pH 9.13). Due to the low solubility of rhodamine 110 ethanol (30 vol %) was added during preparation of this stock solution. From these stock solutions a sample mixture containing 3.2 μM rhodamine 110, 8.0 μM 2,7-dichlorofluorescein, 10.0 μM fluorescein and 18.0 μM 5-carboxylfluorescein was prepared by appropriate dilution with 10 nM borate buffer.

2.5 Procedures

The sample mixture was electrokinetically injected using a pinched injection scheme [10]. The separation was performed with field strength in the separation channel of 0.43 kV/cm. For the breakthrough test the voltage was applied between the sample reservoir and overall waste reservoir (see Fig. 2) with 500 V steps up to 4 kV, which was a limit of the power supply. The reservoirs were filled with 10 mM borate buffer (pH 9.13).

3. Results

The visual control of the anodic bonding in infrared light showed that pairs of wafers have been bonded without any voids. No dependence on the bonding area was found. The bond strength test, which was performed using the razorblade technique [8, 9], showed that the surface energy of anodic bonding exceeded the mechanical strength of the material. For the investigation of applicability of the polysilicon-mediated glass-to-glass bonded microsystems for the electrophoretic separations, the breakthrough voltage test was performed (Figure 5). It can be seen that no breakthrough happened up to 4 kV applied, which was a limit of the power supply.

The performance of the microsystems was also tested for electrophoretic separations of a sample mixture containing 3.2 μM rhodamine110, 8 μM 2,7-dichlorofluorescein, 10 μM fluorescein and 18 μM 5-carboxyfluorescein (Figure 6). The measured laser induced fluorescence response values for the peaks were in a range of 0.8-4.8 and a good sensitivity for this relatively dilute sample mixture was obtained. The peak for 18 μM 5-carboxyfluorescein (peak 4 on fig. 6) had a signal-to-noise ratio of 35.

4. Discussions

The sputtered polysilicon layer with a thickness of 100 nm fulfils three requirements. First, it can be successfully used as an adhesion layer for the photoresist to withstand the etching in 40 % HF. Second, it enables the anodic bonding. Finally, it has a conductivity lower then the conductivity of a buffer solution and thus doesn't disturb the performance of the device. Sputtering of the polysilicon is furthermore a fast process that can be done in a cassette deposition system, ensuring high throughput. The anodic bonding is also compatible with potential integration of metal electrodes due to the relatively low temperatures. The comparison of some parameters for anodic bonding and traditional fusion bonding is presented on figure 7.

The anodic bonding with polysilicon intermediate layer is not a valid method for all types of glass. It is not possible to anodically bond a pure silica substrate (quartz) to polysilicon layer, due to the low concentration of sodium ions in quartz.

5. Conclusions

A new fabrication sequence for micromachining of glass microfluidic devices for capillary electrophoresis has been developed. A polysilicon layer was used as an adhesion layer for the photoresist and subsequently as a mediator for the anodic bonding. This reduces the number of microfabrication steps compared with other recipes. In addition, the anodic bonding gives a higher yield then direct bonding techniques due to lower requirements on surface roughness and cleanliness. Polysilicon-mediated glass-to-glass bonded structures exhibited stable performance in electrophoretic separations.

6. Acknowledgements

This research was sponsored from the Danish Research Council, on frame program "Micro Total Analysis Systems". Case number is 9901288.

7. References

1. A. van den Berg and T. S. J. Lammerink. “μ-TAS: Microfluidics aspects, integration concept and applications” Microsystem technology in chemistry and life sciences, A. Manz, H. Becker (Eds.) (1997) 21-49
2. V. L. Spiering et al. “Technologies and microstructures for separation techniques in chemical analysis” SPIE 2882, 91-100
3. Hans Joachim Ache “Chemical analytical systems: objectives and latest developments” Fresenius J Anal Chem 355 (1996) 467-474
4. J. M. Ramsey, S. C. Jacobson and M. R. Knapp. “Microfabricated chemical measurement systems” Nature Medicine, Vol. 1 (October 1995) 1093-1096
5. Luc Bousse. “Electrokinetic microfluidics systems” SPIE 3877 (1999) 2-8
6. Y. Fintschenko and A. van den Berg. Review “Silicon microtechnology and microstructures in separation science”, J. Chromatography A 819 (1998) 3-12
7. S. C. Jakeway, A. J. de Mello and E. L. Russell. Review “μ-TAS for biological analysis” Fresenius J Anal Chem 366 (2000) 525-539
8. Wafer direct bonding: tailoring adhesion between brittle materials, Andreas Plößl and Gertrud Kräuter, Materials Science and Engineering, R25 (1999), p.1-88
9. Silicon to Silicon Wafer Bonding for Microsystems Packing and Formation, Ph.D. Thesis, Steen Weichel, MIC DTU (2000)
10. Madou, M., Fundamentals of Microfabrication CRC Press LLC, Boca Raton, FL 1997

8. Captions

Figure 1. The anodic bonding mechanism is presented. It is important, that polysilicon layer is sputtered also on the side edges of the bottom wafer, thus getting into the electric contact with anode.

Cathode: $4\,Na^{+} + 4\,e^{-} \rightarrow 4\,Na^{0}$

Anode: $Si + 2O^{2-} \rightarrow SiO_2 + 4\,e^{-}$

Figure 2. The layout of the fluidic channels fabricated in glass for electrophoretic separations is shown. The length of the separation channel is 3.5 cm, the width is 120 μm, while the channel is narrowed to 30 μm in the detection cell (see the close-up view in the circle). The inlet and outlet channels have a width of 250 μm.

Figure 3. Schematic view of the process sequence for the fabrication of microchannels on the buttom substrate. (a) Sputtering of a 100 nm polysilicon layer; (b) spinning of the photoresist; (c) exposure and development of the resist; (d) etching of the polysilicon layer; (e) etching of the glass in 40 % HF; (f) strip-off the resist; (g) anodic bonding of the lead glass.

Figure 4. Picture of the injection cross of the anodically bonded chip.

Figure 5. Current-voltage characteristic of a bonded glass microsystem with polysilicon intermediate layer. The voltage potential was applied between the sample reservoir and overall waste reservoir. The channel length between the reservoirs was 7.3 cm.

Figure 6. Electropherogram using laser induced fluorescence (LIF) detection, pinched injection. Peaks: 1- 3.2 μм rhodamine 110; 2- 8.0 μм 2,7-dichlorofluorescein; 3- 10.0 μм fluorescein; 4- 18.0 μм 5-carboxyfluorescein. E=0.43 kV/cm.

Figure 7. The comparison of some parameters of fusion and anodic bonding is presented.

9. Figures

Figure 1.

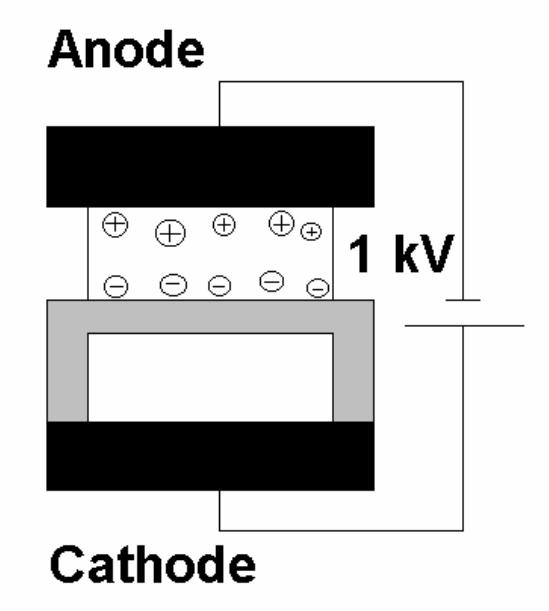

Figure 2.

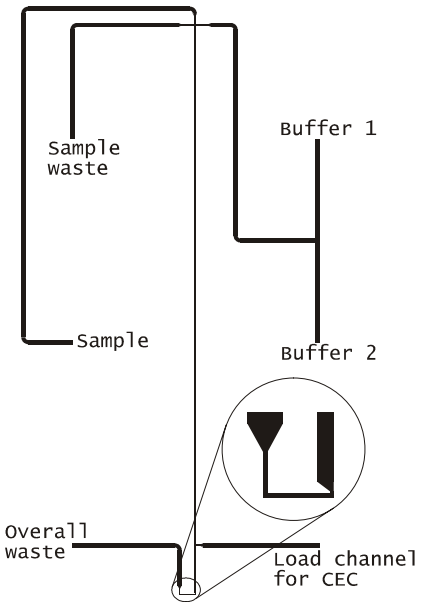

Figure 3.

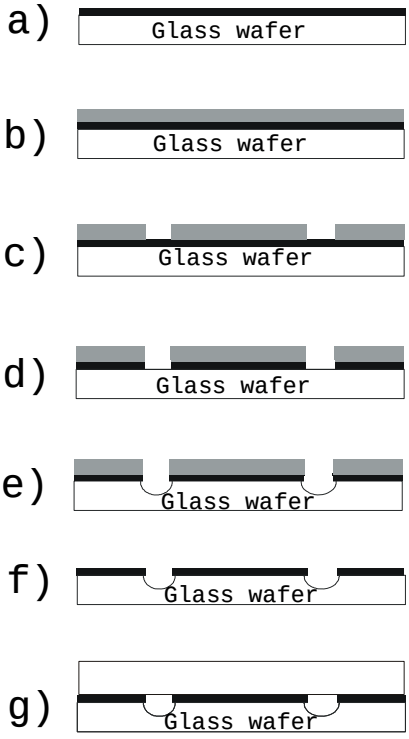

Figure 4.

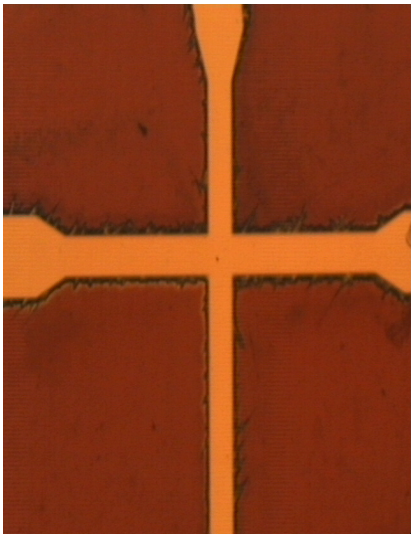

Figure 5.

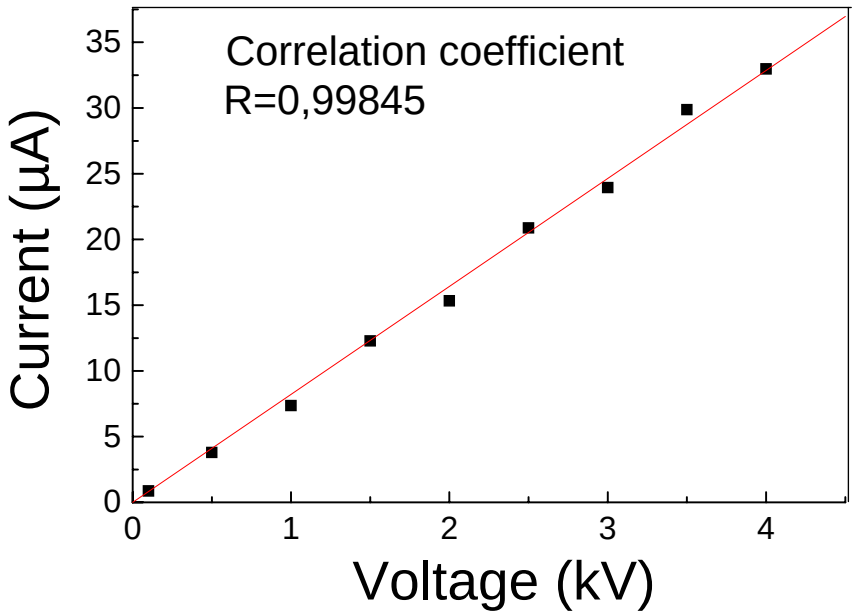

Figure 6.

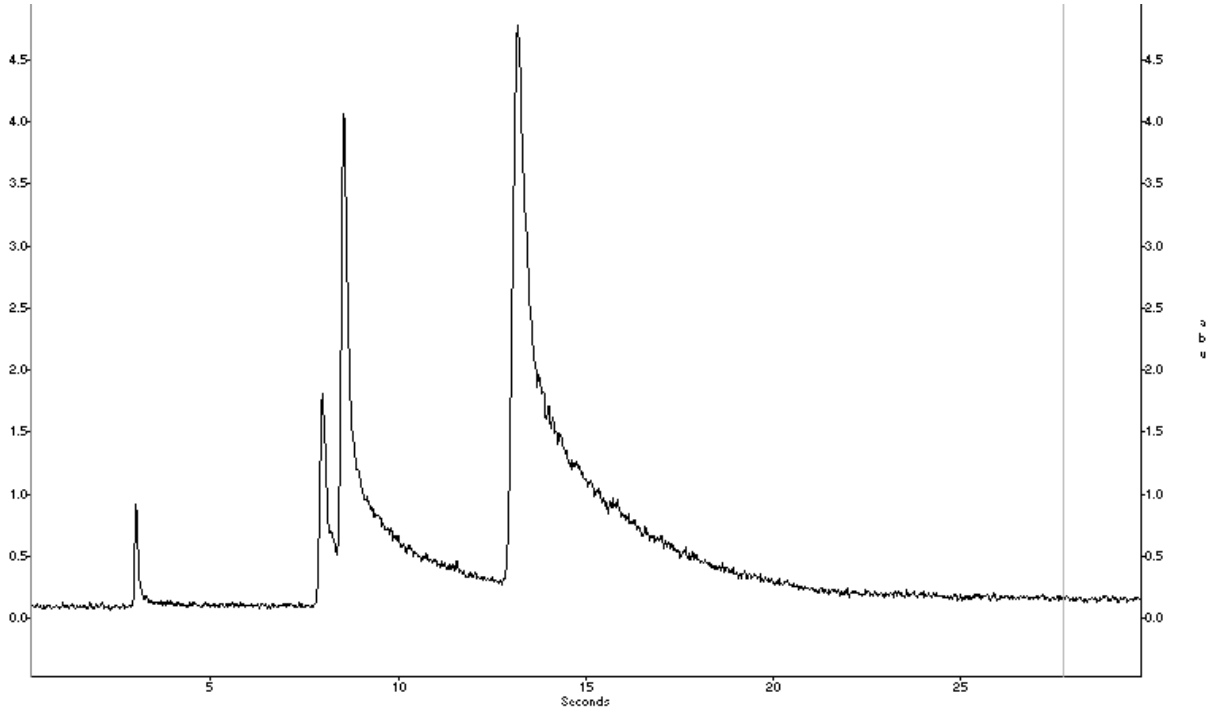

Figure 7.

	Fusion bonding	Anodic bonding
Surface roughness	< 1 nm	< 1 μm
Wafer curvature	< 10 μm	< 300 μm
Typical temperature	560-650 ˚C for borofloat	200-400 ˚C for borofloat
Bonding of quartz wafer	Yes	No
Dependence on area	Yes	No

Integrated Preconcentration, Labeling, Separation and Signal Enhancement of Proteins on a Single Microfluidic Device

Daria Petersen[1, 2], Robert S. Foote[3], Oliver Geschke[2], and J. Michael Ramsey[1]*

* Corresponding author

[1] *Department of Chemistry, University of North Carolina at Chapel Hill (UNC), North Carolina 27599, USA*

[2] *Dept. of Micro and Nanotechnology (MIC), Technical University of Denmark (DTU), Bldg 345 East, DK 2800 Kongens Lyngby, Denmark*

[3] *Chemical and Analytical Science Division, Oak Ridge National Laboratory (ORNL), P.O. Box 2008, Oak Ridge, Tennessee 37831- 6142, USA*

Keywords: preconcentration, on-chip protein labelling, non-covalent dyes, capillary sieving electrophoresis (CSE), μ-TAS, Lab-on-a-chip

ABSTRACT

We have developed a fully integrated glass microsystem for protein analysis, combining preconcentration, labelling, capillary sieving electrophoresis (CSE), dilution (destaining), and detection steps on the same chip. This is a first demonstration of compatibility of on-chip protein preconcentration on a sol-gel filter with on-chip non-covalent labelling. The performance using both on-column and post-column labelling was compared for Sypro Orange® and Sypro Red® dyes. Post-column labelling was shown to be comparable to on-column labelling with respect to both sensitivity and separation efficiency.

Prior to detection a post-column dilution step was performed to lower the sodium dodecyl sulphate (SDS) concentration to below the critical micelle concentration (cmc). The dilution step occurred under suppressed EOF (electroosmotic flow) conditions and resulted in a higher dilution of SDS-dye micelles compared to the proteins. For the post-column labelling both the labeling and SDS dilution was integrated in one step. The dissolution of SDS micelles containing labeling dye decreased the baseline level and increased the signal to noise by factor 10. Separations performed with the post-column labeling / dilution of proteins resulted in separation efficiency and detection limits comparable with that achieved using on-column labelling and post-column dilution. The performance of the device was compared using Sypro Orange® and Sypro Red® dyes. Additionally, integrated protein concentration on porous sol-gel filter is demonstrated to be compatible with both on-column and post-column non-covalent labelling strategies, resulting in further signal enhancement. This is a first demonstration of a fully integrated glass microsystem for protein analysis, combining preconcentration, labelling, separation, dilution (destaining), and detection steps on the same chip.

INTRODUCTION

With the emphasis in biological research shifted from genomics to proteomics, fast and efficient tools for proteome analysis are needed. A number of techniques that are useful for proteome research has been demonstrated on microsystems, including sample filtration [1], cell manipulation [2], cell lysis [3], enzyme digestion [4], sample preconcentration techniques [5], [6], [7], various separation methods, derivatization with fluorescent agents for subsequent laser induced fluorescence (LIF) detection [8], [9], and interfaces for MS detection [10]. The separation and analysis of native proteins at low concentrations is an important direction towards microfluidic research of single cell proteome.

Laser induced fluorescence (LIF) for the detection of proteins requires a natural fluorophore or derivatization with a fluorescent marker molecule. Fast reaction time is a vital parameter for on-chip labelling of proteins. Non-covalent protein derivatization methods (recently reviewed by Coyler et al.[3]) are more suitable for on-chip integration because they do not need elevated temperatures, they require less sample handling and shorter reaction times compared to covalent labelling. Gel electrophoresis is frequently employed for the separation of complex protein mixtures. When the characterisation of protein mass or estimation of protein purity is needed, sodium dodecyl sulphate – polyacrylamide gel electrophoresis (SDS-PAGE) is a suitable technique due to its size-based separations. For non-covalent pre-labeled proteins separated by SDS-PAGE, Guttman et al. [8] have reported a non-linear relationship between the molecular weight and electrophoretic mobility.

Of special interest for on-chip protein analysis are dyes, which can be employed for non-covalent labelling in presence of a detergent (for example, SDS) above the critical micelle concentration. With detergent-coated sample molecules, the labelling is uniform and proportional to the molecular weight in contrast to variable amount of labels per protein typical for covalent labelling methods. High concentrations of detergent are also needed for molecular weight determination by SDS-assisted sieving electrophoresis where the SDS maintains denaturation of the sample molecules and assures similar mass to charge ratio of proteins independent of their isoelectric points (pI). Non-covalent fluorogenic dyes, such as Sypro Red®, Sypro Orange®, Sypro Ruby®, Sypro Tangerine®, 5-dodecanoyl amino fluorescein, 5-hexadecanoyl amino fluorescein, 5-octadecanoyl amino fluorescein bind both to hydrophobic regions of SDS-protein complexes but also to SDS micelles, thus resulting in high background [4,5]. Bousse et al.[6] demonstrated for on-column labelling with Sypro Red® and Agilent Lower Marker dyes, that post-separation dilution of SDS content to below critical micelle concentration reduces background fluorescence from the dye - SDS complexes and increases the overall signal-to-noise ratio (S/N) from analytes by an order of magnitude [6]. In this paper, labelling and SDS dilution combined in one post-column step is compared to on-column labelling followed by dilution.

To further improve the detection limit, various sample concentration methods can be combined with the on-chip labelling. On-chip sample preconcentration using a sol-gel filter has been demonstrated previously for DNA fragments[8] where up to two orders of magnitude signal enhancement was achieved. In this paper, we report the integration of preconcentration, separation, labelling and signal enhancement by dilution on a single chip for protein analysis.

EXPERIMENTAL SECTION

Microchip fabrication

Microchips (figure 1) were fabricated from White Crown® glass wafers (Telic, Santa Monika, CA, USA), using standard photolithography and wet chemical etching methods described previously [144]. Access holes to the channels were ultrasonically drilled (Sonic-Mill, Albuquerque, NM, USA) in the etched substrate. A closed channel network was

formed by low-temperature bonding of a glass cover plate to the etched substrate, assisted by a thin layer of potassium silicate (KASIL 2130, The PQ Corporation, Valley Forge, PA, USA). The silicate layer functioned both as an adhesive and to form a porous salt bridge for sample pre-concentration [Khandurina, 1999 #3]. Potassium silicate solution was diluted to a final concentration of 0.1 M and spun on the coverplate at 3500 rpm for 7 s. Annealing at 200 °C overnight was used to assist dehydration and siloxane bond formation and thus reinforce the bonding. Dimensions were measured using a stylus-based surface profiler (P-10; Tencor, Mountain View, CA, USA). The etched channels were 14-16 μm deep and 47-51 μm wide at half depth. The width of the porous membrane for preconcentration (the distance between two separate channel networks) was 4.4-5.0 μm. The length of preconcentration cell was 100 μm, measured between the centres of sample and sample waste channels at their intersection with the separation channel. Glass reservoirs were affixed with Norland optical adhesive 68 (Norland Products, Inc., Cranbury, NJ, USA). The length of the separation channel (from preconcentrator/injector to the dilution intersection) was 60 mm (figure 1).

Sample preparation

A mixture of seven proteins with molecular weights ranging from 14 to 70 kDa (Dalton Mark VII-L for SDS gel-electrophoresis, Sigma, Saint Louis, MO, USA) was prepared in sample buffer (CE-SDS protein kit 1874, Bio-Rad Laboratories, Hercules, CA, USA) following the kit manufacturer's instructions.

For on-column protein labelling, Sypro Orange® or Sypro Red® dyes (Molecular Probes, Eugene, Oregon, USA) were added to the run buffer (CE-SDS protein kit 1874, Bio-Rad Laboratories, Hercules, CA, USA) to the final concentration of 1x. Both dyes have initial 5000x manufacturer's recommended concentration in dimethyl sulfoxide (DMSO). Dilution buffer (400 mM Tris borate buffer, pH=8.3) was prepared by dissolving Trizma base (Sigma, St. Louis, LO, USA) and boric acid (Sigma, St. Louis, LO, USA) in deionized water.

For post-column labelling, Sypro Orange® and Sypro Red® dyes were added to the dilution buffer (400 mM Tris borate) to the final concentration of 10x or 100x. For post column labeling with no dilution the Bio-Rad® run buffer with added dye was used as the dilution buffer.

Instrumentation

An Argon ion laser operating at 488nm (Melles Griot, Carlsbad, CA, USA) was used for the excitation of Sypro Orange® labelled proteins (optimum excitation 472 nm). For excitation of Sypro Red® labelled proteins (optimum excitation 548 nm) a Helium-Neon laser at 543 nm (Melles Griot, Carlsbad, CA, USA) was used for the excitation. A high voltage (HV) power supply having 5 outputs and a HV relay box was build in house. Both the control of the power supply, relay box and the data acquisition from the photo multiplier tube (Oriel 71260, Stratford, CT, USA) were controlled by LabView (National Instruments, Austin, TX, USA).

Microchip operation

The presence of SDS minimized protein/wall interactions and the sieving matrix in the run buffer combined with the high buffer concentration (400 mM Tris borate) inhibited the EOF. To avoid protein adsorption to the walls during the preconcentration step and after the postcolumn dilution where the SDS concentration is reduced, all microsystems were coated with acrylamide. The microchip was operated in reversed mode (analytes migrate toward anode). Run buffer was loaded into reservoirs 1, 2, 4 and 6 (Figure 1) and allowed to fill the entire channel network. The protein sample was

loaded into reservoir 3 and both reservoirs 5 were filled with the dilution buffer. For on-column labeling the labeling dye was present in the run buffer (reservoirs 1, 2, 4 and 6). For post-column labeling the labeling dye was present in the dilution buffer (both reservoirs 5).

For analyses without preconcentration, injections were performed by initially applying a potential of 750 V/cm between the sample (reservoir 3) and sample waste (reservoir 2). Potential at reservoir 1 was kept at 0.4 kV in order to create some flow from buffer reservoir to sample waste and thus avoid leaking of sample into the run buffer. This direction of pre-injection allows almost no diffusion/leaking of sample into the separation channel. All other electrodes were floated during this first step. After 5 minutes of pre-injection, a potential of 3.1 kV was applied at the waste (reservoir 6), while run buffer electrode (reservoir 1) was grounded and potentials of 0.3 kV were kept on reservoirs 2 and 3 to prevent the leakage of sample into the separation channel after injection. By varying the potential applied at dilution buffer (reservoirs 5), different dilution ratios (DR) were obtained.

For analysis with sample preconcentration, a potential of 1.2 kV was applied at one of the bridged reservoirs (4) while keeping sample reservoir (3) grounded. All other reservoirs were kept floated during this preconcentration step. The injection/separation step was then performed exactly as described above for the volume defined injection without preconcentration. Detection was performed 10 mm after the dilution intersection at the end of the 60 mm long separation channel. Different dilution ratios (DR) were obtained after the dilution intersection by varying the applied potential at the dilution buffer (reservoirs 5).

RESULTS AND DISCUSSION

An illustration of simultaneous sample preconcentration and on-column labelling is presented in Figure 2 (left image). The adjacent microchannels within the images boundaries were filled with run buffer containing 1x concentration of Sypro Orange® dye recommended by manufacturer (actual concentration is not available). Presence of the dye provided the fluorescence background seen in all channels adjacent to preconcentration membrane area. Upon protein molecules arrival at the membrane, dye was binding to the protein-SDS complex, dramatically increasing the fluorescence signal of the forming sample plug.

Post-column dilution is still possible even when EOF is suppressed. The mechanism of the dilution is different from mixing of flows using EOF. In the case without EOF, ionic streams are combined in the dilution channel. The current in the dilution channel is the sum of the current from the separation channel and from the dilution reservoirs, but the current may be carried by a different ratio of ions before and after the intersection. The dilution of the different ionic species at the dilution intersection thus depends on their apparent conductivities. More neutral analytes become less diluted than more charged and thus mobile ions. The sieving matrix in the Bio-Rad® separation buffer is dextran, which is neutral and therefore it will not become diluted (washed out) after the dilution intersection even though it is not present in the dilution buffer. The SDS-dye complexes have a much higher mobility than the labeled proteins and therefore it is expected to become more diluted compared to the proteins. This higher mobility can be seen from the electropherograms where the first migrating peak is from the SDS-dye complex (Sample had a higher SDS concentration than the run buffer). This dilution will favor the detection limit of the proteins even before the SDS is diluted to below its cmc. Below the cmc the SDS-dye components becomes dissociated. This dissociation will give a baseline reduction since these non-covalent dyes are flourogenic (less fluorescent in free solution). The released dye may also bind to the proteins thereby increasing the peak height even further.

During the separations performed with different DR only the voltage at the dilution reservoirs was changed. This change in voltage modifies the voltage at the dilution intersection, which then changes both the separation field strength and the field strength in the dilution channel. Since the separation length is longer than the length in the dilution channel a higher dilution ratio will increase the overall analysis time.

A comparison of separation efficiency is best done by looking at the resolution of the different peaks rather than at the apparent peak widths. The higher velocity at the detection point should be taken into account since it otherwise will make the peaks appear narrower than what they really are. When calculating N from the peak width, the different field strengths in the separation channel and the detection point therefore has to be taken into account.

For both the on-column and post-column labeling with different DR the resolution was calculated between peak 3 (trypsinogen, 24 kDa) and peak 4 (carbonic anhydrase, 29 kDa). Also the separation efficiency, N, was calculated for peak 1 (α-lactalbumin, 14.2 kDa). Resolution, separation efficiency and theoretical limit of detection (LOD) are presented in Table 1.

Theoretical dilution ratio (graph a on Figure 4) was calculated as a ratio of field strength in the dilution (detection) channel to the field strength in the separation channel, assuming that conductivity is the same in all channels. For on-column labelling, the DR for the SDS-dye complex was also estimated experimentally as a ratio of the average baseline value without dilution to the average baseline value with dilution (graph b on Figure 4). This method gave values similar to theoretical ones. For post-column labeling, experimental DR was determined as the ratio of an average baseline value with dilution to an average baseline value without dilution (graphs c and d on Figure 4 represent correspondingly 100x and 10x concentration of Sypro Orange® in dilution buffer).

Beside the signal enhancement from lowering the baseline, baseline is also getting smoother with dilution, thus significantly increasing the average signal-to-noise ratio.

Average S/N for the experiment without preconcentration and dilution was 9.3. For the experiment with dilution ratio of 4.2 was 105 (average S/N increased by a manifold). Average S/N for the experiment with 1 min preconcentration (standard deviation of the baseline was similar to the experiment with the same dilution ratio of 4.2 without preconcentration) was 304 (a three-fold increase).

Signal-to-noise enhancement from preconcentration step is not linear with log molecular weight of the proteins.

While signal enhancement from dilution step is nearly the same for all peaks (on Fig…., signal enhancement for Dilution Ratio = 4.2 is presented), preconcentration step enhance signal from the later peaks to large extend, thus resulting in a slope in the total signal enhancement by both preconcentration and post-column dilution.

CONCLUSION

The main advantage of miniaturized analytical systems is the possibility to integrate different analytical procedures on the same device. Therefore, the main goal for this project was to perform the proof of the concept experiments to demonstrate that the non-covalent labeling of proteins can be integrated with on-chip preconcentration of proteins on the same device in a single run. This goal has been successfully achieved. A fully integrated glass microsystem for protein analysis was developed and optimized. This microsystem combines preconcentration, labeling, separation, dilution/destaining, and detection steps. To my knowledge, this is the first demonstration of compatibility of on-chip protein preconcentration on a sol-gel filter with on-chip non-covalent labeling. Furthermore, from investigation

of on-column versus post-column protein labeling modes integrated with protein separation by capillary sieving electrophoresis, dilution/destaining, and detection steps on the same chip, the following results have been concluded:

- Non-covalent labeling can be performed simultaneously with preconcentration and separation of proteins (on-column mode) or after the preconcentration and separation has taken place (post-column mode).
- On-chip protein labeling with Sypro Orange® shows detection limits similar to those obtained by labeling with Sypro Red® dye.
- Integration of post-column labeling in one step with post-column dilution (destaining) was successfully demonstrated, with sensitivity similar to that of on-column labeling combined with postcolumn dilution.
- Post-column labeling of proteins combined with dilution resulted in separation efficiency and theoretical detection limits comparable to those achieved with on-column labeling.
- Integrating the labeling and dilution steps simplified the operation of the microsystem.
- Preconcentration was shown to improve the limit of detection (LOD) by more than 15 times.

ACKNOLEDGMENT

This research was sponsored by U.S. Department of Energy, National Nuclear Security Administration, under contract DE-AC05-00OR22725 with Oak Ridge National Laboratory, managed and operated by UT-Battelle, LLC.

This research was supported in part by an appointment to the Oak Ridge National Laboratory Postmaster's Research Participation Program administered jointly by the Oak Ridge Institute for Science and Education and Oak Ridge National Laboratory.

We thank Christopher D. Thomas and Leslie Wilson for the help with fabrication of the microchips.

REFERENCES

(1) Krull, I. S.; Strong, R.; Sosic, Z.; Cho, B. Y.; Beale, S. C.; Wang, C. C.; Cohen, S. *Journal of Chromatography B* **1997**, *699*, 173-208.

(2) Zhang, X.; Stuart, J. N.; Sweedler, J. V. *Analytical and Bioanalytical Chemistry* **2002**, *373*, 332-343.

(3) Colyer, C. *Cell Biochemistry and Biophysics* **2000**, *33*, 323-337.

(4) Jin, L. J.; Giordano, B. C.; Landers, J. P. *Analytical Chemistry* **2001**, *73*, 4994-4999.

(5) Kang, C.; Kim, H. J.; Kang, D.; Jung, D. Y.; Suh, M. *Electrophoresis* **2003**, *24*, 3297-3304.

(6) Bousse, L.; Mouradian, S.; Minalla, A.; Yee, H.; Williams, K.; Dubrow, R. *Analytical Chemistry* **2001**, *73*, 1207-1212.

(7) Jacobson, S. C.; Hergenroder, R.; Koutny, L. B.; Ramsey, J. M. *Analytical Chemistry* **1994**, *66*, 1114-1118.

(8) Khandurina, J., et al., *Microfabricated porous membrane structure for sample concentration and electrophoretic analysis.* Analytical Chemistry, 1999. **71**(9): p. 1815-1819.

FIGURE CAPTIONS

Figure 1. Schematic of the chip layout: 1) run buffer; 2) sample waste; 3) sample; 4) preconcentrator reservoirs, bridged with platinum wire; 5) dilution reservoirs, bridged with platinum wire; 6) waste. Insert (a) shows a schematic of two adjacent channel networks in the glass substrate. When bonded with a cover plate using intermediate silicate layer, the 5 micrometer gap in between these networks bonded with the sol gel, serves as a filter, allowing the flow of buffer ions but retaining and accumulating protein molecules. The insertion (b) sketches the cross section of the chip along the dashed line on the (a) insertion. The thickness of the sol-gel layer is less than 100 nm.

Figure 2. Fluorescence images of simultaneous sample pre-concentration and on-column labeling (left) of protein sample (1 mg/ml) with 1x Sypro Orange® dye, followed by an injection (middle and right) into the separation channel.

Figure 3. Visualisation of post-column labelling of 1 mg/ml total protein with 100x Sypro Orange® is presented.

Figure 4. Data showing a) an injection without preconcentration; b) the effect of 1 min on-chip preconcentration of sample on a porous salt bridge. On-column labeling with 1x Sypro Orange® in the Bio Rad® run buffer was followed by dilution with 89 mM Tris-borate buffer, pH 8.3, at dilution ratio of 4.2 for both experiments. Sample: Dalton Mark VII protein mixture, 2 mg/ml total protein concentration. Protein peaks and their initial concentrations: 1) α -Lactalbumin (19 μM); 2) Trypsin inhibitor (13 μM); 3) Trypsinogen (16 μM); 4) Carbonic anhydrase (9.3 μM); 5) Glyceraldehyde-3phosphate dehydrogenase (7.5 μM); 6) Ovalbumin (6 μM); 7) Bovine serum albumin (4.1 μM).

Figure 5. Signal to noise ratio and theoretical limit of detection for each protein at different dilution rates. On-column labeling with 1x Sypro Orange®, 2 mg/ml protein content in sample. The best average detection limit (LOD=235 nM) was obtained at maximum tested dilution (DR 4.8)

Figure 6. Dependance of dilution ratio (DR) on potential applied at dilution reservoirs: a) theoretical DR calculated as $\frac{E_{dilution}}{E_{separation}}$; b) experimental DR calculated as the decrease of baiseline flouresence for on-column labeling with 1x Sypro Orange®, 2 mg/ml total protein content in sample; c) experimental DR for post-column labeling with 10x Sypro Orange® in the dilution buffer, 1 mg/ml sample; d) experimental DR for post-column labeling with 10x Sypro Orange® in the dilution buffer, 1 mg/ml sample.

Figure 7. The signal enhancement from a) dilution step (DR=4.2), b) preconcentration step (1 min), c) their total. Sample: Dalton Mark VII protein mixture, 2 mg/ml total protein concentration; on-column labeling with 1x Sypro Orange®. Beside the signal enhancement, baseline is getting smoother with dilution, thus significantly increasing the average signal-to-noise ratio. Average S/N for the experiment without preconcentration and dilution was 9. An average S/N for experiment with dilution ratio of 4.2 was 105 (average S/N increased by a manifold). Average S/N for the experiment with 1 min preconcentration (standard deviation of the baseline was similar to the experiment with the same dilution ratio of 4.2 without preconcentration) was 304 (a three-fold increase). Signal-to-noise enhancement from preconcentration step is not linear with log molecular weight of the proteins.

Figure 8. Signal enhancement of protein peaks due to 1 min preconcentration in post-column labeling with 10x Sypro Orange®, 1 mg/ml total protein content in Dalton Mark VII sample, theoretical dilution ratio 4.3.

Figure 9. The effect of potential applied on dilution reservoirs for post-column labeling with 10x Sypro Orange®, preconcentration for 1 min, 1mg/ml total protein content Dalton Mark VII sample: a) 1.7 kV; b) 1.1 kV; c) 0.8 kV.

Figure 10. Post-column labeling with 10x Sypro Orange®, 1 mg/ml total protein content of Dalton Mark VII sample, potential of 0,8 kV applied at the dilution reservoirs: a) injection without preconcentration; b) 1 min preconcentration

Figure 11. Signal to noise ratio for all proteins at different potentials applied on dilution channels. Post-column labeling with 10x Sypro Orange®, 1mg/ml sample.

Figure 12. Signal enhancement of protein peaks due to 1 minute preconcentration combined with post-column labeling with 10x Sypro Orange®, 1 mg/ml total protein content in Dalton Mark VII sample, theoretical dilution ratio 4.3.

Figure 13. Average peak amplitude of the proteins at different DR. Post-column labeling with 10x Sypro Orange®, 1mg/ml total protein content Dalton Mark VII sample.

Figure 14. Postcolumn labeling after preconcentration: the influence of DR. Post-column labeling with 100x Sypro Orange®, 1 mg/ml total protein content of Dalton Mark VII, 1 min preconcentration for all electropherograms, dilution potentials were: 1.4, 1.1 and 0.8 kV.

Figure 15. On-column labeling with 1x Sypro Red® Dye, 1 mg/ml total protein concentration sample Dalton Mark VII. Protein peaks and their initial concentrations: 1) α -Lactalbumin (9.5 μM); 2) Trypsin inhibitor (6.5 μM); 3) Trypsinogen (8 μM); 4) Carbonic anhydrase (4.65 μM); 5) Glyceraldehyde-3phosphate dehydrogenase (3.75 μM); 6) Ovalbumin (3 μM); 7) Bovine serum albumin (2.05 μM).

Figure 16. Protein molecular weight determination. For separations with on-column labeling with 1x Sypro Red® Dye, 1 mg/ml total protein concentration sample Dalton Mark VII, log MW was plotted against the 1/Migration time.

Figure 17. Average peak amplitude per run versus potential applied at dilution reservoirs. Post-column labeling with 10x Sypro Orange®, 1mg/ml sample.

Figure 18. Separation efficiency versus potential applied at dilution reservoirs. Post-column labeling with 10x Sypro Orange®, 1mg/ml sample.

Figure 19. Preconcentration combined with on-column labeling with 1x Sypro Orange®. Sample: Dalton Mark VII, 0.02 mg/ml total protein content, preconcentration for respectively 2, 3 and 5 min, followed by dilution with 89 mM Tris-borate pH 8.3. Potential on the dilution reservoirs 0.4 kV for all runs.

Figure 20. Preconcentration time effect is shown for post-column labelling with 100x Sypro Orange®, 1 mg/ml total protein content of Dalton Mark VII in the sample, potential on dilution reservoirs is 1.1 kV for all runs: a) an injection without preconcentration; b) 1 minute preconcentration; c) 2 minutes preconcentration

Table 1. Performance of on-column versus post-column labeling. [a] SyR = Sypro Red®, SyO = Sypro Orange®; [b] dye concentration relative to manufacturer's recommended concentration for gel-staining; [c] total concentration of Dalton Mark VII-L proteins; [d] separation efficiency for α-lactalbumin,14.2 kDa; [e] average LOD (defined as the concentration giving S/N = 3) of all proteins per run.

Table 2. Performance of on-chip preconcentration. [a] concentration of Sypro Orange® Dye relative to manufacturer's recommended concentration for gel-staining; [b] total concentration of Dalton Mark VII-L proteins, [c] separation efficiency for α-lactalbumin, 14.2 kDa; [d] average for all proteins per run

Figure 1

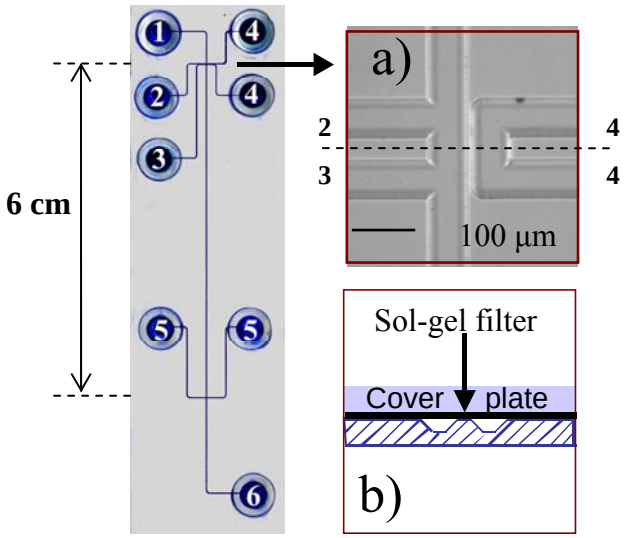

Figure 2

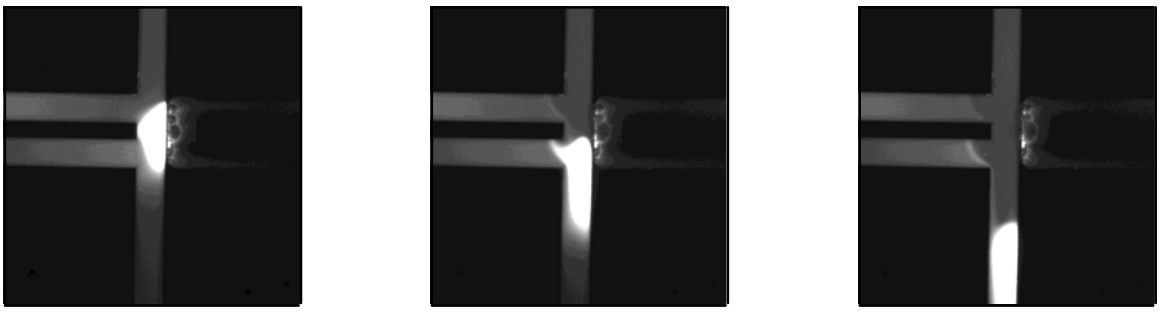

Figure 3

Separation channel

Dilution channel: Side channel for introducing the dilution buffer and the labeling dye

Dilution channel: Side channel for introducing the dilution buffer and the labeling dye

Detection channel for dilution, labeling and detection

Figure 4

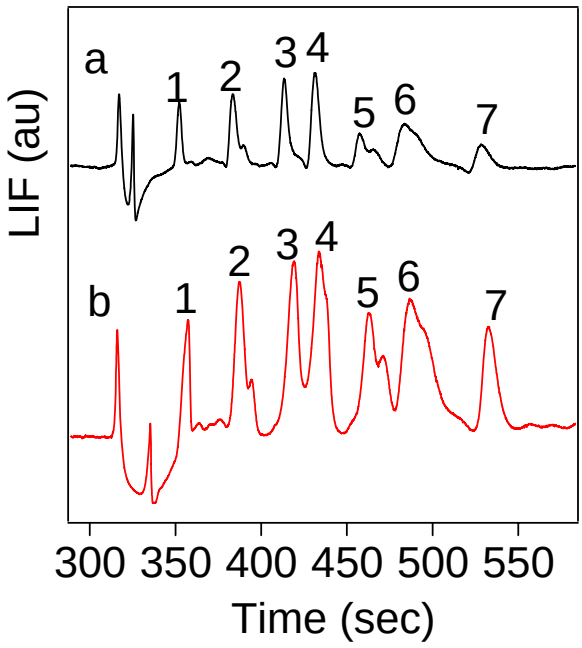

Figure 5

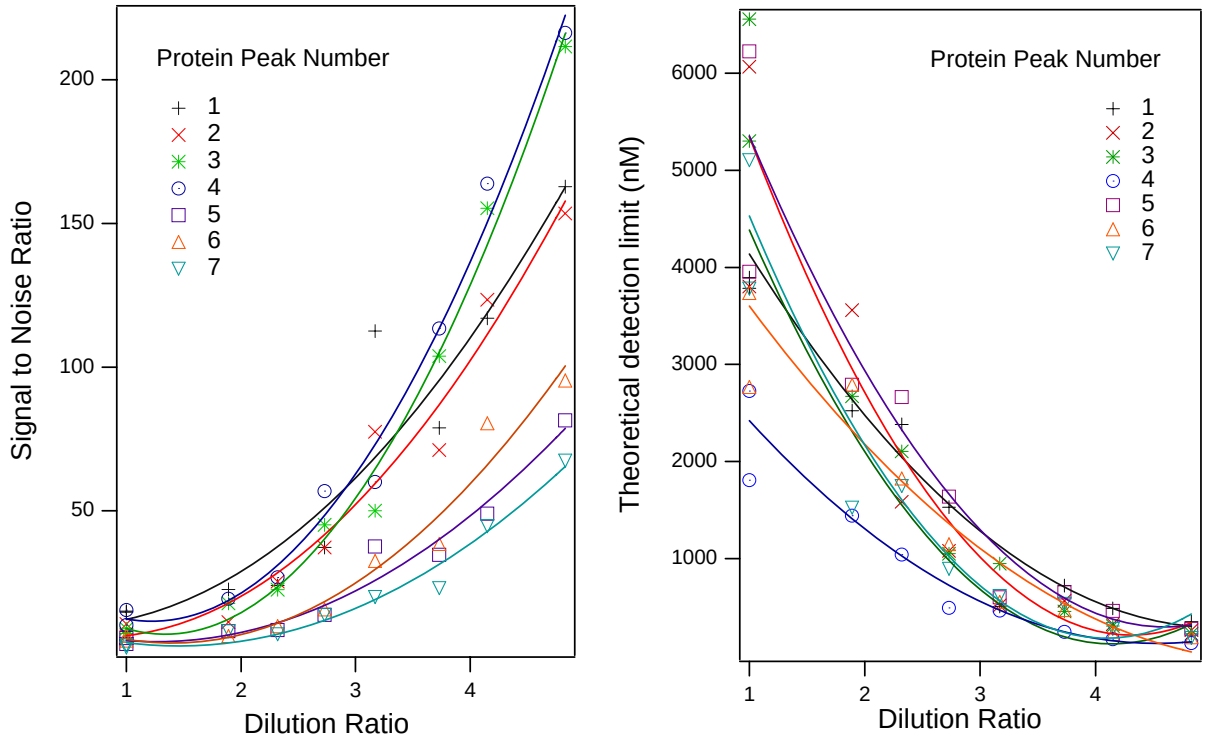

Figure 6

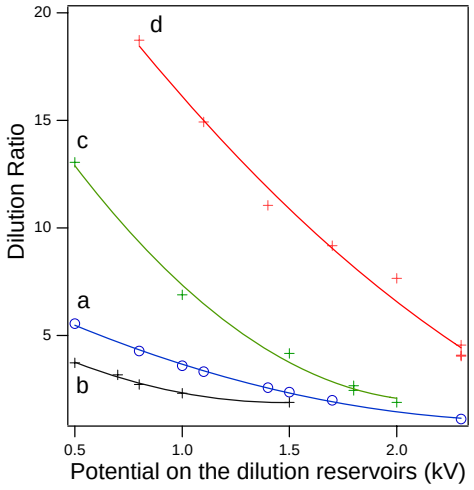

Figure 7

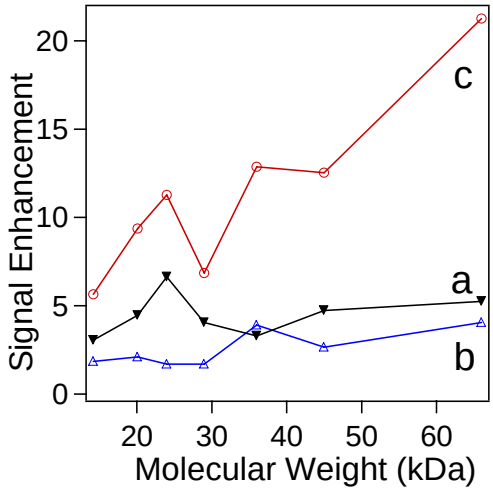

Figure 8

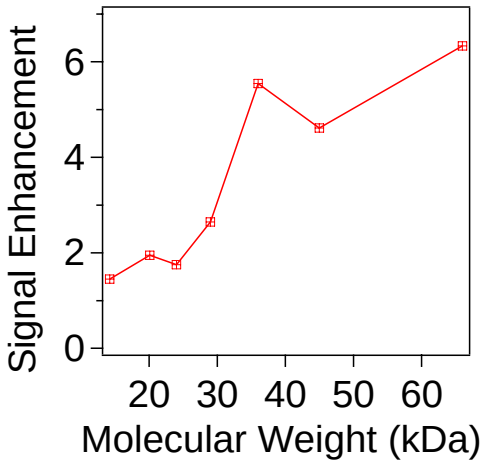

Figure 9

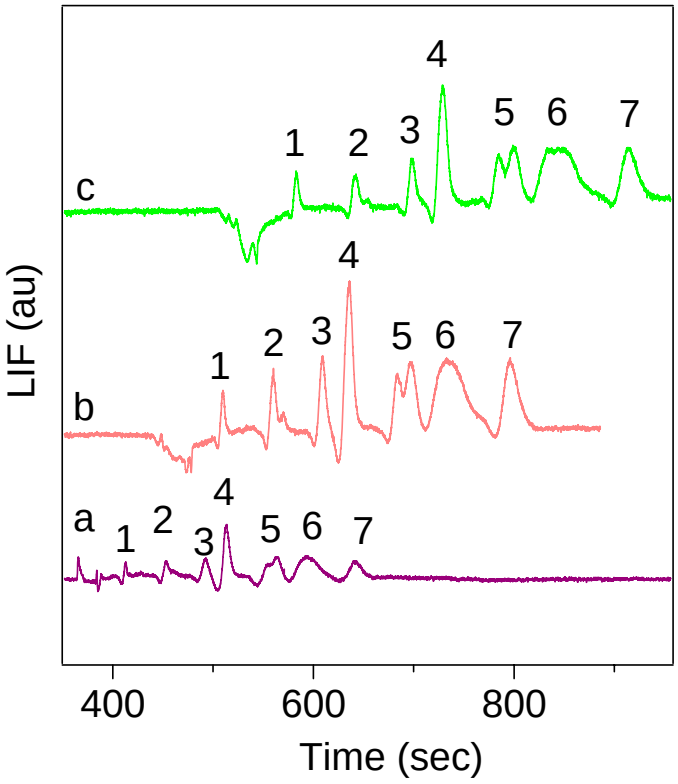

Figure 10

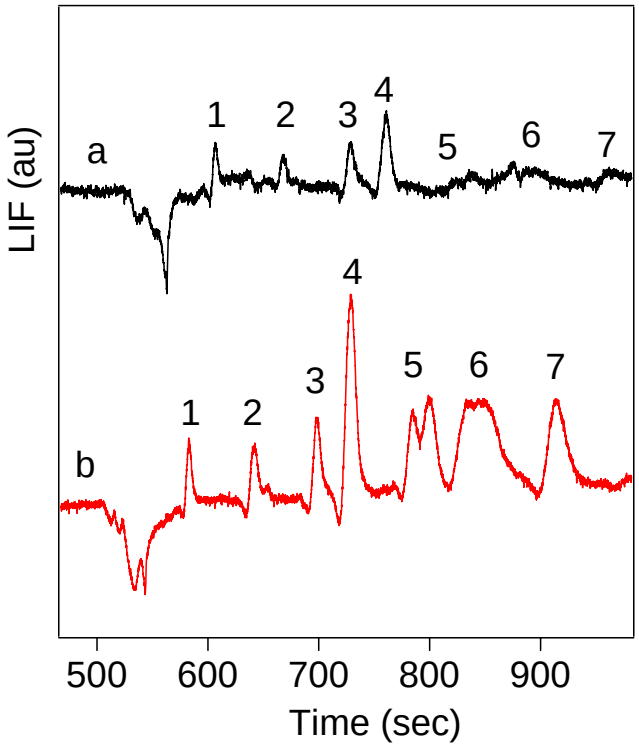

Figure 11

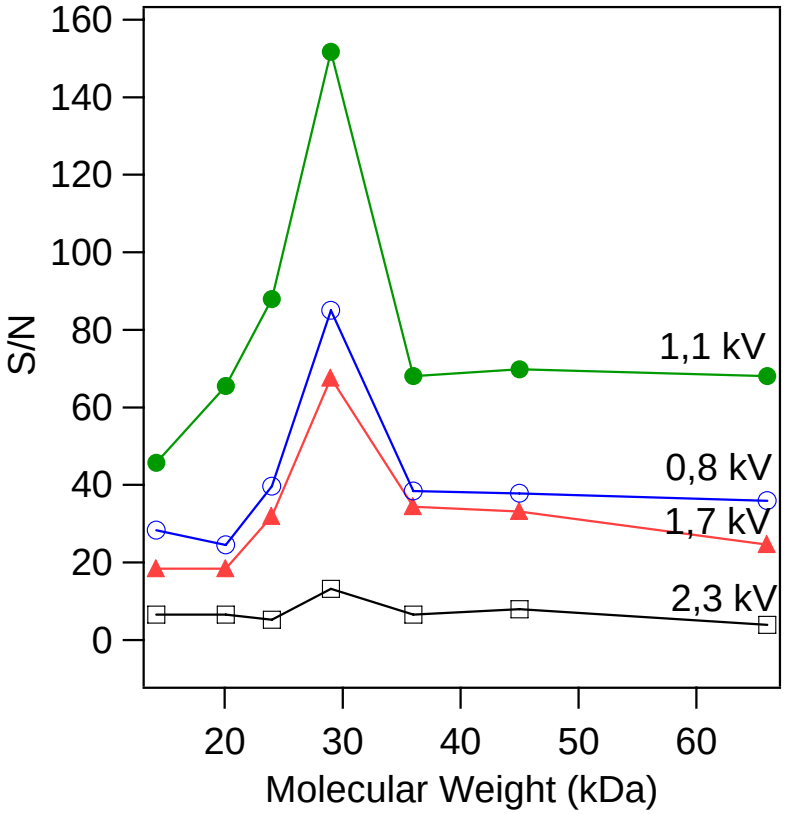

Figure 12

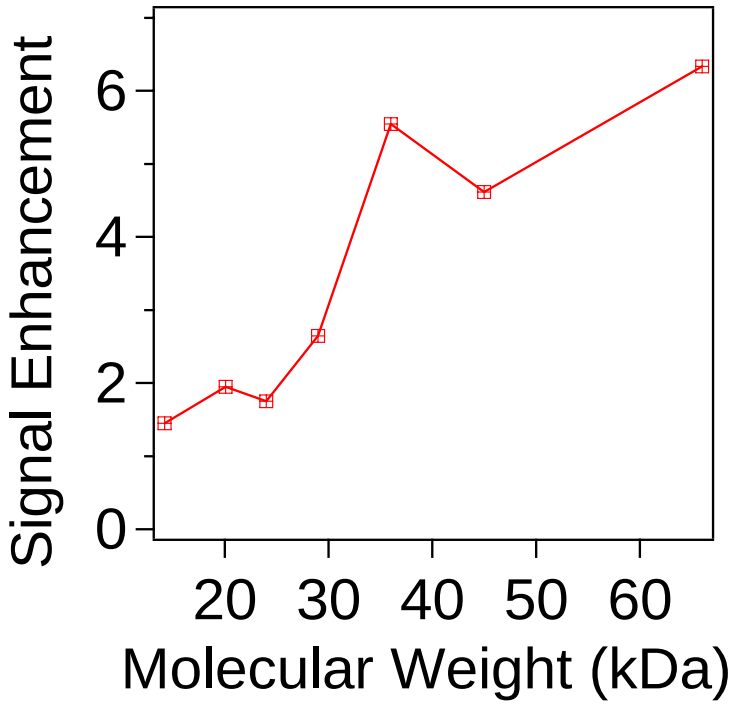

Figure 13

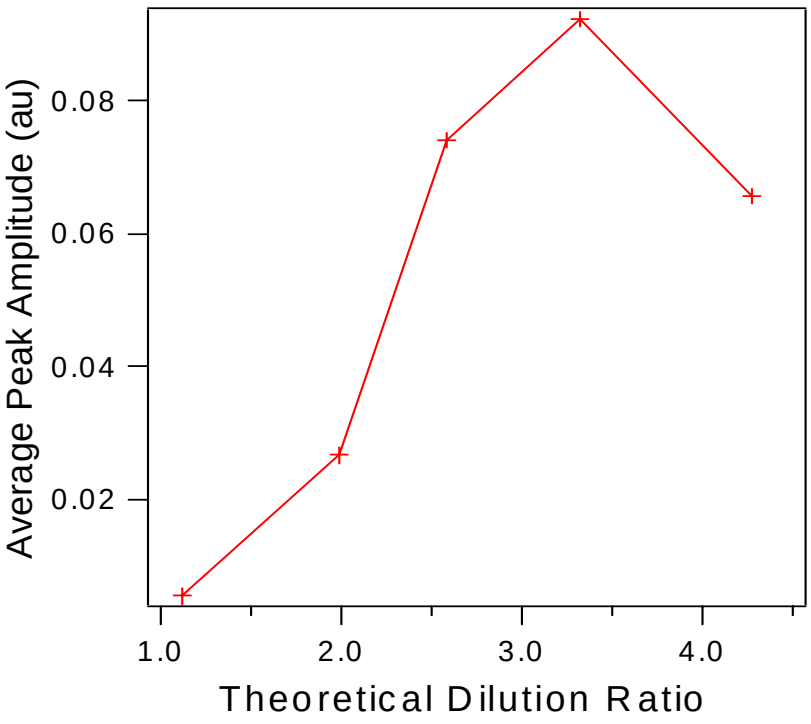

Figure 14

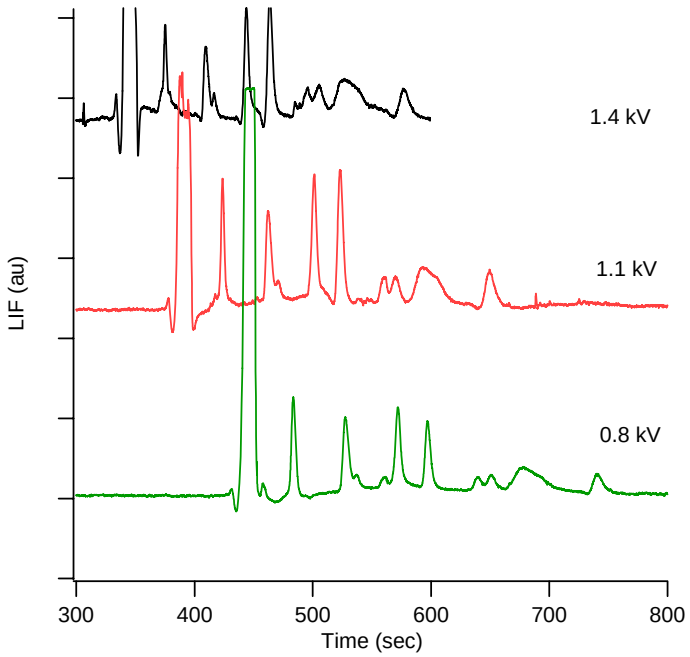

Figure 15

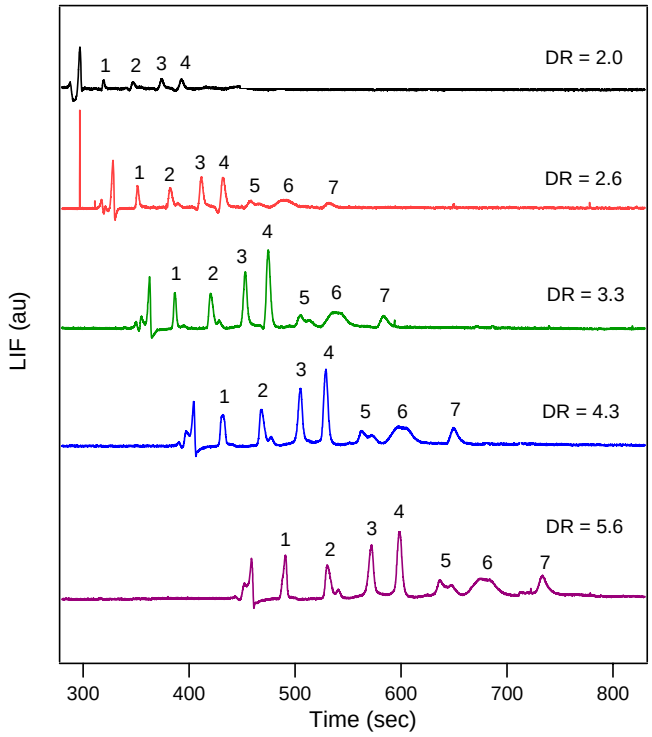

Figure 16

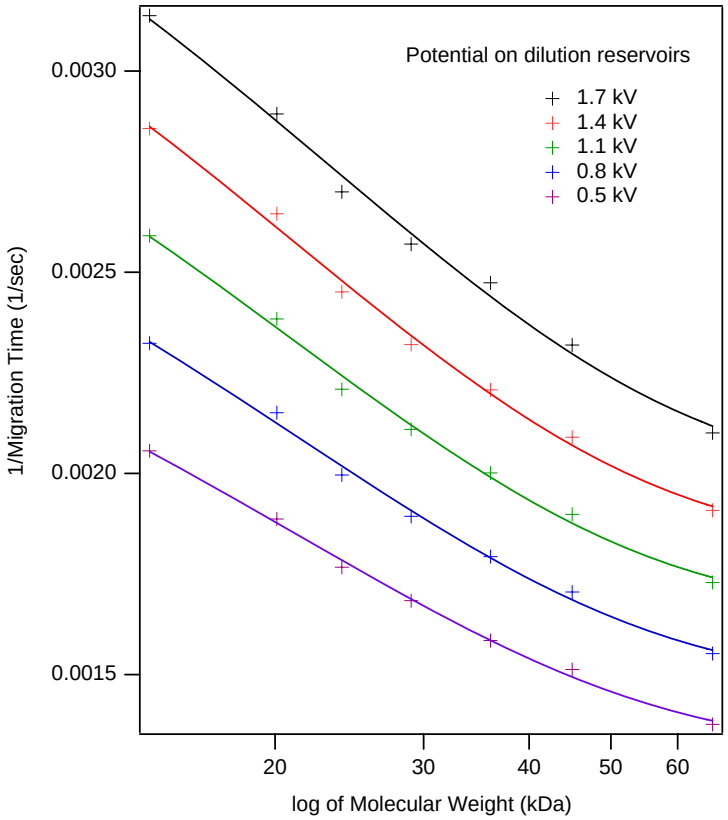

Figure 17

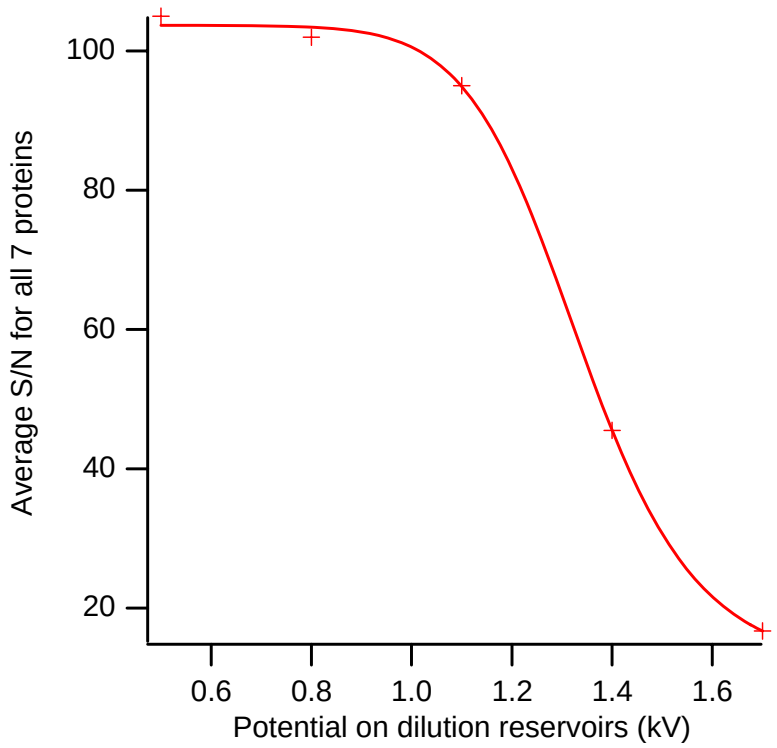

Figure 18

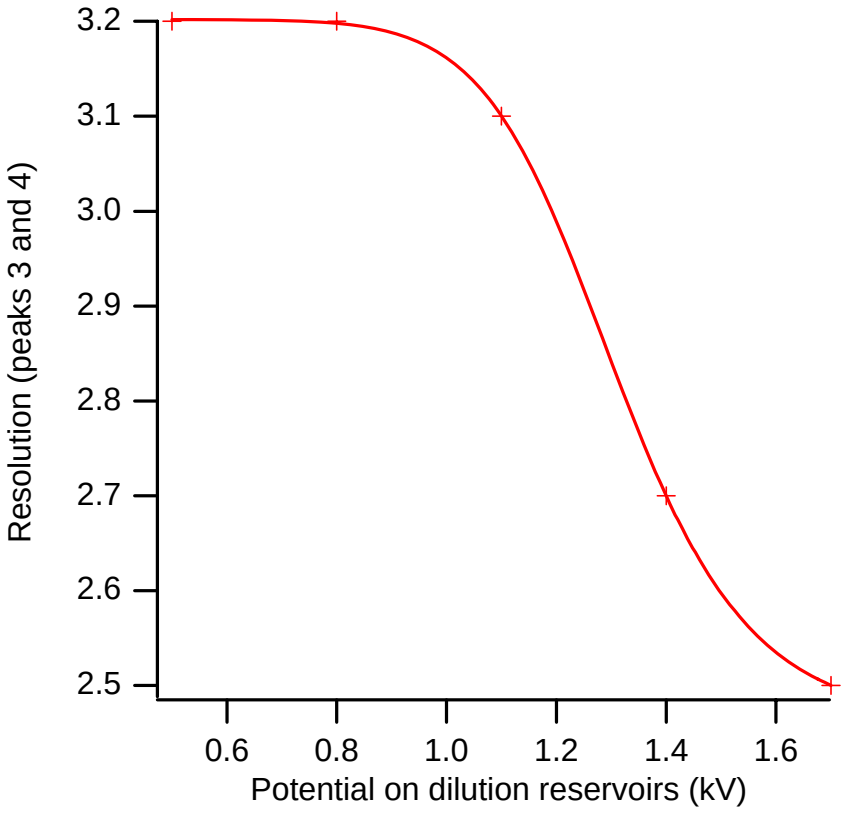

Figure 19

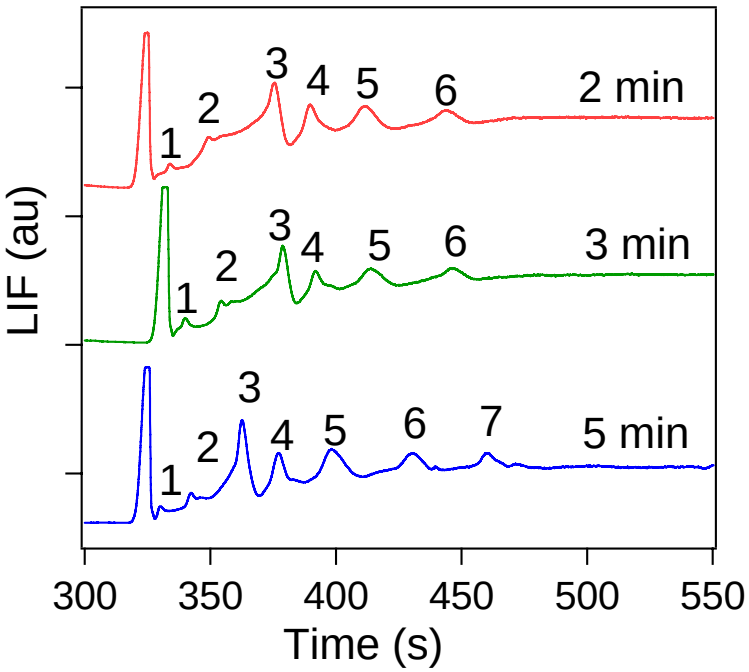

Figure 20

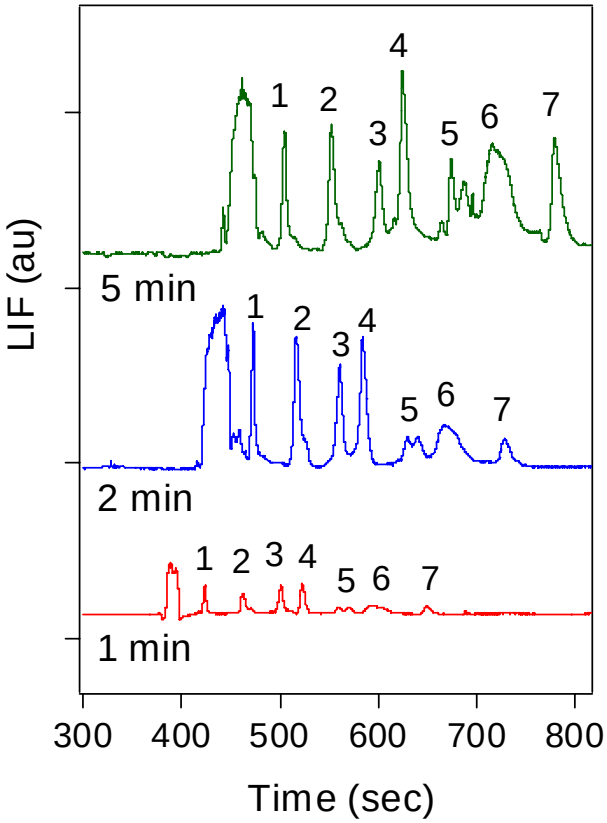

Figure 21

Dye[a]	Dye Conc.[b]	Sample conc. (mg/ml)[c]	Labeling Mode	Average S/N	N (peak 1)[d]	Resolution (peaks 3 and 4)	Average[e] LOD (nM)
SyR	**1x**	1	**On-column**	105	78,700	3.2	168
SyO	1x	2	On-column	151	76,100	2.3	320
SyO	**10x**	1	**Post-column**	8	56,000	2.1	2450
SyO	**100x**	1	**Post-column**	100	110,100	2.6	220

Table 1

Dye Conc.[a]	Sample conc. (mg/ml)[b]	Labeling Mode	Precon. Time (min)	N (peak 1)[c]	Average S/N[d]	Resolution (peaks 3 and 4)	Theoretical LOD (average, nM)[d]
1x	2	On-column	0	76,100	151	2.3	320
“	2	“	1	37,900	304	1.0	104
“	0.02	“	5	91,400	30	1.2	16
10x	1	**Post-column**	0	56,000	8	2.1	2450
“	1	“	1	77,200	84	1.8	240
100x	1	**“**	0	110,100	100	2.6	220
“	1	“	1	38,200	236	2.1	91

Table 2

8.4 List of publications

This appendix contains references of articles published in refereed international conference proceedings.

'Miniaturized Chromatographic Systems with Integrated Optical Detection', Oral presentation

Nickolaj J Petersen, Daria Anachkina, Klaus B. Mogensen, Jörg P. Kutter, Pieter Telleman

6th Annual Meeting of the Danish Society for Analytical Chemistry, Lyngby, Denmark, August 16-17, 2000

'Microfabricated Separation Systems and Integrated Optics', Oral presentation

Jörg P.Kutter, Nickolaj J Petersen, Daria Anachkina, Klaus B. Mogensen, Peter Friis, Anders M. Jørgensen, Jörg Hübner, Pieter Telleman

2nd Symposium of the Nordic Separation Science Society, Lyngby, Denmark, August 18-19, 2000

'Polymer-based Microdevices versus Silicon/glass-based Microdevices for Analytical Applications – a Comparison', Oral presentation

Jörg P.Kutter, Peter Friis, Klaus B. Mogensen, Nickolaj J Petersen, Weimin Rong, Oliver Geschke, Daria Anachkina, Preben M. Elkjær and Pieter Telleman

HPCE2001, Boston, MA, USA, January 14-18, 2001

'Microfabricated tools for Bio/Chemical Analysis', Invited Oral Presentation

Jörg P.Kutter, Anders Wolff, Ulrik Darling Larsen, Claus Riber Poulsen, Ivan R. Perch-Nielsen, Weimin Rong, Anders M. Jørgensen, Peter Friis, Klaus B. Mogensen, Nickolaj J Petersen, Daria Anachkina, Solveig Sturlaugsdottir, Peter Falk, Oliver Geschke and Pieter Telleman

LabAutomation 2001, Palm Springs, CA, USA, January 27-31, 2001

'A New Approach for Fabricating a Zero Dead Volume Electrospray Tip for Non-aqueous Microchip CE-MS', Poster presentation

Daria Petersen, Sami Varjo, Oliver Geschke, Marja-Liisa Riekkola and Jörg P. Kutter

µTAS 2002, Nara, Japan, November 3-7, 2002

'Glass CE Microfluidic Devices with Monolithically Integrated Electrospray Tip for Coupling to MS'; Poster presentation
Oliver Geschke, Daria Petersen, Sami Varjo, Marja-Liisa Riekkola and Jörg P. Kutter
ITP 2002, Helsinki, Finland, September 1 - 4, 2002

'An Integrated Chemiluminescence Detector for Measuring Enzymatically Generated Hydrogen Peroxide', Poster presentation
Anders Michael Jørgensen, Daria Anachkina, Oliver Geschke
µTAS 2002 Nara, Japan, November 3-7, 2002

'An Integrated Microdevice for Protein Preconcentration, Separation and On-chip Labeling' Poster Presentation
Robert S. Foote, Daria Petersen, J. Michael Ramsey
HPCE 2004, Salzburg, Austria, Feb 8-12, 2004

'An integrated microdevice for on-chip preconcentration, separation and labeling of proteins'
Daria Petersen, Robert S. Foote, Oliver Geschke, J. Michael Ramsey
Poster presentation
µTAS 2004, Malmö, Sweden, Sep 26 - Oct 1, 2004

Other Publications

'Analytisk Kemi på Mikrochips' (in Danish)
Nickolaj J. Petersen, Klaus B. Mogensen, Daria Anachkina, Pieter Telleman, Jörg P. Kutter
Dansk Kemi, 81(9), 2000, 17-20

Coauthor for two chapters in the textbook "Microsystem Engineering of Lab-on-a-Chip Devices", ISBN: 3-527-30733-8, Geschke, Klank, Telleman Eds., 2004